

MICROCOPY RESOLUTION TEST CHART
NATIONAL BUREAU OF STANDARDS 1963-A

AFIT/GSO/PH/82D-2



DTIC
ELECTE
FEB 10 1986
S D

A FEASIBILITY STUDY:
THE DETERMINATION OF THUNDERSTORM
INTENSITY WITH A TEMPERATURE SENSING
SHUTTLE-BORNE LIDAR

THESIS

AFIT/GSO/PH/82D-2

Craig Z. Lowery
Capt USAF

DISTRIBUTION STATEMENT A

Approved for public release;
Distribution Unlimited

A FEASIBILITY STUDY:
THE DETERMINATION OF THUNDERSTORM
INTENSITY WITH A TEMPERATURE SENSING
SHUTTLE-BORNE LIDAR

THESIS

Presented to the Faculty of the School of Engineering
of the Air Force Institute of Technology
Air University
In Partial Fulfillment of the
Requirements for the Degree of
Master of Science

by
Craig Z. Lowery
Capt USAF
Graduate Space Operations
December 1982

Accession For	
NTIS CRA&I	<input checked="" type="checkbox"/>
DTIC TAB	<input type="checkbox"/>
Unannounced	<input type="checkbox"/>
Justification	
By	
Distribution /	
Availability Codes	
Dist	Avail and/or Special
A-1	

Preface

This thesis examines the feasibility of placing a DIAL lidar on the space shuttle and have this instrument measure the intensity of thunderstorms. I have always had a great deal of interest in meteorology and in particular the thunderstorm. As an undergraduate, my classmates and I use to chase thunderstorms in hopes of watching tornado formation. Now, with extensive physics and remote sensing courses taught here at AFIT, I can combine my meteorological experience with sensor design concepts and show what a great asset the lidar is to the atmospheric sciences.

I would like to thank my advisor, Major Jim Lange (PhD), who seems to always be two steps ahead of the world, for all of his advice and support. I thank the AFIT research librarian, Linda Stoddart, for locating all my meteorological references which required inter-library loans. Finally, I would like to thank my wife, Gay, for eighteen months of loving support during very trying times here at AFIT.

Craig Z. Lowery

Abstract

This thesis examines the feasibility of operating a lidar (laser radar) from the space shuttle and having this instrument measure the intensity of thunderstorms. Thunderstorm intensity is monitored by measuring the time rate of change in temperature of the top 0.5 km of a thunderstorm. Severe weather occurring on the ground takes place during, or just after a period of rapid cloud top cooling. Temperature is measured with two wavelengths using the differential absorption lidar (DIAL) technique which determines the resonant absorption of oxygen in the oxygen "A" band near $.7700 \mu\text{m}$. One wavelength is set at $.7696 \mu\text{m}$ which is a temperature sensitive oxygen absorbing line while the second wavelength is set at $.7614 \mu\text{m}$ where oxygen absorption is negligible. The lidar can measure the oxygen resonant absorption coefficient at the heights of typical thunderstorm tops. A temperature value is recovered by placing the absorption coefficient into a quickly converging iterative expression. Hypothetical thunderstorms with heights from 10-17 km are probed at shuttle altitudes ranging from 100-250 km. Success of the system is based on useful values of the signal-to-noise ratio.

Table of Contents

	<u>Page</u>
Preface	i
Abstract	ii
I. Introduction	1
II. Literature Review	3
Characteristics of a Thunderstorm	3
Internal Structure of a Thunderstorm	5
Top Structure of a Thunderstorm	8
Forecasting Thunderstorms	9
Satellite Observations of Thunderstorms	11
History of Lidars	12
Lidar Sensing of Temperature	14
DIAL Lidar vs Infrared and Microwave Radiometers	15
Scattering Theory	16
Rayleigh Scattering	16
Mie Scattering	17
Resonant Absorption	18
III. Lidar Equation	20
Multiple Scattering	23
IV. DIAL Theory	25
Remote Sensing of Temperature	25
Relative Humidity	34
Differential Absorption Calculation	34
Predicting α_g with Polynomial Regression	37
V. Atmospheric Considerations	41
Index of Refraction	41
Rayleigh Cross Section	42
Atmospheric Extinction	42
Rayleigh Backscatter Coefficient	45
Attenuation by Gases	47
Attenuation by Aerosols	50
Aerosol Backscatter Coefficient	54
Attenuation by Thunderstorm Tops	54
Miscellaneous Cloud Top Parameters	56
Attenuation by Ozone	56
VI. Laser Considerations	59
Laser Beam Divergence	59
Thermal Blooming	62
Dye Lasers	63
VII. Instrumental Considerations	65
Integration Time	65
Sounding Time	65

Table of Contents (contd)

	<u>Page</u>
Laser Power	65
Peak Power	67
Vertical Resolution	68
Background	70
Signal-to-Noise Ratio	71
VIII. System Results	74
Scenario I	74
Attitude Control	76
Data Collection Intervals	76
IX. Thunderstorm Vertical Velocity	89
Stereographic Observations	98
Damaging Hailstorms	98
Scenario II	99
X. Miscellaneous Considerations	103
Eye Safety	103
Calibration of the Lidar	104
Transmitter Configuration	105
Receiver Configuration	105
System Arrangement	105
Viewing Geometry	105
The Infrared Equivalent	105
XI. Conclusion	112
Recommendations	114
Bibliography	115
Vita	123

I. Introduction

The Space Shuttle Columbia completed its fourth test flight and became operational on 4 July 1982. Now, for the first time, a space vehicle can carry cargo into orbit and return all of it safely back to earth in a relatively economic manner. Such a magnificent capability poses an interesting question: what can the space shuttle be used for? Presentations at the recent Space Symposium held at the U.S. Air Force Academy on 11 October 1982 indicate that the shuttle is an excellent vehicle to conduct scientific research from. In addition, the symposium revealed that proposed scientific experiments have yet to fully utilize the shuttle's unique capabilities. This thesis proposes a new use for the space shuttle.

This thesis examines the feasibility of mounting a lidar (laser radar) in the shuttle's cargo bay and having this device measure the intensity of thunderstorms. Thunderstorm intensity will be monitored by measuring the time rate of change in temperature of the thunderstorm top. Temperature will be measured using a recently developed DIAL technique which determines the resonant absorption of oxygen in the oxygen "A" band near 770 nm. This is the first proposed use of a temperature sensing laser for the monitoring of thunderstorm intensity.

If a thunderstorm becomes severe, a great deal of property damage and a loss of life is possible. Recent research indicates that severe weather occurring on the ground took place during, or just after a period of rapid cloud top cooling. A lidar operating from the space shuttle

could measure the temperature of a particular thunderstorm and provide an indication of the storm's intensity or severity. A shuttle-borne lidar would be an interesting experiment with operational possibilities later on such as providing timely warnings. In this way, such a sensor could prevent millions of dollars of damage and possibly save lives.

II. Literature Review

Characteristics of a Thunderstorm

A thunderstorm is produced by a cumulonimbus cloud and is always accompanied by thunder, lightning, rain, wind, and occasionally with hail and/or tornado (s). The thunderstorm and its associated weather phenomenon is the most violent storm produced in the earth's atmosphere.

In the continental mid-latitudes, thunderstorms usually occur in the spring and summer. Those storms that form in the spring are typically triggered by synoptic scale (storms 1000-2500 km across) disturbances embedded in the jet stream. These spring-time thunderstorms can be quite intense. Such intense or severe storms can reach heights greater than 14 km and produce hail (≥ 3 cm in diameter), strong straight-line winds (≥ 30 m sec⁻¹), intense updrafts (98 m sec⁻¹ reported by Brown and Knupp, 1980), and sometimes tornados. The typical summer-time thunderstorm is usually less severe and is triggered this time by mesoscale (storms 1-999 km across) disturbances and/or surface heating.

All thunderstorms can occur as single cells by themselves, groups of several cells producing a multicell complex, or lined up singly to form a squall line. Occasionally a single local storm will become very severe and becomes what Browning (1977) refers to as a supercell. A few over-simplified characteristics of severe and non-severe thunderstorms can be found in Figure 1.

The shear referred to in Figure 1 is the horizontal force felt by the storm as wind velocity increases with height.

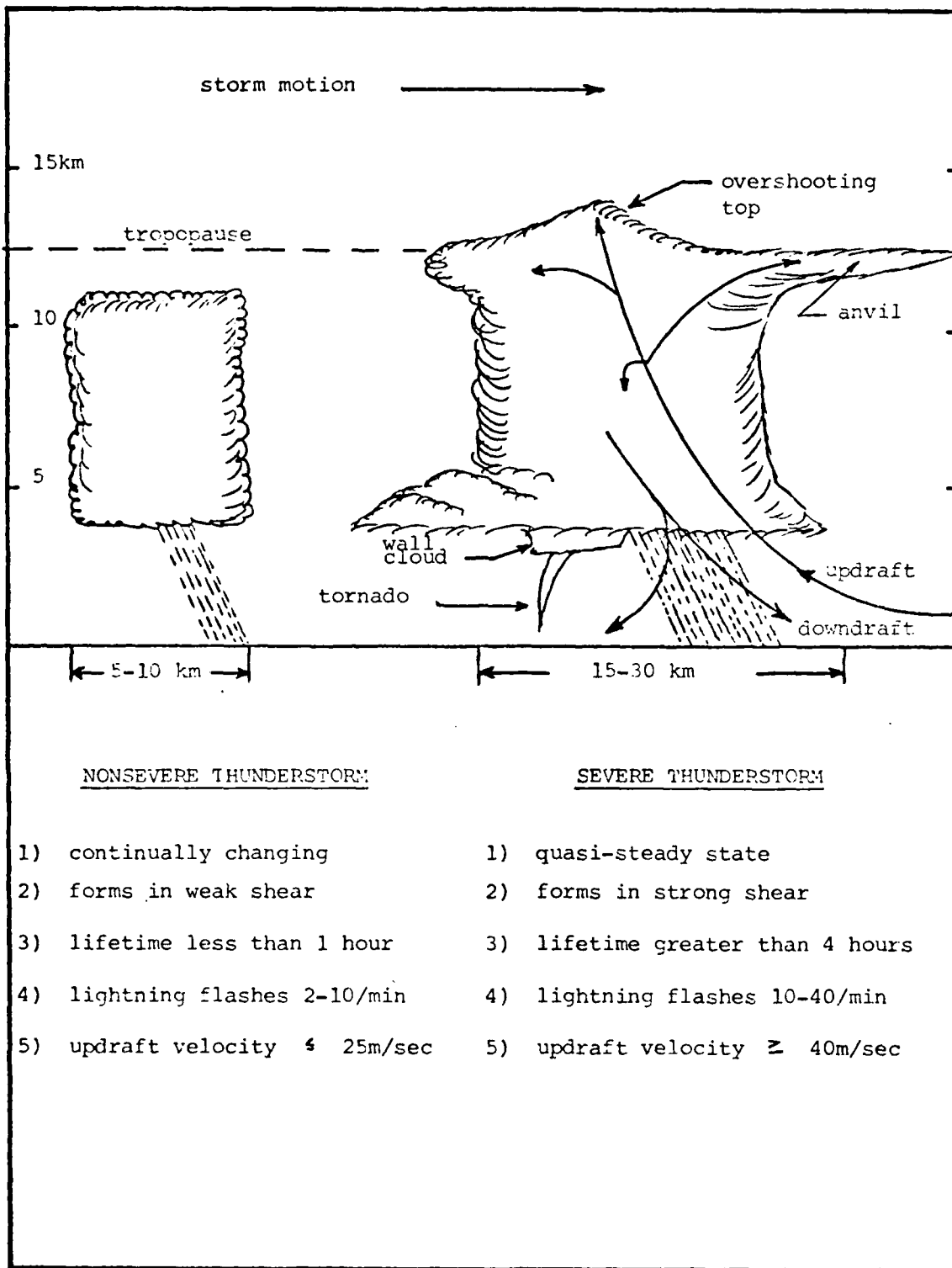


Figure 1. Typical thunderstorm characteristics (after Rust *et al*, 1981; Kropfli and Miller, 1976 with changes).

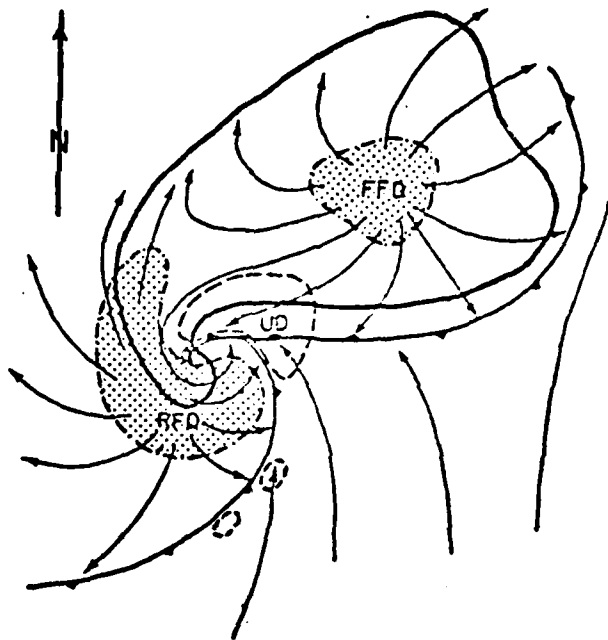
Internal Structure of a Thunderstorm

Research in mesoscale meteorology is dominated by investigations of supercell thunderstorms. Such research is carried out by surface observing networks, radar, aircraft, and satellite. There has been extensive effort to develop computer programs which simulate thunderstorm development; however, to this day the internal dynamics of a thunderstorm are not well understood, and with the lack of good data, computer simulations have not verified well against real world situations. Thus, most thunderstorm models are of a conceptual format (Newton, 1963; Browning, 1964; Marwitz, 1972 a.b.; Lemon and Doswell, 1979b). To briefly review the internal structure of a severe thunderstorm, the model of Lemon and Doswell (1979b) is chosen since it represents an excellent composite of current research on supercells.

Figure 2 is a one-dimensional view of a supercell storm looking down from space. The heavy dark outline represents the shape of the storm as viewed from a weather radarscope. The storm is moving towards the northeast. A mesoscale frontal structure is formed by these storms which closely resemble synoptic scale cold fronts which cover entire continents (Brooks, 1949).

Figure 3 a-d is a three-dimensional schematic of a supercell with the vertical scale distorted and features above 9 km omitted. Figure 3a shows the main updraft rotating upward. The forward flank downdraft is formed by falling precipitation and supplemented by mid-altitude prevailing winds deflected downward.

Figure 3b illustrates the unique feature of a supercell, a second downdraft. This rear flank downdraft forms as cool dry air slams into the



FFD is the forward flank downdraft

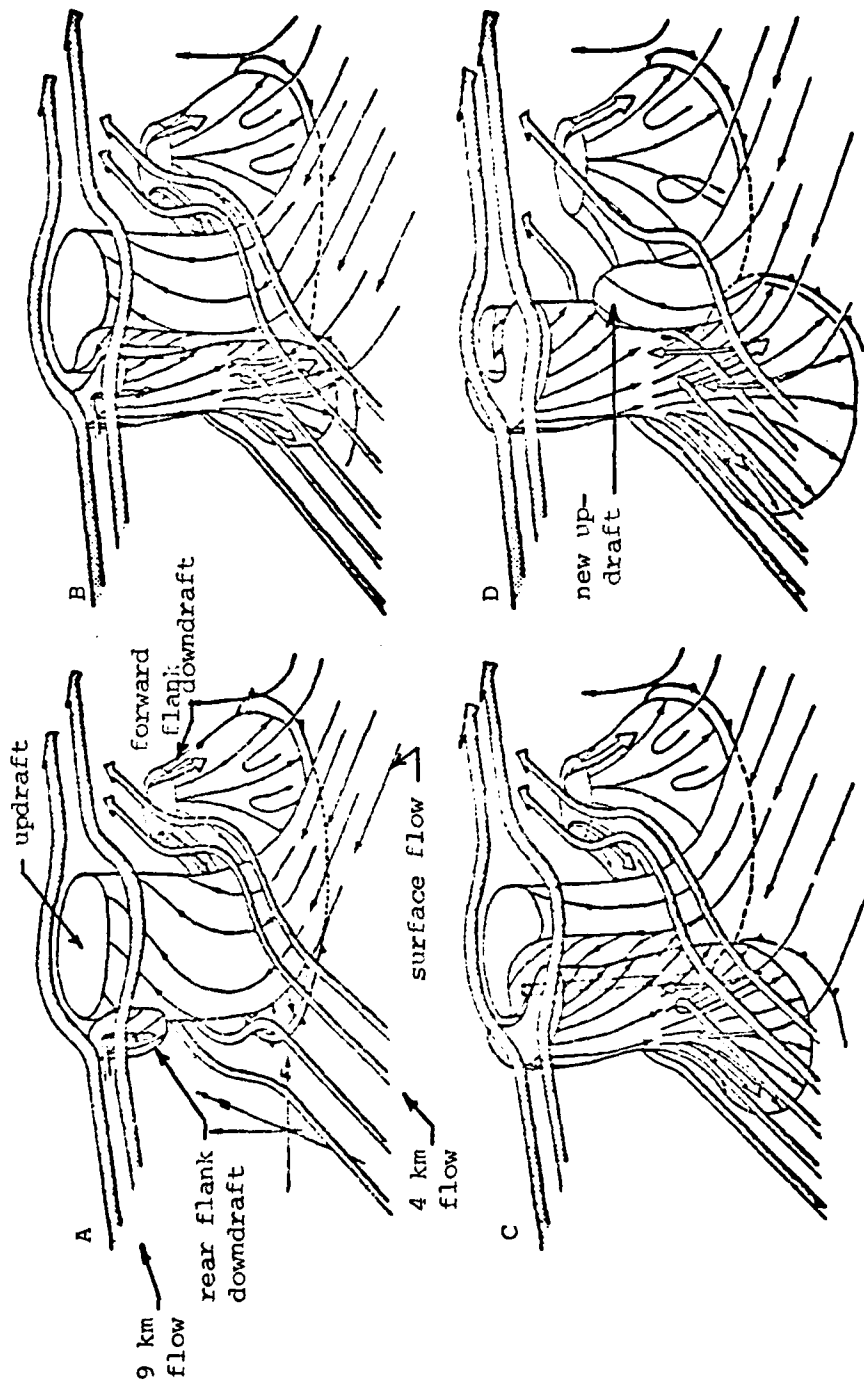
UD is the updraft

RFD is the rear flank downdraft

T is the tornado location

Figure 2. Top view of a supercell thunderstorm (after Lemon and Doswell, 1979b).

Figure 3. Internal thunderstorm structure (after Lemon and Doswell, 1979b).



updraft column and is deflected downward. Figure 3c shows the proposed location of a tornado existing in a region of intense vertical velocity and temperature gradients.

Figure 3d shows the dissipating stage where downdrafts have choked off the warm moist updraft. Tornado touchdown is possible here.

Top Structure of a Thunderstorm

The study of overshooting cloud tops or towers protruding above the anvil floor by several kilometers has been the subject of much research in recent years (McCann, 1979). Overshooting tops have been directly correlated with thunderstorms producing tornados, hail, and strong wind gusts (see Figure 1).

There are two evolving schools of thought concerning overshooting storm tops. The first theory claims that severe weather will occur on the ground during or soon after an overshooting top collapses. Hard data backs this theory. The second theory concerning overshooting tops claims that severe weather occurs on the ground during or soon after rapid top growth. Hard data backs this theory also (McCann, 1979).

Fujita (1973a) maintains that a collapsing top will create a tornado at ground level. Here it is claimed that the updraft carries warm moist air above the anvil floor. This now protruding top soon becomes precipitation heavy causing the top to collapse upon itself. The resulting downdraft twists around the rotating updraft which produces enough surface vorticity to generate a tornado.

Lemon et al (1975) claims that rotation of the updraft causes the top to collapse through a process in fluid mechanics called vortex valve. This too is a trigger mechanism for tornadogenesis.

Adler and Fenn (1979c) studied thunderstorm vertical growth rates and top structure from infrared geosynchronous satellite data. These researchers showed that the rate of storm growth and minimum cloud top temperature correlate with reports of severe weather on the ground.

Reynolds (1980) studied top temperatures of damaging hailstorms with infrared geosynchronous satellite data. He determined that hailfall occurred at close to the time of the maximum rate of storm growth. In other words, hail was reported under an overshooting top as the top reached its maximum height (coldest temperature).

Forecasting Thunderstorms

The National Weather Service (NWS) defines a severe thunderstorm as one or more of the following: 3/4 inch (1.9 cm) or larger hail, strong winds of 50 knots (26 msec^{-1}) or greater, and tornado(s).

Ostby and Higginbotham (1982) examined tornado predictability and intensity. They considered all reported tornados (8,825) for the period 1971-1980. Figure 4 shows the 10 year statistics for the number of weak, strong, and violent tornados for each state. Figure 5 shows the number of tornado deaths during the 10 year period which occurred in either a tornado watch or in a severe thunderstorm watch.

Lemon (1979a) points out that the NWS's thunderstorm and tornado warning programs need considerable improvement. The Doppler radar will improve warnings, but the nation-wide network will not be operational until the 1990 time frame (Lemon et al, 1977; Burgess and Devore, 1979; Wilson, 1980). Stereographic observations from geosynchronous satellites of thunderstorm height changes is a promising new tool; however, it is

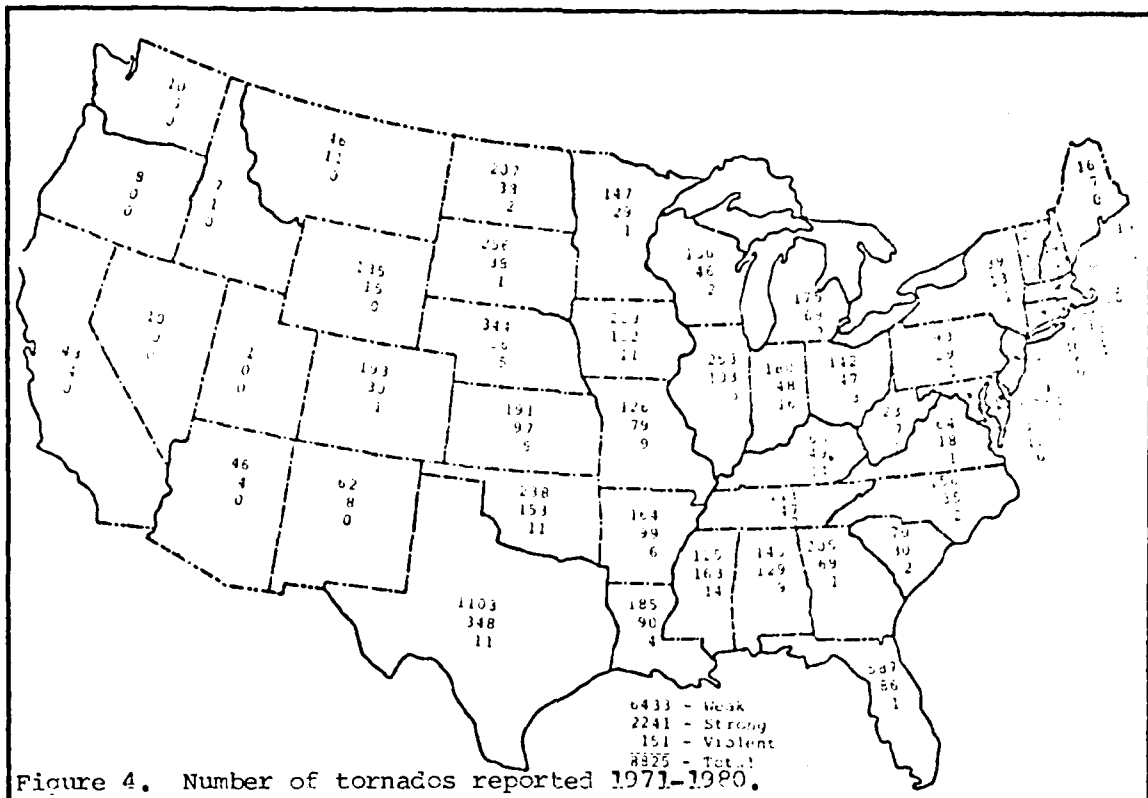


Figure 4. Number of tornadoes reported 1971-1980.

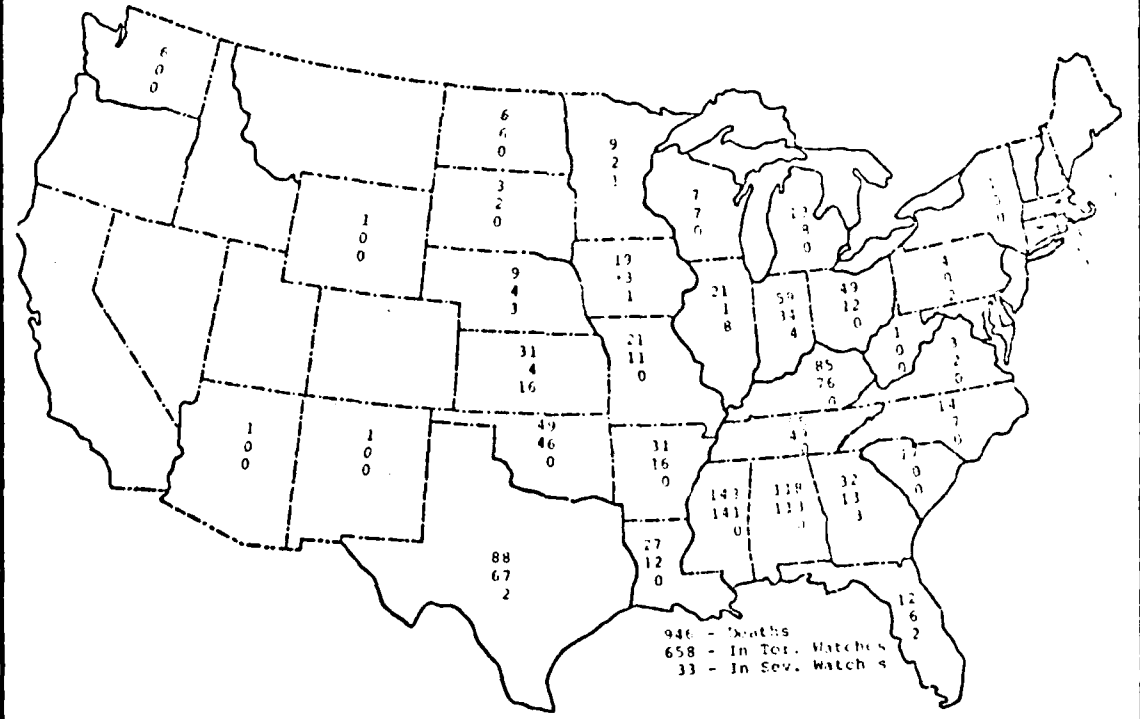


Figure 5. Number of tornado deaths 1971-1980 (figures 4&5 after Ostby and Higginbotham, 1982).

only now being demonstrated, and researchers would like more satellites (Hasler, 1981).

Any improvement in forecast reliability in the near future will lower the false alarm rate (no occurrence of a tornado when forecast). A high false alarm rate may produce public apathy. If the loss of life is to be prevented, severe thunderstorm and tornado warnings must improve (Johnson, 1977).

Satellite Observations of Thunderstorms

Distinct severe thunderstorm characteristics were first identified by using visual images from the old TIROS 1 satellite. Whitney and Fritz (1961) and Whitney (1963) identified severe thunderstorms to be (1) visibly brighter than surrounding clouds, (2) rounded in appearance, (3) have scalloped edges, (4) some evidence of cirrus blowoff, and (5) dimensions of 100 to 200 miles. Later, Boucher (1967) observed severe storms to have larger tops than non-severe storms.

Severe local storm research became very popular in the 1970s with the advent of geosynchronous satellites featuring ever improving spatial and temporal resolution in both the visible and infrared. Anvil brightness was examined by Arn (1975) and Tuckman (1982). Purdom (1976) and Beckman (1982) studied merging thunderstorms. Anvil growth rate has been linked to severe thunderstorms by Sikdar (1970), Purdom (1971), Adler and Fenn (1976), Yuen (1977), and Negri (1977). Fujita (1978) was able to isolate an incident of pulsating anvil growth, while Marshall and Peterson (1979) studied a storm whose anvil grew in area at a rate of $700 \text{ km}^2 \text{ min}^{-1}$ yet did not become severe. Anderson (1979) also reports

unusual anvil characteristics while investigating anvil outflow patterns.

Adler and Fenn (1979a) used short interval 3-5 minute infrared images from geosynchronous satellites to examine the rate of change in temperature of severe and non-severe thunderstorm tops. This led to a relationship between storm growth rate as compared to the storm's updraft velocity (Adler and Fenn, 1979b). Pryor (1978) and Reynolds (1980) investigated the top temperatures of hailstorms.

The latest technique developed to study thunderstorms by satellite is stereographic observations (Hasler, 1981; Fujita, 1982; Heymsfield et al, 1982). This method features good horizontal and vertical resolution (1 km x 1/2 km) but is useful only in daylight. Stereographics uses two geosynchronous satellites focused on the same cloud from different viewing positions to yield accurate measurements of height changes.

History of Lidars

A lidar is a laser often used for observing the atmosphere. Lidar is an acronym for light detection and ranging. The lidar's principle of operation closely parallels that of the weather radar (radio detection and ranging). Some researchers refer to the lidar as "laser radar" or "optical radar."

The lidar generates a short, powerful light pulse that propagates through the atmosphere. The light from the laser pulse is backscattered by atmospheric gases and by suspended aerosols and is collected by a receiving telescope. The telescope contains a narrow band interference

filter which removes background sky light and directs a filtered-returned signal into a photomultiplier tube where the signal is enhanced.

Three years after lasers became operational, Guy Goyer and R. Watson (1963) are credited as the first to point out that the laser is a powerful tool for remote sensing of the atmosphere. Shortly thereafter, Fiocco and Smullin (1963) used a ruby lidar to analyze the mesosphere. In addition, Ligda (1963) was the first to use the lidar for meteorological purposes in the troposphere. Indeed, the lidar has many applications as a tool for remote sensing of the atmosphere (Collis, 1970; Derr, 1977). The wide selection of papers presented at the Eleventh International Laser Radar Conference (NASA, 1982) emphasizes the exceedingly broad range of potential applications of lidar to the atmospheric sciences from the analysis of aerosols to wind measurements.

NASA recently completed a survey of the scientific problems and the feasibility of conducting lidar experiments from the space shuttle. The study identified a number of experiments that would be of scientific interest and be technically feasible with state-of-the-art technology (NASA, 1979).

According to Atlas and Korb (1981) a shuttle-borne lidar could conduct experiments such as the measurement of all atmospheric state variables (temperature, pressure, humidity, and wind) as a function of altitude above any surface location. Since this thesis examines a use for a shuttle-borne temperature sensing lidar, this literature review will be restricted to laser methods of measuring temperature.

Lidar Sensing of Temperature

Techniques to measure temperature with optical devices began with Elterman (1964) when he employed a searchlight to measure stratospheric density profiles. Temperature profiles are computed from the density measurements by assuming that the atmosphere is in hydrostatic equilibrium. Twenty-seven years later, Chanin and Hauchecorne (1980) performed essentially the same experiment using a lidar. Searchlight procedures are not accurate in the troposphere where all sensible weather occurs, but lidars are quite useful.

Raman lidar systems using rotational Raman scattering from a mix of atmospheric O_2 and N_2 gases can recover temperature profiles (Gill et al, 1974; Cohen et al, 1976). Nevertheless, Raman scattering has a low cross-section, or probability of occurrence. Hence this technique has low sensitivity which makes it inappropriate for atmospheric probing from shuttle altitudes.

Atmospheric temperatures can also be recovered from the three wavelength method. Such a system transmits two wavelengths centered on the absorption lines of a gas while the third wavelength is used to calibrate the lidar. This method is similar to the DIAL technique reviewed below (Mason, 1975, Endemann and Byer, 1981). This method is feasible from the ground or an airplane but not at shuttle altitudes.

DeLuisi et al (1975) developed another three wavelength technique to measure temperature. In addition, this method uses two zenith angles to obtain separate density profiles. This technique is not fully developed, and results are very restrictive. Russel and Morley (1982) refined a one wavelength,

single-angle analysis technique to arrive at a density profile. This system is well suited for atmospheric sounding from the space shuttle.

The final laser technique to measure temperature is the DIAL technique. DIAL is an acronym for differential absorption lidar. Korb and Weng (1979) theorized that one wavelength centered on a resonant absorption line could be used to make highly accurate temperature measurements and is called the on-line wavelength. A second wavelength is tuned to an off-line frequency where there is no molecular absorption. The absorption coefficient at line center is very sensitive to temperature through the Boltzmann distribution. Oxygen is the ideal element to use with its wide absorption band near 770 nm. Furthermore, oxygen is uniformly mixed throughout the atmosphere (Smith and Platt, 1977; Kolshoven et al, 1980; Murray et al, 1980; Lebow et al, 1982). This latter technique yields very accurate temperature measurements (less than 1°C error) and is the technique employed in this thesis to recover thunderstorm cloud top temperatures.

DIAL Lidar vs Infrared and Microwave Radiometers

The Global Atmospheric Research Program (GARP, 1973) requires atmospheric temperatures to be $\pm 1^\circ\text{C}$ for 2 km vertical layers up to the tropopause so that numerical models forecasting the weather can be improved.

Infrared and microwave radiometers are currently capable of 1.5 - 3.0°C for a 5-10 km vertical layer (Kolshoven et al, 1980). The proposed new Advanced Meteorological Temperature Sounder (AMTS) will deliver $\pm 1^\circ\text{C}$ accuracy; however, the vertical resolution is limited to 4 km.

These passive radiometry techniques require extensive atmospheric modeling to derive the temperature profile from the measured data. A lidar in low earth orbit can deliver temperature errors less than 1°C and vertical resolution from 10 m to 2 km (Atlàs and Korb, 1981; Russel, 1982).

Scattering Theory

There are several scattering phenomena that attenuate a laser beam as it propagates through the atmosphere. These phenomena are Rayleigh scattering, Mie scattering, resonant absorption, and Raman scattering (Ely, 1972). This thesis will consider the first three scattering phenomena which are tabulated at different wavelengths and altitudes by McClatchey et al (1971).

Rayleigh Scattering

Rayleigh theory considers the scattering of incident radiation off particles whose diameters are very much smaller than the incident wavelength. The irradiance of light can be measured at a distance r from a scattering atom or molecule and expressed as

$$\epsilon = \epsilon_0 \frac{\sigma_r}{r^2} \quad (1)$$

where ϵ_0 = irradiance of incident radiation (watt m^{-2})

σ_r = Rayleigh cross section (m^2).

Kerker (1969) explains that Rayleigh theory represents the irradiance as

$$\epsilon = \epsilon_0 \frac{2\pi^2 (n-1)^2 (1 + \cos^2 \theta)}{r^2 N^2 \lambda^4} \quad (2)$$

where λ = wavelength of incident light

N = particle number density

n = apparent index of refraction of the gas

θ = scattering angle in the forward direction.

Thus, the Rayleigh cross section per solid angle is

$$\frac{d\sigma_r}{d\Omega} = \frac{2\pi^2 (n-1)^2 (1 + \cos^2 \theta)}{N^2 \lambda^4} \quad (3)$$

or

$$\sigma_r = \int_{4\pi} \frac{d\sigma_r}{d\Omega} 2\pi \sin \theta d\theta. \quad (4)$$

Mie Scattering

Mie theory considers the scattering of incident radiation off particles about the same size as the incident wavelength. Expressions for Mie theory are complicated, since the scattered irradiance is a function of scattering angle, ratio of particle diameter to wavelength, and the particle's complex index of refraction (Ely, 1972). The irradiance of Mie scattered light at a distance r from a scatterer can be written as

$$\epsilon = \epsilon_0 \lambda^2 \frac{(i_1^2 + i_2^2)}{8\pi^2 r^2} \quad (5)$$

where ϵ_0 = irradiance of incident radiation

λ = wavelength of incident radiation

i_1 and i_2 = irradiance functions perpendicular and parallel to the scattering plane.

Equation 1 can be rewritten for Mie theory as

$$\epsilon = \frac{\epsilon_0 \sigma_m}{r^2} \quad (6)$$

where σ_m = Mie theory cross section. Thus, σ_m can be written as

$$\sigma_m = \lambda^2 \frac{(i_1^2 + i_2^2)}{8\pi^2} \quad (7)$$

McClatchey et al (1971) points out that the Mie cross section σ_m consists of the sum of an absorption cross section σ_a and a scattering cross section σ_s such that

$$\sigma_m = \sigma_a + \sigma_s \quad (8)$$

McClatchey also computes extensive tables using Mie theory when computing aerosol extinction at most laser wavelengths using different model atmospheres and altitudes.

Resonant Absorption

Resonant absorption is generally referred to as the gaseous equivalent to Mie theory. In Mie theory, the imaginary component of the index of refraction accounts for σ_a ; however, in resonant theory absorption is

characterized by an absorption coefficient α_{gv} . Here the first subscript g refers to an absorbing gas and the second subscript refers to the particular frequency at which absorption is taking place.

Every molecule in the atmosphere has certain allowed transitions between its electronic, vibrational, and rotational energy states. Accordingly, the absorption coefficient can be very large at certain frequency bandwidths.

A laser beam propagating through the atmosphere will have photons absorbed by atmospheric molecules and removed from the beam if the photon's energy equals that of a molecular energy transition. In equation form

$$E = h\nu \quad (9)$$

where E = energy needed for molecular transition

$h\nu$ = energy of a photon from laser beam.

The many possible transitions of particular molecule are referred to as lines or resonances. These lines are not infinitely sharp in a frequency spectra, but are collision broadened for altitudes up to the tropopause.

There is an extensive development of resonant absorption α_{gv} in Chapter IV of this thesis.

III. Lidar Equation

A lidar mounted in the cargo bay of the space shuttle can transmit power earthward and incident on a volume located at the top of a thunderstorm. The power arriving at the cloud top can be expressed by Bouger's law as

$$P_T(z) = P_O \exp \left[- \int_{Z_T}^{Z_L} \alpha(z) dz \right] \quad (10)$$

where Z_L = height of shuttle above surface (km)

Z_T = height of thunderstorm top (km)

P_O = transmitted power (watts)

P_T = power at thunderstorm top (watts)

$\alpha(z)$ = total atmospheric extinction coefficient (km^{-1})

$\int \alpha(z) dz$ = atmospheric attenuation.

Some of this laser power reaching the cloud top will be backscattered to space. This backscattered power is the product of the backscatter coefficient for the volume being sensed and the depth of this volume. The total power per solid angle backscattered to space, which is the intensity I_B , can be expressed as

$$I_B = P_T(z) B(z) d \quad (11)$$

and

$$d = \frac{ct}{2} P \quad (12)$$

where I_B = intensity backscattered to space (watts sr^{-1})

$P_T(z)$ = power at thunderstorm top (watts)

$B(z)$ = volume backscatter coefficient ($\text{km}^{-1}\text{sr}^{-1}$)

d = vertical resolution (depth of volume) (km)

C = speed of light (km/sec)

t_p = pulse width (sec).

The amount of laser backscattered power that actually enters the lidar's receiving telescope can be expressed as

$$P_L(z) = \frac{A_R}{R^2} I_B \exp - \int_{Z_T}^{Z_L} \alpha(z) dz \quad (13)$$

where $P_L(z)$ = power received by lidar (watts)

A_R = area of receiving telescope (km)

R = distance from cloud top to lidar (km).

Note that $\frac{A_R}{R^2}$ is the solid angle subtended by the receiver at range R , since lidar systems are usually configured with the divergence angle of the transmitted beam less than the receiver's field of view.

All of these equations can be combined to yield the lidar equation for a shuttle-borne lidar

$$P_L(z) = P_0 e A_R \frac{C t_p B(z)}{2 R^2} \exp \left[-2 \int_{Z_T}^{Z_L} \alpha(z) dz \right] \quad (14)$$

where e is the lidar's system efficiency, the product of the optical system efficiency and the receiving system efficiency. The volume backscatter coefficient $B(z)$ is defined as the fractional amount of incident power scattered per steradian in the backward direction per unit path length.

The volume backscatter coefficient is the sum of scattering contributions from all atmospheric constituents (gases, aerosols, and cloud ice crystals) and includes both inelastic and elastic processes. It can be expressed as

$$B(z) = \sum_{i=1}^n B_i(z) = \sum_{i=1}^n N_i \frac{d\sigma_i(z)}{d\Omega} \quad (15)$$

where i = summation over all scattering processes

N_i = number density involved in i^{th} process (km^{-3})

$d\sigma(z)/d\Omega$ = backscattering cross section of the i^{th} process ($\text{km}^2\text{sr}^{-1}$)

$B(z)_i$ = backscatter coefficient ($\text{km}^{-1}\text{sr}^{-1}$).

So in equation 14, $B(z)$ can be replaced with $B_g + B_A + B_C$ where the subscripts apply to gases, aerosols, and cloud particles respectively.

The total extinction $\alpha(z)$ is the sum of the extinction coefficients of all processes in the atmosphere hence

$$\alpha(z) = \alpha_g(z) + \alpha_A(z) + \alpha_C(z) \quad (16)$$

where α_g = extinction due to atmospheric gases (resonant absorption) (km^{-1})

α_A = extinction due to aerosols (km^{-1})

α_C = extinction due to cloud particles (km^{-1}).

Furthermore, each of these coefficients is composed of a contribution from scattering and absorption. The equation for total extinction can be rewritten as

$$\alpha = S_g + K_g + S_A + K_A + S_C + K_C \quad (17)$$

where S_i = scattering due to the i^{th} constituent (km^{-1})

K_i = absorption due to the i^{th} constituent (km^{-1}).

and i is either for gases, aerosols, or cloud particles (g, A, c).

Combining the above results with equation 14, the lidar equation for an instrument mounted on the shuttle can be expressed as

$$P_L(z) = P_0 e^{-A_r} \frac{C t_p}{2} \left[\frac{B_g(z) + B_A(z) + B_C(z)}{R^2} \right] \exp \left[-2 \int_{Z_T}^{Z_L} [\alpha_g(z) + \alpha_A(z) + \alpha_C(z)] dz \right]. \quad (18)$$

Multiple Scattering

The lidar equation expressed by equation 18 considers the theory of single scattering as the beam scatters off gases, aerosols, and cloud particles. Actually equation 18 is only an approximation since multiple scattering prevails in reality. Multiple scattering greatly increases the backscattered signal as the laser beam enters a dense scattering situation such as a cloud top.

Figure 6 illustrates the multiple scattering phenomena. From shuttle altitude and down to a cloud top, weak single scattering prevails as the laser illuminated volume is entirely restricted to the volume enclosed within the divergence angle θ of the laser beam. In other words, single scattering occurs when θ is less than the receiver's field of view ϕ . Multiple scattering occurs as the beam enters the cloud top and spreads as shown in Figure 6 by the shaded region. Photons in this shaded region require three or more scatterings before being directed back to the receiver since this region is greater than ϕ (Hobbs and Deepak, 1981).

Multiple scattering is neglected in this thesis and equation 18 will not be modified.

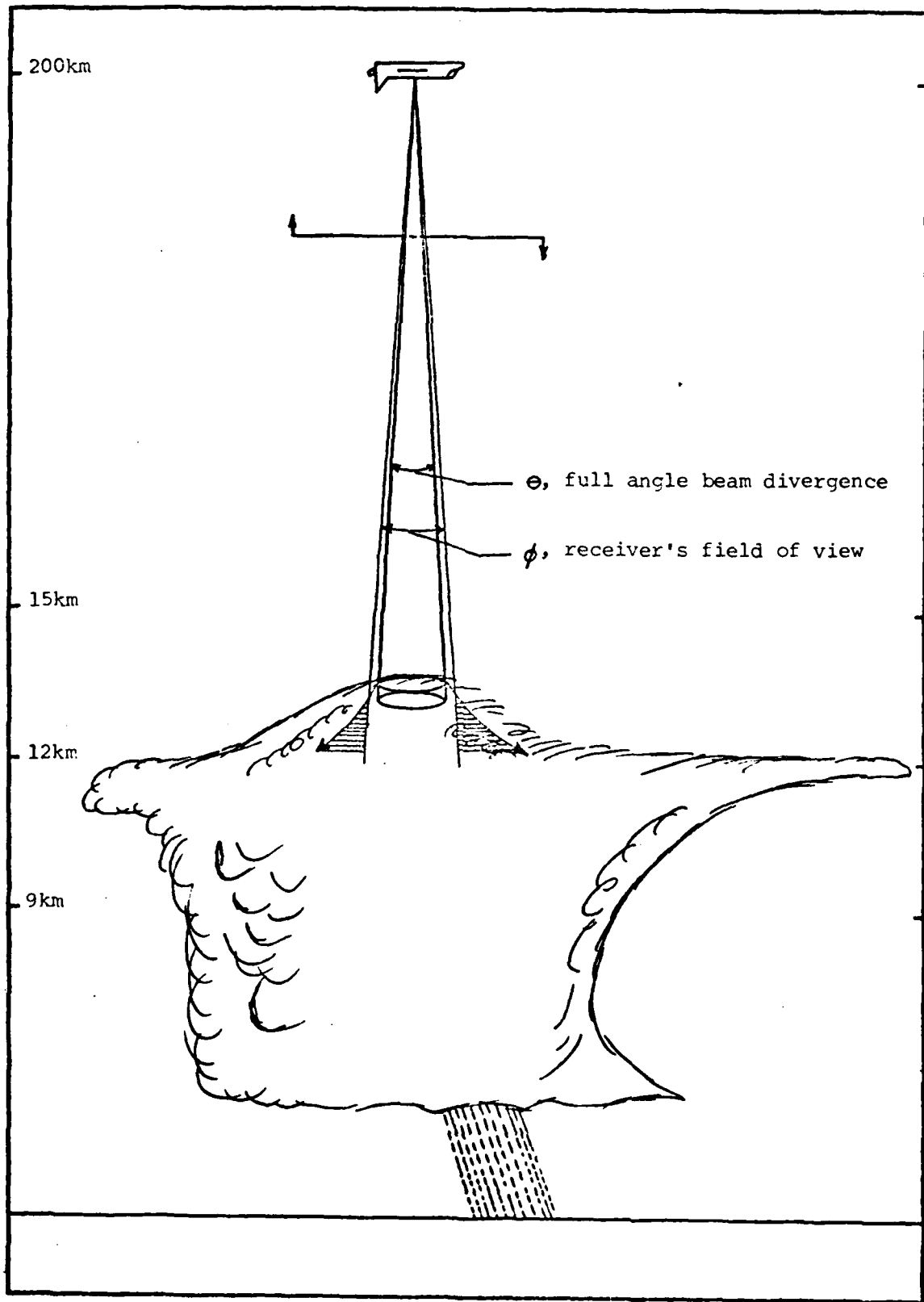


Figure 5. Multiple scattering of a laser beam on an irregular area (after Hobbs and Deepak, 1981 with changes).

IV. Dial Theory

The laser technique used to measure temperature in this thesis is the differential absorption lidar (DIAL) technique (see literature review). A lidar on-board the space shuttle using the DIAL technique will transmit two wavelengths along the same path down to the top of a thunderstorm. The first wavelength, an on-line wavelength, is selected to match the center of a resonant absorption oxygen line in the oxygen "A" band near 770 nm. The second wavelength, an off-line wavelength, is used as a reference and is chosen at a nearly spectral position where there is almost no absorption from the oxygen "A" band. This DIAL technique is designed so that scattering and absorption properties of the atmosphere are identical except for the resonant absorption at the on-line wavelength.

Remote Sensing of Temperature

Kalshoven et al (1980) outlined a procedure to determine atmospheric temperature measurements by using the DIAL technique. This technique will be modified by the author so that thunderstorm cloud top temperatures can be recovered by operating a DIAL lidar from the space shuttle.

The differential absorption coefficient (extinction due to gases) α_g can be found by the ratio of power on-line to power off-line returned to the lidar's receiving telescope. This can be expressed in equation form developed by Kalshoven et al (1980) and modified by the author as

$$\int_0^z \alpha_{g_0} dz = - \frac{1}{6.9} \left[\frac{1}{2} \ln \left(\frac{P^O}{P^I} \right) \right] \quad (19)$$

where z = distance between lidar and cloud top (km)

6.9 = scale height for an isothermal atmosphere (km)

α_{g0} = differential absorption coefficient at line center or extinction due to gases (km^{-1})

P^0 = received on-line power (watts)

P^r = received reference power (watts).

The differential absorption coefficient hereafter called the absorption coefficient or extinction coefficient due to gases can be found analytically with an expression derived by Elasser (1960) as

$$\alpha_g(\bar{\nu}) = \frac{S\alpha_s P_s \sqrt{T_s}}{\pi} \left[\frac{P \sqrt{T}}{(\bar{\nu} - \bar{\nu}_0)^2 T P_s^2 + \alpha_s P T_s^2} \right] \quad (20)$$

where $\alpha_g(\bar{\nu})$ = absorption coefficient at wave number $\bar{\nu}$

S = line strength

α_s = collisional broadening half-width at half maximum at standard pressure and temperature or 273.16°K, 1013.25 mb

P_s = pressure at STP

P = pressure at specified level

T_s = temperature at STP

T = temperature at specified level

$\bar{\nu} - \bar{\nu}_0$ = frequency bandwidth of absorption line

$\bar{\nu}_0$ = wave number of center of absorption line

STP refers to conditions at standard temperature and pressure.

A more conventional form of this equation for use in the atmosphere where pressure and temperature change with height is

$$\alpha_{g_o} = N(P,T) S(T) F(\bar{\nu} - \bar{\nu}_o) \quad (21)$$

where $N(P,T)$ = atmospheric number density for oxygen (molec m^{-3})

$S(T)$ = line strength (molec $^{-1}$ m^2 cm^{-1})

$F(\bar{\nu} - \bar{\nu}_o)$ = line shape function (cm).

The number density can be found from

$$N(P,T) = q W n_s \frac{P}{P_s} \frac{T_s}{T} \quad (22)$$

where P_s = pressure at STP (1013.25 mb)

P = pressure at specified height (mb)

T_s = temperature at STP (273.16°K)

T = temperature at specified height (°K)

q = dry air mixing ratio for O_2 (0.209)

n_s = dry air number density at STP (2.69×10^{25} molec/ m^3)

W = correction factor for atmospheric water vapor.

Kalshoven et al (1980) was able to derive an empirical expression for W given as

$$W = 1 - 2.23 \times 10^9 \frac{RH}{P} \exp \left(- \frac{5385}{T} \right) \quad (23)$$

where RH = relative humidity (.80 for 80%).

W was found to be nearly one and contributes < 2% to the computation for number density.

Line strength S for oxygen can be found from Penner (1959) as

$$S = \int_0^{\infty} \alpha_g(\bar{\nu}) d\bar{\nu} \quad (24)$$

$$= \frac{8\pi^3 \bar{\nu}_0}{3 h c M Q(T)} \exp(-h c E''/k T) \left[\frac{1 - \exp(-h c \bar{\nu}_0/k T)}{h c \bar{\nu}_0} \right] \\ * f(J'') R_{eV}^2 \quad (25)$$

where $\bar{\nu}_0$ = wave number of resonant line center

M = mass of the molecule

Q(T) = the partition function

T = temperature

E'' = energy in wave numbers of the lower state

J'' = total angular momentum quantum number

f(J'') = statistical weight

R_{eV} = combined electronic-vibrational transition moment

c = speed of light

h = Planck's constant

k = Boltzmann's constant

* = multiplication operator.

Burch and Gryvnak (1969) were able to simplify this expression and derive an expression for line strength of the oxygen "A" band at a particular line as

$$S_{J''} = \frac{S_V F_{J''}}{Q(T)} \exp(-h c E''/k T). \quad (26)$$

The rotational partition function Q(T) is given by

$$Q(T) = \sum_{J''} F_{J''} \exp(-h c E''/k T) \quad (27)$$

where F_J is a weighting function.

Finally, McClatchey et al (1971) expressed line strength in a very operational format as

$$S(T) = S(T_S) \frac{T_S}{T} \exp \left[1.439 E'' \left(\frac{1}{T_S} - \frac{1}{T} \right) \right] \quad (28)$$

where $S(T_S) = O_2$ line strength at STP ($\text{molec}^{-1} \text{ m}^2 \text{ cm}^{-1}$)

$E'' =$ energy in lower level of the oxygen molecule (cm^{-1}).

Burch and Grynak (1969) have compiled extensive tables of $S(T_S)$, E'' , J'' , etc. for lines throughout the oxygen "A" band.

The line shape function $F(\bar{\nu} - \bar{\nu}_0)$ is a combination of Lorentz and Doppler broadening and is typically expressed by the Voigt integral as

$$F(\bar{\nu} - \bar{\nu}_0) = \frac{F'}{\sqrt{\pi}} \int_0^{\infty} \frac{\cos(x t)}{\exp(a t + \frac{t^2}{4})} dt \quad (29)$$

where $x = \frac{\bar{\nu} - \bar{\nu}_0}{\alpha_D} (\ln 2)^{1/2}$ (30)

$$a = \frac{\alpha_L}{\alpha_D} (\ln 2)^{1/2} \quad (31)$$

$$F' = \left(\frac{\ln 2}{2} \right)^{1/2} \frac{1}{\alpha_D} \quad (32)$$

and $\alpha_D =$ Doppler broadened halfwidth (cm^{-1})

$\alpha_L =$ Lorentz broadened halfwidth (cm^{-1})

Expressions for α_D and α_L are

$$\alpha_D = \bar{\nu}_0 \left(\frac{2 k T \ln 2}{mc^2} \right)^{1/2} \quad (33)$$

$$\alpha_L = \alpha_L^S \left(\frac{P}{P_S}\right) \left(\frac{T_S}{T}\right)^{1/2} \quad (34)$$

where m = molecular mass for O_2 (5.31×10^{-26} kg)

α_L^S = collision halfwidth for O_2 at STP.

According to Penner (1959) and Kalshoven et al (1980), the line shape function $F(\bar{\nu}-\bar{\nu}_0)$ reduces to

$$F(0) = F' \exp \left[\frac{2}{\sqrt{\pi}} a \int_0^{\infty} \exp(-z^2) dz \right] \quad (35)$$

where $F(0)$ = line shape at line center

z = height

a = correction factor.

The value of the correction factor "a" varies with the molecule of interest. For oxygen

$$a = 2.14 \times 10^5 \frac{\alpha_L^S}{\nu_0} \frac{P}{T} \quad (36)$$

where α_L^S is expressed in cm^{-1}

P is expressed in mb

T is expressed in $^{\circ}K$

ν_0 is expressed in cm^{-1} .

Solving the Voigt integral can be avoided by using a good analytical approximation such as

$$F(0) = \frac{1}{3\alpha_L} \left[1 - \frac{\exp(1)}{10a} \right]. \quad (37)$$

At heights of typical thunderstorms this equation is 93% accurate (Penner, 1959).

Recalling Equation 21, and combining all of the above equations, the absorption coefficient is calculated by

$$\begin{aligned} \alpha_{g_0} &= N(P,T) S(T) F(\bar{v} - \bar{v}_0) \\ &= q n_s W T^{-3/2} \left(\frac{P}{P_s}\right) \left(\frac{T_s}{T}\right) S(T_s) \left(\frac{T_s}{T}\right) \exp \left[1.439 E'' \left(\frac{1}{T_s} - \frac{1}{T}\right) \right] \frac{1}{3\alpha_L} \\ &\quad \left(1 - \frac{\exp 1}{10a}\right) \end{aligned} \quad (38)$$

where $\frac{1}{\alpha_L} = \frac{1}{\alpha} \left(\frac{P}{P_s}\right) \left(\frac{T_s}{T}\right)^{.5}$. (39)

Therefore,

$$\begin{aligned} \alpha_{g_0} &= q n_s W T^{-3/2} S(T_s) \exp \left[1.439 E'' \left(\frac{1}{T_s} - \frac{1}{T}\right) \right] \frac{1}{\alpha_L} \left(1 - \frac{\exp 1}{10a}\right) \\ A_0 T^{-3/2} W \exp \left(-1.439 \frac{E''}{T}\right) \left[1 - \frac{\exp 1}{10a}\right] \end{aligned} \quad (40)$$

where $A_0 = \frac{qn_s}{3} T_s^{3/2} \frac{S(T_s)}{\alpha_L} \exp \left(1.439 \frac{E''}{T_s}\right) \cdot \circ_K^{3/2} m^{-1}$ (41)

This equation can be solved for temperature and arrive at Kalshoven's et al (1980) iterative expression for temperature. Equation 40 can be re-written as an iterative expression

$$\alpha_{g_0} = A_0 T_{i+1}^{-3/2} W \exp \left(-1.439 E''/T_{i+1}\right) \left(1 - \frac{\exp(1)}{10a}\right) . \quad (42)$$

Now solving for T_{i+1} so that an equation yielding a laser derived temperature can be found:

$$\frac{\alpha_{g_0}}{A_0 T_i^{-3/2} W \left(1 - \frac{\exp(1)}{10a}\right)} = \exp(-1.439 E''/T_{i+1})$$

$$\ln \left[\frac{\alpha_{g_0}}{A_0 T_i^{-3/2} W \left(1 - \frac{\exp(1)}{10a}\right)} \right] = - \frac{1.439 E''}{T_{i+1}}$$

$$T_{i+1} = \frac{-1.439 E''}{\ln \left[\frac{\alpha_{g_0}}{A_0 T_i^{-3/2} W \left(1 - \frac{\exp(1)}{10a}\right)} \right]}$$

$$T_{i+1} = \frac{+1.439 E''}{\ln \left[A_0 T_i^{-3/2} W \left(1 - \frac{\exp(1)}{10a}\right) \frac{1}{\alpha_{g_0}} \right]} \quad (43)$$

Where T_i is a seed temperature value (a standard atmosphere value) and is not critical to the results of T_{i+1} . Kalshoven et al (1981) tested this DIAL technique at sea level using the .7684 μm O_2 line and found a temperature accuracy of 0.6°K .

To investigate the rate of change of absorption with respect to temperature, the first derivative of equation 40 can be taken with respect to temperature. Equation 40 is rewritten for convenience

$$\alpha_{g_0} = A_0 T^{3/2} W \exp(-1.439 E''/T) \left[1 - \frac{\exp(1)}{10a} \right].$$

It is appropriate to omit the weak pressure components to α_{g_0} such that

$$\alpha_{g_0} = T^{-3/2} \exp\left(\frac{-1.439 E''}{T}\right). \quad (44)$$

Now taking the derivative

$$\begin{aligned}
 \frac{d\alpha_{gO}}{dT} &= -\frac{3}{2} T^{-5/2} \exp\left(\frac{-1.439 E''}{T}\right) + T^{-3/2} \left(\frac{1.439 E''}{T^2}\right) \exp\left(\frac{-1.439 E''}{T}\right) \\
 &= \exp\left(\frac{-1.439 E''}{T}\right) \left[-\frac{3}{2} T^{-5/2} + 1.439 E'' T^{-7/2} \right] \\
 &= T^{-5/2} \exp\left(\frac{-1.439 E''}{T}\right) \left[-\frac{3}{2} + \frac{1.439 E''}{T} \right] \quad (45)
 \end{aligned}$$

Substituting α_{gO} in Equation 44 into the term on the left

$$\frac{d\alpha_{gO}}{dT} = \frac{\alpha_{gO}}{T} \left(-\frac{3}{2} + \frac{1.439 E''}{T} \right) \quad (46)$$

Terms can now be rearranged to yield

$$\frac{d\alpha_{gO}}{\alpha_{gO}} = \frac{dT}{T} \left(\frac{1.439 E''}{T} - \frac{3}{2} \right) \quad (47)$$

This equation says that the shuttle lidar sensitivity to temperature changes improves by choosing higher energy lines within the oxygen "A" band. However, if E'' is increased by choosing another line, the line strength becomes far too weak, and the absorption coefficient becomes too small. A trade-off must be made.

The on-line wavelength chosen in this thesis is .7696 μm . This choice lies within that portion of the oxygen "A" band offering optimum temperature sensitivity and absorption (Kalshoven et al, 1980).

The off-line or reference wavelength is chosen to be .7614 μm since oxygen absorption at this wavelength is negligible compared with that at the on-line wavelength (Smith and Platt, 1977).

Relative Humidity

Relative humidity RH or atmospheric water vapor will slightly affect the calculation for the number density of O_2 . RH is defined as the ratio of the actual mixing ratio of a parcel of air at a specific pressure and temperature to the mixing ratio that saturated air would have at the same pressure and temperature or

$$RH = \frac{w}{w_s} \quad (100) \quad (48)$$

where w , w_s are the mixing and saturated mixing ratio respectively. A mixing ratio is merely the mass of water vapor contained by a mass of dry air (Hess, 1956).

The calculation of the O_2 number density $N(P,T)$ (see Equation 22) requires a correction for atmospheric water vapor expressed in Equation 23. The values of RH required in this equation will vary according to height (AWSM 105-124, 1969) as

Surface - 3 km	50%
4 - 6 km	30%
7 - 10 km	10%
11 - 20 km	5%

Differential Absorption Coefficient Calculation

The differential absorption coefficient for molecular oxygen at $.7696 \mu m$ can now be calculated using the previously developed DIAL theory in a sequential manner consisting of seven steps.

This example will calculate the absorption coefficient α_{g_0} at 10 km altitude and will demonstrate the appropriate units to use.

The following spectral information is provided:

$$\lambda = .7696 \mu\text{m}$$

$$\bar{\nu}_0 = 12,988.734 \text{ cm}^{-1} *$$

$$E'' = 1421.436 \text{ cm}^{-1} *$$

$$S(T_S) = 3.377 \times 10^{-30} \text{ molec}^{-1} \text{ m}^2 \text{ cm}^{-1} *$$

$$\alpha_L^S = .038 \text{ cm}^{-1} *$$

$$P_S = 1013.25 \text{ mb}$$

$$P = 281 \text{ mb (McClatchey's et al (1971) mid-latitude summer atmosphere)}$$

$$T_S = 273.16^\circ\text{K}$$

$$T = 235^\circ\text{K (McClatchey's et al (1971) mid-latitude summer atmosphere)}$$

where * indicates values tabulated by Burch and Gryvnak (1969).

The resonant absorption coefficient α_{g_0} or extinction due to oxygen "A" band absorption α_g (km^{-1}) (subscription g refers to O_2 gas) are names for the same quantities. Recall that α_{g_0} can be calculated from Equation 21 as

$$\alpha_{g_0} = N(P,T) s(T) F(\bar{\nu} - \bar{\nu}_0)$$

where the following seven steps are required to solve the expression.

A. A correction for atmospheric water vapor W must be found from Equation 23.

$$W = 1 - \left[2.23 \times 10^9 \frac{.10}{281 \text{ mb}} \exp\left(-\frac{5385}{285^\circ\text{K}}\right) \right] = .9999$$

B. The number density of O_2 at 10 km can now be calculated from Equation 22.

$$N(P,T) = (.209) (.9999) (2.69 \times 10^{25} \text{ molec m}^{-3}) \left(\frac{273.16^\circ\text{K}}{235^\circ\text{K}} \right) \left(\frac{281 \text{ mb}}{1013.25 \text{ mb}} \right)$$

$$= 1.8126 \times 10^{24} \text{ molec m}^{-3}$$

C. Line strength $S(T)$ using Equation 28

$$S(T) = (3.377 \times 10^{-30} \text{ molec}^{-1} \text{ m}^2 \text{ cm}^{-1}) \left(\frac{273.16^\circ\text{K}}{235^\circ\text{K}} \right) \exp \left[1.439 (1421.436) \left(\frac{1}{273.16^\circ\text{K}} - \frac{1}{235^\circ\text{K}} \right) \right]$$

$$= 1.5082 \times 10^{-30} \text{ molec}^{-1} \text{ m}^2 \text{ cm}^{-1}$$

D. The Lorentz broadened halfwidth α_L for the resonant line using Equation 34.

$$\alpha_L = (0.038 \text{ cm}^{-1}) \left(\frac{281 \text{ mb}}{1013.25 \text{ mb}} \right) \left(\frac{273.16^\circ\text{K}}{235^\circ\text{K}} \right)^{1/2} = 0.0114 \text{ cm}^{-1}$$

E. The weak pressure correction factor "a" using Equation 36.

$$a = 2.14 \times 10^5 \left(\frac{0.038 \text{ cm}^{-1}}{12,988.734 \text{ cm}^{-1}} \right) \left(\frac{281 \text{ mb}}{235^\circ\text{K}} \right) = 0.7486$$

F. Line shape at line center $F(0)$ using Equation 37.

$$F(\bar{\nu} - \bar{\nu}_0) - F(0) = (3) \left(\frac{1}{0.0114 \text{ cm}^{-1}} \right) \left[1 - \frac{\exp(1)}{(10)(0.7486)} \right] = 17.4012 \text{ cm}$$

G. The absorption coefficient α_{g0} can now be calculated using Equation 21.

$$\alpha_{g0} = (1.8126 \times 10^{24} \text{ molec m}^{-3}) (1.5082 \times 10^{-30} \text{ molec}^{-1} \text{ m}^2 \text{ cm}^{-1})$$

$$(17.4012 \text{ cm}) (10^3 \text{ m km}^{-1}) = .0513 \text{ km}^{-1}$$

This sequential scheme of seven steps can readily be programmed using a suitable computer language. The absorption coefficient was computed in this manner from the surface to 17 km using McClatchey's et al (1971)

mid-latitude summer atmosphere. These values are displayed in Table I which compare to Kalshoven's et al (1980) work when extended to 17 km and using an on-line wavelength of .7684 μm . Figure 7 displays α_{g_0} as a function of height.

Predicting α_g with Polynomial Regression

It may be of interest to calculate the O_2 extinction coefficient using regression analysis to statistically model the relationship between the independent variable (height) and a dependent variable (α_{g_0}).

The exact form of the true functional relationship between the O_2 extinction coefficient and height is assumed to be unknown so it is appropriate to use a polynomial model as the approximating function. Regression analysis of this nature assumes that height can be measured with negligible error (Hines and Montgomery, 1980).

To determine the relationship between the two variables a cubic equation will be fitted using the least squares method. This cubic equation can be written as

$$\alpha_{g_0} = a + bz + cz^2 + dz^3 \quad (49)$$

where z = height (km)

α_{g_0} = O_2 absorption coefficient or extinction due to gas at line center (km^{-1}).

The regression coefficients (a,b,c,d) can be found by solving the following system of equations. These equations can be solved numerically using Gaussian elimination with partial pivoting (Ketter and Prawel, 1969):

Table I

Oxygen Absorption Coefficient α_{gO} (km^{-1}) from Surface to 17 km

<u>altitude (km)</u>	<u>α_{gO} (km^{-1})</u>
0	.2848
1	.2604
2	.2326
3	.2023
4	.1746
5	.1488
6	.1254
7	.1042
8	.0832
9	.0669
10	.0513
11	.0393
12	.0284
13	.0202
14	.0164
15	.0118
16	.0066
17	.0005

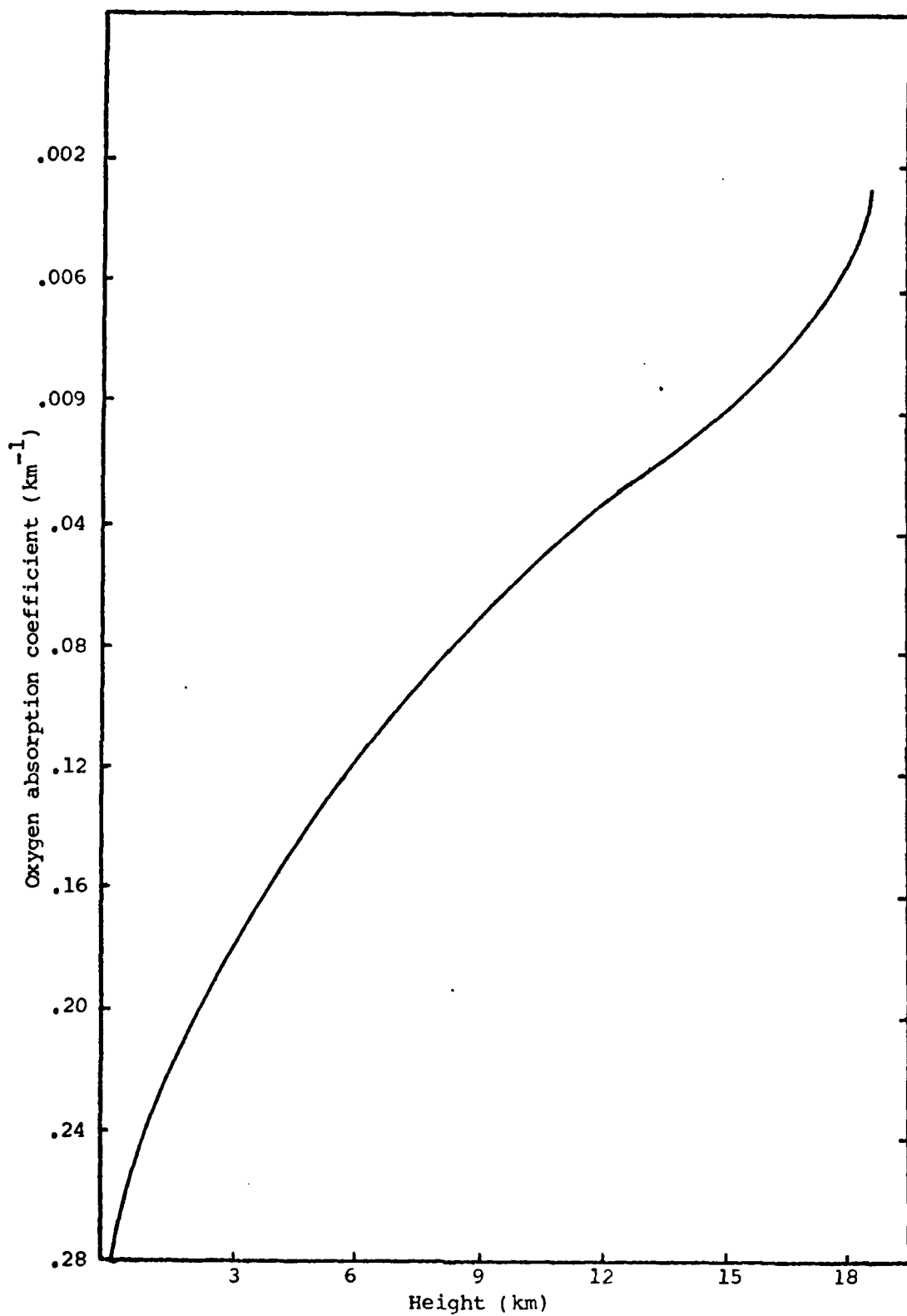


Figure 7. Oxygen absorption coefficient vs height

$$\begin{bmatrix} n & \sum Z_i & \sum Z_i^2 & \sum Z_i^3 \\ \sum Z_i & \sum Z_i^2 & \sum Z_i^3 & \sum Z_i^4 \\ \sum Z_i^2 & \sum Z_i^3 & \sum Z_i^4 & \sum Z_i^5 \\ \sum Z_i^3 & \sum Z_i^4 & \sum Z_i^5 & \sum Z_i^6 \end{bmatrix} \begin{bmatrix} a \\ b \\ c \\ d \end{bmatrix} = \begin{bmatrix} \sum K_i \\ \sum Z_i K_i \\ \sum Z_i^2 K_i \\ \sum Z_i^3 K_i \end{bmatrix} \quad (50)$$

where n = the number of data points and $K = \alpha_{g0}$

The coefficient of determination R^2 can be computed by

$$R^2 = \frac{a \sum K_i + b \sum Z_i K_i + c \sum Z_i^2 K_i - 1/n (\sum K_i)^2}{\sum (K_i^2) - 1/n (\sum K_i)^2} \quad (51)$$

Using the data points from Table I, the cubic regression model yields

$$R^2 = 1.00$$

$$a = 0.30$$

$$b = -0.03$$

$$c = 9.02 \times 10^{-4}$$

$$d = 5.90 \times 10^{-6}$$

The model can now be expressed as

$$\alpha_{g0} = 0.30 - 0.03z + 9.02 \times 10^{-4} z^2 + 5.90 \times 10^{-6} z^3 \quad (52)$$

A correlation coefficient of 1.00 ($R^2 = \sqrt{1.0} = 1$) implies that approximately 100% of the variability in the O_2 resonant absorption coefficient is explained by the cubic relationship with height.

This regression model is reasonably successful in computing α_g only near the .7696 μm line. Accuracy will decrease dramatically if lines on either side of .7696 are chosen.

V. Atmospheric Consideraions

Index of Refraction

Edlen (1953) computed the index of refraction at 1013 mb and 288°k for any particular wavelength as

$$(n-1)10^{-8} = 6432.8 + \frac{2949810}{146-(\lambda^{-2})} + \frac{25540}{41-(\lambda^{-2})} \quad (53)$$

where n = index of refraction

λ = wavelength (μm).

Likewise, Barrell and Sears (1939) found the index of refraction of moist normal air in the range 10 to 30°C at 960 to 1066 mb for any particular wavelength as

$$\begin{aligned} (n-1)10^6 = & 0.378125 + \left[\frac{0.0021414}{\lambda^4} + \frac{0.00001793}{\lambda^6} \right] \\ & * \left[P \frac{1 + (1.049 - 0.0157 T)P 10^{-6}}{1 + 0.003661 T} \right] \\ & - \left[0.0624 - \frac{0.000680}{\lambda^2} \right] \frac{f}{1 + 0.003661 T} \end{aligned} \quad (54)$$

where T = air temperature (°c)

P = barometric pressure (mm Hg)

f = vapor pressure (mm Hg).

Elterman (1968) computed the index of refraction n at various wavelengths using Equation 53. He safely neglects the effects of water vapor by working in and around the visible spectrum. Elterman's (1968) value for n at .8 μm will be used in this thesis for calculations at .7696 and .7614 μm . This value is

$$n(.8 \mu\text{m}) = 1.00027503.$$

Rayleigh Cross Section

Rayleigh theory (see literature review) applies when laser radiation scatters off atmospheric gases. The probability of scattering off an individual gaseous constituent is the cross section. The Rayleigh cross section σ_r can be expressed by

$$\sigma_r(\lambda) = \frac{8\pi^3(n-1)^2}{3\lambda^4 N_S^2} \frac{6 + 3\delta}{6 - 7\delta} \quad (55)$$

where σ_r = Rayleigh scattering cross section (cm^2)

N_S = molecular number density at STP (cm^{-3})

λ = wavelength (cm)

δ = depolarization factor (.035 from Gucker and Basu, 1953).

Elterman (1968) reports that the expression $6 + 3\delta/6 - 7\delta$ accounts for the depolarization caused by the anisotropy of atmospheric molecules. He further calculates σ_r at .8 μm which will be used at the on and off line wavelengths. This value is

$$\sigma_r (.7696 \mu\text{m}, .7614 \mu\text{m}) = 9.990 \times 10^{-28} \text{ cm}^2.$$

Atmospheric Extinction

The total extinction α expressed in Equation 16 consists of three components. The atmospheric extinction component α_g is due to scattering and absorption by gas molecules and is discussed in this section. This extinction due to atmospheric gases α_g can be calculated at different heights according to

$$\alpha_g = \sigma_r(\lambda) N(z) (10^5 \text{ cm km}^{-1}) \quad (56)$$

where α_g = extinction due to gas (km^{-1})

N = molecular number density which is a function of height.

The reader should note that the above computation for α_g is correct at the nonabsorbing wavelength (.7614 μm). At the absorbing wavelength (.7696 μm), the O_2 absorption coefficient $\alpha_{g\text{O}}(z)$ (see the remote sensing of temperature section) must be added to α_g to obtain the extinction at an absorbing wavelength. Values for the Rayleigh molecular number density N can be obtained from the U.S. standard atmosphere or McClatchey et al (1971).

Table II lists the molecular number density, atmospheric extinction coefficient at the off-line wavelength (.7614 μm), and the extinction coefficient at the on-line wavelength (.7696 μm) where O_2 absorption values from Table I have been added to the computation for α_g . The heights ranging from 0-17 km were arbitrarily chosen; however, this thesis is only concerned with values from 10 - 17 km which are average top heights of severe and non-severe thunderstorms. It is possible for thunderstorms to exceed 17 km. If $\alpha_{g\text{O}}$ is needed for such rare storms than a new O_2 line should be chosen so that $\alpha_{g\text{O}}$ is larger and therefore measureable at extreme altitudes. An ideal resonant absorption line in this case would be the .7677 μm (13,021.283 cm^{-1}) oxygen line. Once again a trade-off is necessary. If .7677 μm is used to measure super high thunderstorms, then system signal-to-noise ratio (discussed in Chapter VII) becomes useless for smaller storms because of extreme absorption at lower altitudes from O_2 .

Table II

Atmospheric Number Density N , Off-line ($.7614 \mu\text{m}$), and On-line ($.7696 \mu\text{m}$)
Extinction due to Gas α_g all as a Function of Height z

Height z (km)	N (cm^{-3})	α_g ($.7614 \mu\text{m}$) km^{-1}	α_g ($.7696 \mu\text{m}$) km^{-1}
0	2.547×10^{19}	2.544×10^{-3}	.2873
1	2.311	2.309	.2627
2	2.093	2.091	.2347
3	1.891	1.889	.2042
4	1.704	1.702	.1763
5	1.531	1.530	.1503
6	1.373	1.371	.1268
7	1.227	1.225	.1054
8	1.093	1.092	.0843
9	9.712×10^{18}	9.702×10^{-4}	.0679
10	8.598	8.589	.0522
11	7.585	7.577	.0401
12	6.486	6.478	.0290
13	5.543	5.538	.0208
14	4.738	4.733	.0169
15	4.049	4.045	.0122
16	3.461	3.458	.0069
17	2.959	2.956	.0007

Rayleigh Backscatter Coefficient

The volume backscatter coefficient B_g ($\text{km}^{-1} \text{sr}^{-1}$) for atmospheric gases in the lower 100 km of atmosphere can be found according to Hinkley (1976) from

$$B_g = B_r = N 5.45 \left[\frac{\lambda (\mu\text{m})}{.55} \right]^{4.09} \times 10^{-23} \quad (57)$$

where B_r = Rayleigh backscatter coefficient ($\text{km}^{-1}\text{sr}^{-1}$)

N = atmospheric number density (cm^{-3})

λ = optical wavelength (μm) .

Values for N can be taken from Table II or calculated by using a suitable model atmosphere such as McClatchey's et al (1971) mid-latitude summer atmosphere reproduced in part in Table III. N can be calculated by

$$N = \frac{\rho N_0}{\bar{A}} \quad (58)$$

where ρ = atmospheric density which is a function of pressure and temperature (g cm^{-3})

N_0 = Avogadro's number (6.023×10^{23})

\bar{A} = gram atomic weight of dry air (28.699 g).

The exponent on Equation 57 is 4.09 instead of 4.0 as prescribed by Rayleigh's theory (see Equation 2) to account for the slight wavelength dependence of the refractive index of air.

Equation 57 is appropriate in all cases except at those wavelengths where molecules have absorption coefficients much greater than the oxygen "A" band (Hinkley, 1976).

Table III

Mid-Latitude Summer Atmosphere
(after McClatchey et al, 1971)

<u>Z(km)</u>	<u>Pressure (mb)</u>	<u>Temp (°K)</u>	<u>Density (cm m⁻³)</u>
0	1.013x10 ³	294.0	1.191x10 ³
1	9.020x10 ²	290.0	1.080x10 ³
2	8.020x10 ²	285.0	9.757x10 ²
3	7.100x10 ²	279.0	8.846x10 ²
4	6.280x10 ²	273.0	7.998x10 ²
5	5.540x10 ²	267.0	7.211x10 ²
6	4.870x10 ²	261.0	6.487x10 ²
7	4.260x10 ²	255.0	5.830x10 ²
8	3.720x10 ²	248.0	5.225x10 ²
9	3.240x10 ²	242.0	4.669x10 ²
10	2.810x10 ²	235.0	4.159x10 ²
11	2.430x10 ²	229.0	3.693x10 ²
12	2.090x10 ²	222.0	3.269x10 ²
13	1.790x10 ²	216.0	2.882x10 ²
14	1.530x10 ²	216.0	2.464x10 ²
15	1.300x10 ²	216.0	2.104x10 ²
16	1.110x10 ²	216.0	1.797x10 ²
17	9.500x10 ¹	216.0	1.535x10 ²
18	8.120x10 ¹	216.0	1.305x10 ²
19	6.950x10 ¹	217.0	1.110x10 ²
20	5.95 x10 ¹	218.0	9.453x10 ¹

Using Equations 57 and 58, B_g is found using McClatchey's et al (1971) mid-latitude summer atmosphere. Such values are presented at both the on-line wavelengths and the off-line wavelengths in Table IV.

Attenuation by Gases

In this thesis, a highly coherent laser beam is transmitted from an orbiting space shuttle down through the atmosphere. Unfortunately, the beam will be attenuated every kilometer along its path as photons are scattered and absorbed or otherwise removed from the beam. The following sections will develop relationships in an attempt to model laser beam attenuation with height caused by atmospheric gases, aerosols, and cloud particles.

The eventual development of an equation expressing how gases attenuate a laser beam calls for an initial assumption. It will be assumed that the atmosphere can be modeled as isothermal from 10 km to the "top" of the atmosphere (about 80 km).

Using McClatchey's et al (1971) mid-latitude summer atmosphere, temperature at 10 km, $T_{10} = 235^{\circ}\text{k}$ while temperature at 80 km, $T_{80} = 216^{\circ}\text{k}$. So the variation of temperature with height is

$$.919 < \frac{T_{80}}{T_{10}} < 1$$

Thus, an isothermal assumption is somewhat reasonable. According to Hess (1959), pressure decreases exponentially with height in an isothermal atmosphere by

$$P = P_0 \exp \left(- \frac{Z}{H} \right) \quad (59)$$

Table IV

Volume Backscatter Coefficient B_g ($\text{km}^{-1} \text{sr}^{-1}$)
for Mid-Latitude Summer Atmosphere

Height km (km)	On-Line .7696 μm	Off-Line .7614 μm
0	3.416×10^{-4}	3.569×10^{-4}
1	3.097×10^{-4}	3.236×10^{-4}
2	2.798×10^{-4}	2.924×10^{-4}
3	2.537×10^{-4}	2.651×10^{-4}
4	2.294×10^{-4}	2.397×10^{-4}
5	2.068×10^{-4}	2.161×10^{-4}
6	1.860×10^{-4}	1.944×10^{-4}
7	1.672×10^{-4}	1.747×10^{-4}
8	1.499×10^{-4}	1.566×10^{-4}
9	1.339×10^{-4}	1.399×10^{-4}
10	1.193×10^{-4}	1.246×10^{-4}
11	1.059×10^{-4}	1.107×10^{-4}
12	9.376×10^{-5}	9.795×10^{-5}
13	8.266×10^{-5}	8.636×10^{-5}
14	7.067×10^{-5}	7.383×10^{-5}
15	6.034×10^{-5}	6.305×10^{-6}
16	5.154×10^{-5}	5.385×10^{-5}
17	4.402×10^{-5}	4.600×10^{-5}
18	3.743×10^{-5}	3.910×10^{-5}
19	3.183×10^{-5}	3.326×10^{-5}
20	2.711×10^{-5}	2.833×10^{-5}

where P_0 = initial pressure

P = pressure at another height

z = height (km)

H = scale height (km).

The scale height H is calculated from

$$H = \frac{\bar{R} T}{g} = 6.9 \text{ km} \quad (60)$$

where \bar{R} = universal gas constant

g = acceleration of gravity.

Pressure can be defined through the ideal gas law as

$$P_i = N_i k T_0 \quad (61)$$

where P_i = pressure at some altitude i

N_i = number density at altitude i

k = Boltzmann constant

T_0 = temperature at altitude i .

So by substitution into Equation 59:

$$N_i k T_0 = N_0 k T_0 \exp\left(\frac{-z}{H}\right)$$

$$\frac{N_i}{N_0} = \exp\left(-\frac{z}{6.9}\right) \quad (62)$$

Thus, number density is also exponentially distributed with height in an isothermal atmosphere.

The lidar equation (see Equation 18) defines atmospheric attenuation due to gases ρ_g as

$$Q_g = \int_{Z_T}^{Z_L} \alpha_g(z) dz \quad (63)$$

where Z_L = altitude of shuttle lidar (km)

Z_T = height of thunderstorm top (km)

α_g = atmospheric extinction coefficient due to gases (km^{-1}).

It will be assumed that α_g follows the exponential distribution described by an isothermal atmosphere. Integrating the right-hand side of Equation 59, Q_g can be found by

$$Q_g = \alpha_g(Z_T) \int_{Z_T}^{Z_L} \exp\left(-\frac{z}{6.9}\right) dz \quad (64)$$

$$Q_g = \alpha_g(Z_T) 6.9 \left[\exp\left(-\frac{Z_L - Z_T}{6.9}\right) \right] \quad (65)$$

Consider, $Z_L = 200$ km and $Z_T = 10$ km. Then $Z_L - Z_T = 190$ and the exponent of Equation 65 approaches one. The extreme distances separating the shuttle from a cloud top implies that Equation 65 can be rewritten as

$$Q_g = \alpha_g(Z_T) 6.9 \quad (66)$$

Extensive tables of $\alpha_g(Z)$ at many laser wavelengths have been compiled by Elterman (1968). In this thesis, the values of $\alpha_g(Z)$ listed at $.8 \mu\text{m}$ are used for both the on-line and off-line wavelengths (see Table II).

Attenuation by Aerosols

Aerosol particles in the atmosphere vary in size from clusters of a few molecules up to particles of $100 \mu\text{m}$ in radius. Aerosols can be divided into three size categories (Pruppacher and Klett, 1980):

1. Aitken particles - particles with dry radii $r \leq 0.1 \mu\text{m}$ (individual atoms and molecules)
2. large particles - particles with dry radii $0.1 \leq r \leq 1.0 \mu\text{m}$ (smoke, haze)
3. Giant particles - particles with dry radii $1.0 \mu\text{m} < r < 10 \mu\text{m}$ (dust).

This thesis distinguishes between aerosol particles and cloud particles. Aerosols will be considered as particles with radii $r < 10 \mu\text{m}$.

Aerosol particles are injected into the atmosphere by natural and by anthropogenic sources. Most particles originate from the earth's surface, interiors of volcanoes, or outer space. Particles of terrestrial origin are formed by gas-to-particle conversions or by mechanical and chemical disintegration of the earth's solid and liquid surfaces. Some typical particles are made of soil and rock debris, sea salt, volcanic debris, sulfates, nitrates, and ammonium salts.

Using exponentially derived data, aerosol particle size distribution can be expressed according to Junge's (1972) power law as

$$\frac{dN(r)}{dr} = Cr^{(D+1)} \quad (67)$$

where $dN(r)$ = number density of particles between particle radius r and dr

C = normalizing constant

D = shaping constant, $2 \leq D \leq 4$, for particle radii .1 to $10 \mu\text{m}$.

Elterman (1968) expanded the Junge distribution and computed extensive tables of atmospheric extinction due to aerosols α_A at different wavelengths

from altitudes of 0-50 km. His research examined over 79 density profiles demonstrating how the aerosol extinction coefficient changes with height.

Detailed studies by Junge (1972) in air over Germany found that the total aerosol concentration decreased exponentially up to about the tropopause. Above the tropopause, the aerosol concentration decreases rapidly toward zero at 50 km. The data supplied by Elterman (1968) at .8um indicates that α_A is distributed according to a power law from near 12 km to 50 km. A least squares curve fit technique was applied to this data to model the power law.

The power curve can be expressed as

$$Z = a\alpha_A^b \quad (68)$$

where Z = height (km)

α_A = aerosol extinction coefficient (km^{-1})

a,b = regression coefficients.

The regression coefficients a and b are found by solving the following system of linear equations (Ketter and Prawell, 1969):

$$\begin{bmatrix} n & \sum \alpha_{Ai} \\ \sum \alpha_{Ai} & \sum \alpha_{Ai}^2 \end{bmatrix} \begin{bmatrix} a \\ b \end{bmatrix} = \begin{bmatrix} \sum Z_i \\ \sum Z_i \alpha_{Ai} \end{bmatrix} \quad (69)$$

where n = number of data points

α_{Ai} = aerosol extinction coefficient at a given height (km^{-1}).

The coefficient of determination can also be expressed in a numerical manner by

$$R^2 = \frac{a \sum Z_i + b \sum \alpha_{Ai} Z_i - \frac{1}{n} (\sum Z_i)^2}{\sum (Z_i^2) - \frac{1}{n} (\sum Z_i)^2} \quad (70)$$

The model results are

$$R^2 = .80$$

$$a = 2.1197$$

$$b = -.25.$$

Equation 68 can now be rewritten as

$$Z = 2.1197 (\alpha_A)^{-.25} \quad (71)$$

or

$$\alpha_A = \left(\frac{Z}{2.1197} \right)^{-4} \quad (72)$$

Equation 72 indicates that α_A (from approximately 10 - 50 km) decreases rapidly to almost zero.

Atmospheric attenuation due to aerosols Q_A is defined in Equation 18 as

$$Q_A = \int_{Z_T}^{Z_L} \alpha_A(z) dz$$

where symbols are as previously defined.

The correct functional relationship needed to evaluate Q_A is found by integrating the right-hand side of Equation 72 such that

$$Q_A = \int_{Z_T}^{Z_L} \left(\frac{Z}{2.1197} \right)^{-4} dz \quad (73)$$

$$= \left[\frac{1}{2.1197} \right] \int_{Z_T}^{Z_L} (Z)^{-4} dz$$

$$= \left[\frac{1}{2.1197} \right]^{-4} \left(\frac{1}{3} \right) z^{-3} \quad \left| \begin{array}{l} z_L \\ z_T \end{array} \right.$$

$$Q_A = 6.73 (z_L^{-3} - z_T^{-3}) . \quad (74)$$

Aerosol Backscatter Coefficient

The aerosol particles considered in the above derivation range from .1 to 10 μm in radius. This implies that Mie scattering theory applies, since the laser wavelength is on the same scale as the particles. The aerosol backscatter coefficient B_A (required in the lidar equation) must be found using Mie theory (Hinkley, 1976).

Investigators typically avoid solving complex differential equations in computing B_A . In general cases, a simplifying relationship is established between α_A and B_A (Hobbs and Deepak, 1981). This relation is referred to as the backscatter-to-extinction ratio k and is experimentally measured. The backscatter-to-extinction ratio k for aerosols of the size considered in this thesis was found by Fernald (1972) to be

$$k = \frac{B_A}{\alpha_A} = .03 \text{ sr}^{-1} . \quad (75)$$

It is then a simple matter to compute B_A from

$$.03 \alpha_A = B_A . \quad (76)$$

Attenuation by Thunderstorm Tops

The top 0.5 km of a thunderstorm in this thesis will be modeled as a cirrus ice cloud. This assumption is consistent with Byers and Braham's (1949) model of a thunderstorm calling for the upper regions of

the cumulonimbus cloud to be made of cirrus type ice crystals. Cirrus clouds are composed of several types of ice crystals such as bullet-shaped crystals, single rosettes, hexagonal columns, and irregular crystals (Pruppacher and Klett, 1980). Ice crystal concentrations range between 1 to $5 \times 10^4 \text{ cm}^{-3}$.

It may be wondered if a laser beam can even penetrate a cloud without suffering severe attenuation. Platt (1979) has conducted extensive research with lidars probing clouds. He reports that for low-level water clouds, laser penetration is about 100 m; however, for cirrus clouds, laser penetration is found to be $>4 \text{ km}$. This is true since cirrus clouds have very low water liquid water content thus low internal scattering from the water molecule.

Spinhirne et al (1982) used a high-altitude research aircraft with a Nd:YAG lidar mounted in the plane to actually measure the volume backscatter coefficient by over-flying cirrus clouds. The measured value of the cirrus cloud top volume backscatter coefficient B_c is $0.02 \text{ km}^{-1} \text{ sr}^{-1}$.

The extinction coefficient due to the presence of cloud particles α_c can be found through a backscatter-to-extinction ratio k . Platt (1973) probed cirrus clouds with a lidar and had great success with a value $k = .05 \text{ sr}^{-1}$. Accordingly, this thesis will use the following values for B_c and α_c :

$$B_c = .02 \text{ km}^{-1} \text{ sr}^{-1}$$

$$\alpha_c = \frac{B_c}{k} = \frac{.02 \text{ km}^{-1} \text{ sr}^{-1}}{.05 \text{ sr}^{-1}} = .4 \text{ km}^{-1} .$$

The only other assumption that investigators make is that B_c and α_c will be constant throughout the depth of cloud being probed (1/2 km in this thesis).

Atmospheric attenuation due to cloud particles Q_c is defined in Equation 18 as

$$Q_c = \int_{Z_T - 1/2 \text{ km}}^{Z_T} \alpha_c dz = .5 \alpha_c. \quad (77)$$

Miscellaneous Cloud Top Parameters

With knowledge of α_c , it is possible to compute other cloud top parameters such as cloud particle number density N_c and the liquid water content W_c existing on ice crystals. The number density is

$$N_c = \frac{B_c}{2\pi a^2} \quad (78)$$

where a = cloud particle radius (a typical value is 50 μm).

The cloud water content can be found by

$$W_c = \frac{4}{3} \pi a^2 \rho N_c \quad (79)$$

where ρ = cloud particle mass density (.92 gm cm^{-3} for ice clouds, Russell, 1982).

Attenuation by Ozone

The extinction due to ozone α_3 is a strong function of altitude z and wavelength λ . Elterman (1968) defines α_3 as

$$\alpha_3 = A_v(\lambda) D_3(z) \quad (80)$$

where A_v = pure ozone absorption coefficient (cm^{-1})

D_3 = ozone equivalent thickness (cm km^{-1}).

A_v for the wavelength used in this thesis is $1.00 \times 10^{-2} \text{ cm}^{-1}$.

Values for D_3 have been tabulated by Elterman (1968) for heights of 0-50 km.

This thesis is concerned with ozone O_3 at heights from 20-50 km. Elterman (1968) shows that $\alpha_3(20 \text{ km}, .8 \mu\text{m}) = 1.64 \times 10^{-4} \text{ km}^{-1}$ while $\alpha_3(50 \text{ km}, .8 \mu\text{m}) = 1.86 \times 10^{-6} \text{ km}^{-1}$. Since these values are extremely small compared to α_g , α_A , and α_C the effects of ozone are not considered in this thesis. Figure 8 is a profile of α_3 at $.8 \mu\text{m}$ as a function of height (Elterman, 1968).

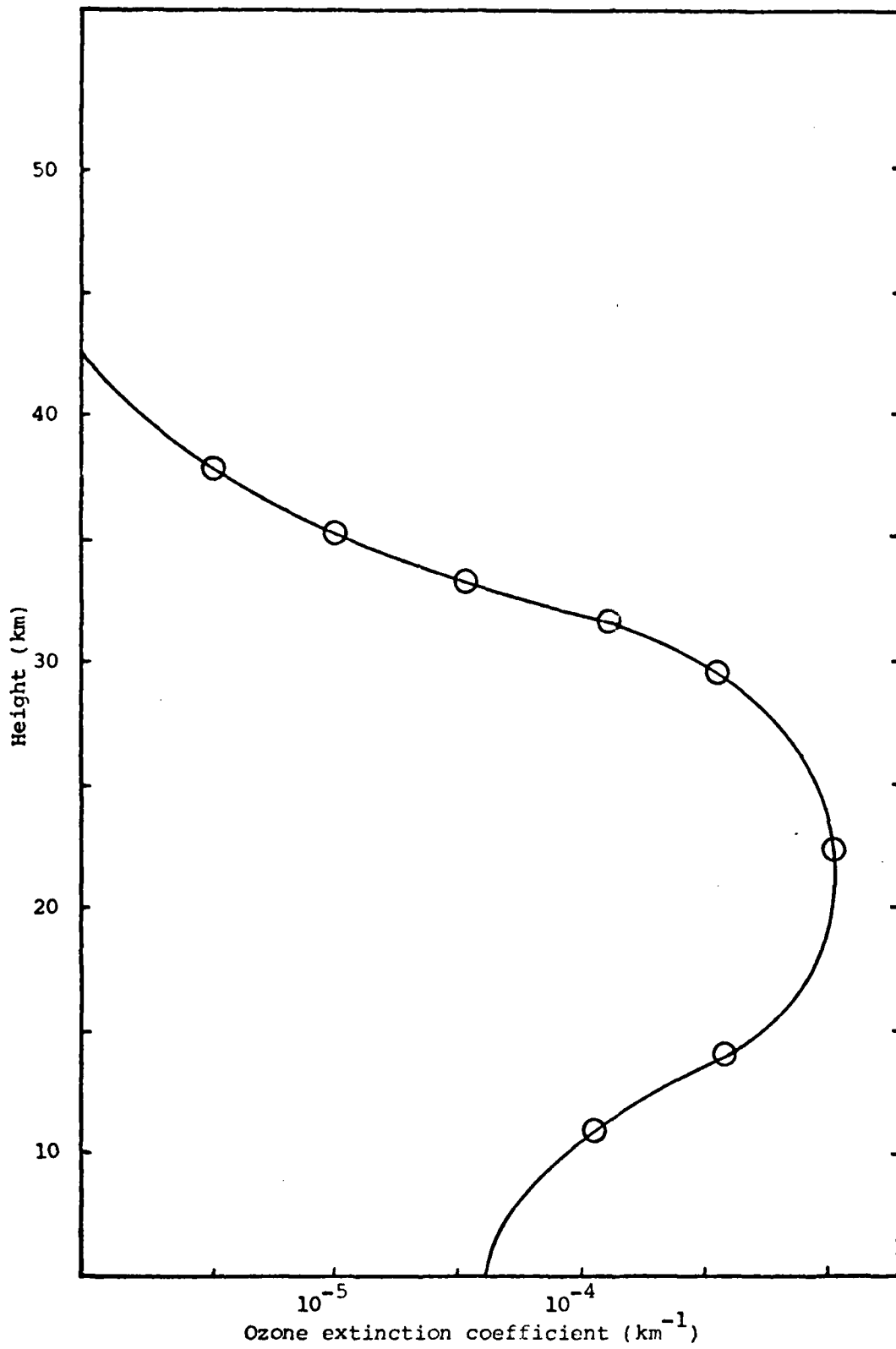


Figure 8. Sketch of ozone extinction vs height

VI. Laser Considerations

Laser Beam Divergence

As a laser beam leaves the optical cavity and propagates it will slowly diverge because of diffraction. Assuming the laser beam is a Hermit-Gaussian type, beam divergence θ can be expressed as

$$\begin{aligned}\theta &= \frac{2\lambda}{\pi W_0} \\ &= \frac{4}{\pi} \frac{\lambda}{2W_0} \\ &1.27 \frac{\lambda}{2W_0}\end{aligned}\tag{81}$$

where θ = full angle beam divergence

λ = laser operating wavelength

W_0 = beam spot size (actually this is the beam radius value) at beam waist (O'Shea et al, 1978).

Another factor of interest to the laser user is spot size on the target W . This thesis is interested in aiming the laser beam at the rising towers protruding above the anvil floor so it would be desirable for W to be less than the diameter of an updraft tower. Typical thunderstorm updraft radius range from 1-3 km (Kropfli and Miller, 1976).

A Hermit-Gaussian beam with a spot size W on a target at a distance z can be expressed according to Nielsen (1980) as

$$W(z) = W_0 \left[1 + \left(\frac{\lambda z}{\pi W_0^2} \right)^2 \right]^{1/2}\tag{82}$$

where z is the distance from the minimum spot size (essentially the laser's front end) to the target. It must be noted that Equation 82 is valid only when the target which in this case is a storm top lies in the laser's far field. A laser's near field is that distance z where the beam remains well collimated. The Rayleigh range can now be defined as that distance z where the laser beam begins to spread. The Rayleigh range Z_R in equation form is

$$Z_R = \frac{\pi W_0^2}{\lambda} \quad (83)$$

Once the target distance Z_T exceeds 20-100 times Z_R , the laser beam enters the far field region and Equation 82 becomes effective. Figure 9 illustrates the situation considered in this thesis.

It will now be demonstrated that a storm top lies in the laser's far field and W at the storm top will be found. This example will assume that the lidar is in a 200 km orbit with a thunderstorm top at 10 km. Spot size on target can be found using Equation 82 re-written here for convenience

$$W(Z) = W_0 \left[1 + \left(\frac{\lambda z}{\pi W_0^2} \right)^2 \right]^{1/2}$$

W_0 = laser beam radius at instrument aperture (assume a typical value of 1 cm (Nielsen, 1980))

$W(Z)$ = beam radius at target

λ = laser operating wavelength ($.7696 \times 10^{-6}$ m)

z = distance from lidar to storm top (190 km here).

To use this formula, the target must lie in the far field. The far field check is performed by testing if z is 20 to 100 times greater than Equation 83:

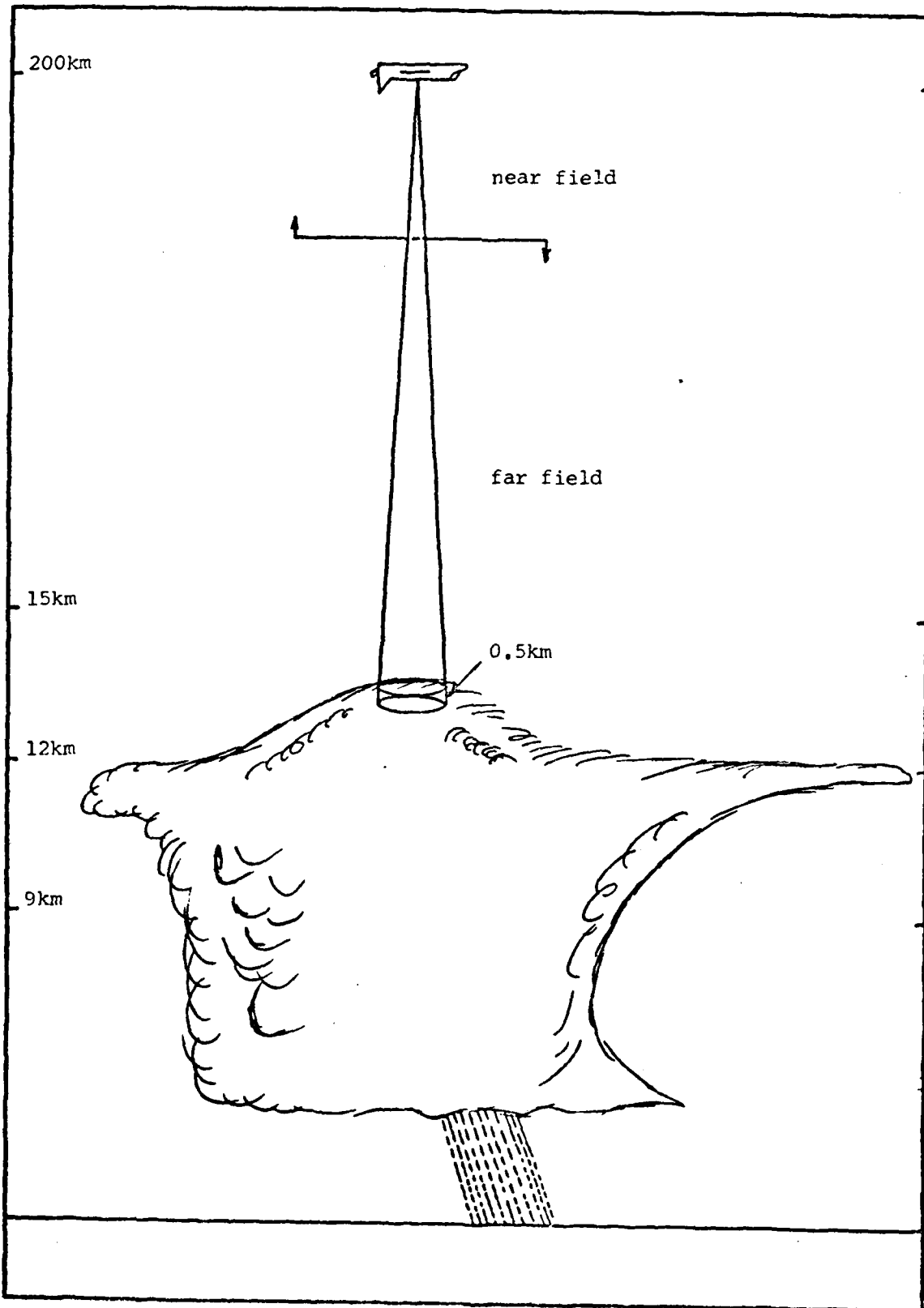


Figure 9. Orbiting shuttle-loom fiber with diameter $d = 0.5$ km in the far field.

far field check, $z > 100 \text{ times } \frac{\pi W_0^2}{\lambda}$

$$190,000 \text{ m} > \frac{\pi (.01 \text{ m})^2}{.7696 \times 10^{-6} \text{ m}}$$

$$190,000 \text{ m} > (100) (408 \text{ m})$$

$$190,000 \text{ m} > 40,800 \text{ m.}$$

So target (storm top) is in the far field.

The beam radius on target $W(190 \text{ km})$ according to Equation 82 is 4.655 m. The circular area illuminated at the cloud top is 68.059 m².

These values are much smaller than the average updraft. Such values indicate, for the first time, an orbiting sensor could observe cloud top structure on a scale previously obtainable only by high altitude aircraft.

Thermal Blooming

The atmosphere absorbs photons from the beam as it propagates. This absorbed energy is not lost but instead heats and expands the channel of air surrounding the beam. This rise in temperature of the air channel is thermal blooming, and the effect is to cause the beam to spread farther than Equation 82 predicts.

Thermal Blooming is greatly reduced by pulsing the beam, since a short pulse does not stay in one location long enough for the air channel to expand. The time scale of thermal blooming can be found according to Nielsen (1980) as

$$t_j = \frac{W}{j} \quad (84)$$

where t_j = time required for thermal blooming to occur

W = beam radius at specified distance

j = speed of sound (3×10^4 cm/sec).

The previous example found $W(190) = 4.66$ m. This implies $t_j = 1.55 \times 10^{-2}$ sec. The pulse width used in this thesis is 3.33×10^{-6} sec. So thermal blooming does not have time to occur and will therefore be neglected.

Dye Lasers

Dye lasers must be used when DIAL experiments are being performed such as the DIAL procedure employed by this thesis. DIAL experiments require two wavelengths: one at the absorption line of the molecule studied and a second nearby wavelength where absorption by the molecule is negligible. Furthermore, the absorption lines of most molecules are not at standard laser wavelengths. Dye lasers can meet all DIAL experimental requirements since they can be tuned to non-standard wavelengths. Dye lasers can be frequency tuned to any frequency in the visible spectrum. Such lasers work well in the pulse mode and are characterized by high output power, high gain, and low cost.

The active medium of dye lasers consist of an organic dye dissolved in a solvent. Industry is developing a dye laser that does not require a dye cell. Instead a rotating solid plastic disc is impregnated with dye (Greco, 1980). A suitable dye that can be used to reach the wavelengths chosen in this thesis (both wavelengths centered near $.76 \mu\text{m}$) is nileblue--A perchlorate (O'Shea et al,

1978) or oxazine 725 dye in ethanol (Greco, 1980).

Dye lasers are optically pumped which implies that another laser can be used to pump the dye laser. The only requirement is for the pumping laser to have an output near the peak dye absorption band. A dye laser operating in the oxygen "A" band could be pumped by nitrogen or krypton lasers. The krypton laser is chosen as the pumping laser in this thesis since Kalshoven et al (1980) had great success with such a system while operating in the oxygen "A" band.

VII. Instrumental Considerations

Integration Time

The integration time t_I will be defined as that time interval for which the lidar receiving telescope is turned on or receiving signal and noise photons. This integration time for Kt_s pulses can be expressed as

$$t_I = \frac{2dKt_s}{c} \quad (85)$$

where d = vertical resolution (km)

K = number of pulses per second (PPS)

t_s = sounding time (see below)

c = speed of light (km sec^{-1}).

The integration time can be calculated using the correct values from the list of laser characteristics found in Table V.

Sounding Time

The sounding time t_s is defined as that time interval required to place 1000 shots (Kt_s pulses) into a cloud top. Sounding time will be taken as 20 seconds ($20 \text{ sec} \times 50 \text{ shots sec}^{-1} = 1000 \text{ shots}$).

Laser Power

Huffaker (1978) indicates that the space shuttle can allocate a maximum of 3000 watts to a shuttle-borne lidar. The lidar system developed for this thesis is a three laser system where two of these are dye lasers. The first dye laser is tuned to an O_2 absorption line, the second dye laser is tuned to a nearby spectral

Table V

Laser Characteristics

Energy per Pulse (E_p)	6J
Laser Output Power	300 watt
Peak Power (P_p)	1.8 MWatt
**Shuttle Power available to Lidar	3000 Watt
Lidar System Efficiency	10%
Pulse Width (t_p)	3.33×10^{-6} sec
Vertical Resolution (d)	0.5 km
*Receiver Diameter	1.25 m
On-line Wavelength	.7696 μm
Off-Line Wavelength	.7614 μm
*Optical Filter Bandpass ($\Delta\lambda$)	1 nm
*Receiver FOV	1 mrad
Pulse Repetition Rate (k)	50 pps
Integration Time t_I	3.33×10^{-3} sec
Sounding Time t_s	20 sec

* indicates values recommended by Greco (1980)

** indicates value recommended by Huffaker (1978)

position where O_2 absorption is negligible. The third laser (a krypton gas laser) will optically pump the first two. Such a complex system of three lasers along with a well designed optical system is generally considered to be about 10% efficient (Huffaker, 1978). Therefore, laser output power could be as large as 300 watts.

The energy per pulse using this power level is calculated as

$$E_p = \frac{P_A e}{K} \quad (86)$$

where E_p = energy per pulse (J)

P_A = power available to laser (watts)

e = laser system efficiency (see Eq. 14).

Using Equation 86, E_p will be taken as 6J per pulse. Commercial lasers developing 6J per pulse will be available by the mid eighties according to Huffaker (1978) and Greco (1980).

Peak Power

High powered pulsed lidars operated from the shuttle will develop very high peak power. High peak powers could represent a danger to the human eye for an observer viewing the laser directly from the earth's surface. Eye safety is discussed in Chapter X of this thesis. Peak power P_p can be found by

$$P_p = \frac{E_p}{t_p} \quad (87)$$

where t_p = the pulse width (see Table V).

Vertical Resolution

The vertical resolution, or depth of the volume sensed, will be taken as 0.5 km. Penetrating a thunderstorm top beyond 0.5 km is thought to be impossible since the laser beam would be greatly attenuated by the presence of super-cooled water droplets suspended in the updraft.

Another problem can occur if the beam could penetrate the cloud top much beyond 0.5 km. The laser beam will encounter warmer (243°K) temperatures as penetration increases. Cloud microphysics predicts hexagonal ice plates in clouds at a temperature range of $243\text{--}261^{\circ}\text{K}$ (Pruppacher and Klett, 1980).

Platt (1978 a,b) showed that super, large backscatter returns are possible if lidar signals are reflected off horizontally oriented hexagonal ice plates. This phenomenon occurs only if the zenith angle ψ is zero. Figure 10 illustrates this situation with a crystal of thickness t . To make matters worse, these plate shaped crystals fall naturally with their long axis horizontal.

Platt (1978 a) further explains that sudden high increases in the signal-to-noise ratio (see this chapter) are possible when laser light is reflected off even a single horizontally oriented hexagonal ice plate as the lidar is scanned across the vertical (zero zenith angle). Therefore, it will be assumed that no such ice crystals exist in the colder top 0.5 km of a thunderstorm.

A final barrier that could stop a laser beam from ever reaching the storm top is for dense cirrus clouds to hide the thunderstorm altogether. Such cirrus are produced by previous convection.

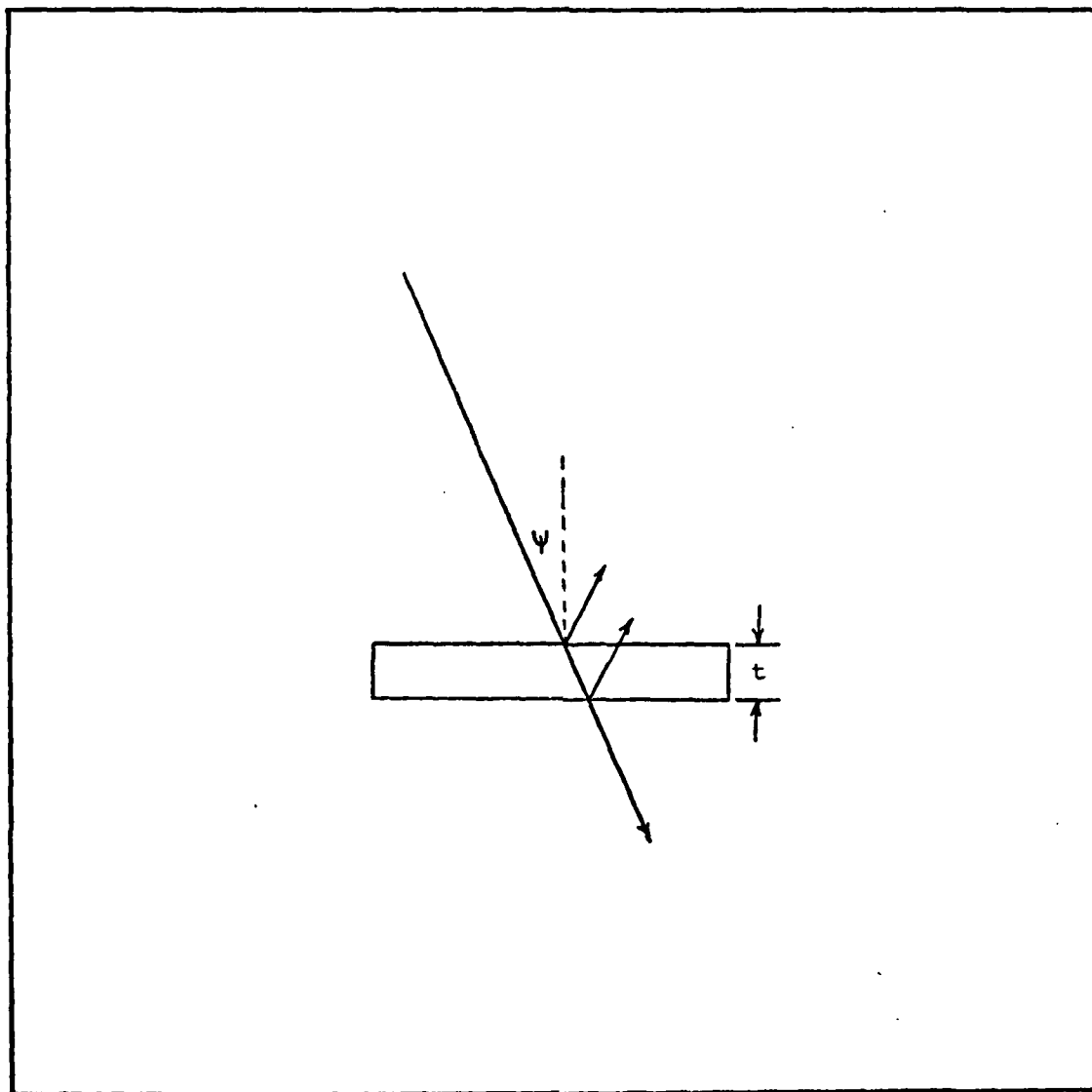


Figure 10. Side view of hexagonal plate ice crystal with laser beam incident at zenith angle ψ .

This canopy of cirrus over thunderstorms does occasionally form (Adler and Fenn, 1979c). This problem is disregarded in this thesis.

The vertical resolution d can be computed by

$$d = \frac{c \tau p}{2} \quad (88)$$

where symbols are as previously defined.

Background

The onboard receiving telescope will receive return radiation from thunderstorm tops and from the background. Three observations will be considered:

- a. sunlit cloud with albedo $A = .8$
- b. sunlit ocean with albedo $A = .1$
- c. moonlit cloud with albedo $A = .8$.

The albedo A is the percentage of radiation reflected by a body.

Background radiance L_λ (watt $m^{-2} \text{sr}^{-1} \mu m^{-1}$) can be found according to Russell (1982) as

$$L_\lambda = \frac{AE_\lambda(\lambda) \cos \psi}{\pi} \quad (89)$$

where $E_\lambda(\lambda)$ = solar spectral irradiance (watt $m^{-2} \mu m^{-1}$)

ψ = zenith angle.

The zenith angle ψ is chosen to be zero so that only worse case situations are considered such as local noon with the sun directly overhead or the full moon directly overhead at night. The value of $E_\lambda(\lambda)$ at $.76 \mu m$ will be 1211 watts $m^{-2} \mu m^{-1}$ (Thekaekara, 1974).

Table VI displays upward spectral radiance for a downward pointing lidar operating near .76 μm . Values in Table VI reflect worse case background situations. Moonlit values correspond to the ratio:

$$\frac{E_{\lambda}(\text{sun})}{E_{\lambda}(\text{moon})} = 10^{-6} \quad (90)$$

according to Russell (1982).

Table VI

Upward Spectral Radiance ($\text{watts m}^{-2} \text{ nm}^{-1} \text{ sr}^{-1}$) at .76 μm

	Sunlit	Moonlit
Cloud top	3.084×10^{-1}	3.084×10^{-7}
Ocean	3.855×10^{-2}	3.855×10^{-8}

Signal-to-Noise Ratio

The power received by the lidar's receiver P_r given by Equation 18 contains three sources of noise which collectively limit the sensitivity of the receiver. Noise results from the random arrival of photons from cloud induced laser returns and the background. This random arrival is described by a Poisson distribution. Another source of noise is the random generation of dark current. This dark current occurs within the photomultiplier even if no photons are incident. It can be neglected in photomultipliers if they are cooled to liquid nitrogen temperatures (77°K).

Investigators typically discuss noise in terms of photoelectrons produced by the detector. Accordingly, the signal-to-noise ratio S/N can be written as (Smith and Platt, 1978):

$$S/N = \frac{n_s}{(n_s + n_b)^{1/2}} \quad (91)$$

where n_s = signal count from cloud top

n_b = background count.

Signal counts are calculated by

$$n_s = \frac{\lambda}{hc} e P_L t_I \quad (92)$$

where λ = laser wavelength (m)

h = Planck's constant (6.63×10^{-34} J-sec)

c = speed of light (3.0×10^8 m sec⁻¹)

e = system efficiency (.10)

P_L = received power collected by receiver optics (watts)

t_I = integration time (3.33×10^{-3} sec).

Included in e is the optical system efficiency and the receiving system (photomultiplier) efficiency. The quantity $\frac{hc}{\lambda}$ is the energy per photon.

Background counts are calculated by

$$n_b = \frac{\lambda}{hc} e P_b t_I \quad (93)$$

where P_b (watts) is the power from the cloud background and is calculated by

$$P_b = \Omega \Delta\lambda A_r L \quad (94)$$

where Ω = receiver's field of view (sr)

$\Delta\lambda$ = receiver's optical bandpass filter (nm)

A_r = area of receiver (m^2)

L_λ = background radiance (watts m^{-2} nm^{-1} sr^{-1}).

VIII. System Results

Scenario I

The lidar equation (see Equation 18) can now be solved using the quantities defined in the atmospheric considerations chapter and the laser system characteristics specified in Table V.

Tables VII - XIII display the numerical results of solving the lidar equation for varying shuttle altitudes and thunderstorm heights. Signal-to-noise calculations are performed for situations of a worse case daylight (local noon) and a worse case at night with a full moon overhead.

The results shown in Tables VII - XIII indicate that the shuttle-borne lidar proposed in this thesis can successfully probe the top 0.5 km of a thunderstorm and return a measurable signal. The nighttime values of S/N are very good as would be expected with reduced background radiance from the storm tops.

Two scenarios will be considered in this thesis. This first scenario will demonstrate the shuttle lidar's ability to determine a single temperature. At the end of the following chapter on thunderstorm vertical velocities, a second scenario will consider a second temperature measurement of the same area at a later time.

Consider a scenario where the shuttle is orbiting at 200 km. Suppose that through coordination with meteorologists on the ground using weather radar, the shuttle lidar is aimed at an overshooting top at 10 km above the surface. Using the results shown in Table XI, Equation 19 can be solved for the resonant absorption coefficient α_{g_0} such that

$$\alpha_{g_0} = -\frac{1}{6.9} \frac{1}{2} \ln \left(\frac{3.359 \times 10^{-11} \text{ watts}}{6.821 \times 10^{-11} \text{ watts}} \right)$$

$$= .0513 \text{ km}^{-1}$$

This is the actual value of α_{g_0} calculated using Equation 40 and tabulated in Table I. This value of α_{g_0} is then placed into Equation 43 where temperature is arrived at in an iterative fashion using a seed temperature from a standard atmosphere at the storm height provided by weather radar, spotter plane, or the shuttle lidar itself. To demonstrate, A_0 must be found using Equation 41:

$$A_0 = \frac{(2.09) (2.69 \times 10^{25} \text{ molec m}^{-3}) (273.16^\circ\text{K})^{3/2} (3.37 \times 10^{-30} \text{ m}^2 \text{ molec}^{-1} \text{ cm}^{-1})}{(3) (.038 \text{ cm}^{-1})}$$

$$* \exp \left[\frac{(1.439) (1421.436 \text{ cm}^{-1})}{273.16^\circ\text{K}} \right]$$

$$= 1340.56^\circ\text{K}^{3/2} \text{ m}^{-1} .$$

Since the on-line wavelength (.7696um) is in the region of weak line strengths, Kalshoven et al (1981) indicate that the value for A_0 should be increased 30%. This was determined through actual experimentation. Thus, A_0 will be taken as $1742.73^\circ\text{K}^{3/2} \text{ m}^{-1}$.

Now the cloud top temperature measured from a storm with a top at 10 km can be recovered using Equation 43 and a seed temperature of 235°K from McClatchey's et al (1971) mid-latitude summer atmosphere at 10 km:

$$T_{i+1} = \frac{(1.439) (1421.436 \text{ cm}^{-1})}{\ln \left[(1742.73^{\circ\text{K}})^{3/2} \text{ m}^{-1} (.9999) (235^{\circ\text{K}})^{-3/2} \right]}$$

$$* \left(1 - \frac{e}{(10) (.7486)} \right) \frac{10^3}{.0513 \text{ km}^{-1}} \Bigg]$$

$$= 235.09^{\circ\text{K}}.$$

If needed, further iterations could be performed using the previous result for T_i as the seed temperature until successive results give the same results to within $0.1^{\circ\text{K}}$.

Attitude Control

The space shuttle's ability to hold a navigation axes oriented to nadir is 0.5 degrees (3 sigma) up to one hour (Huffaker, 1978). In addition, there is another two degrees of error possible due to misalignment of the navigation subsystem to the cargo bay. Therefore, shuttle aiming accuracy for a lidar mounted in the cargo bay is ± 2.5 degrees.

Data Collection Intervals

The space shuttle operates in low earth orbit typically at 200 km with an orbital velocity of 5 km sec^{-1} . This implies that the time interval during which a storm top remains within range of the lidar is limited. Indeed, this short loitering time is a major factor for any orbit except a geosynchronous one.

It must be determined how many data collection intervals or how many 20 second sounding periods are available to the instrument during a typical flyover. Figure 11 illustrates a flyover with a thunderstorm top at 12 km. It can be seen that about four 20 second data collection intervals are possible before the instrument becomes signal-to-noise

Table VII

Tabulated Results from Solving Lidar Equation
Shuttle Altitude = 100 km

Storm Top (km)	Storm Top (ft)	Return Power On-Line (μW)	Return Power Off-Line (μW)	S/N Daylight	S/N Moonlight
10	32810	1.497×10^{-4}	3.040×10^{-4}	9.86	438.78
11	36091	1.808×10^{-4}	3.110×10^{-4}	11.90	482.23
12	39372	2.171×10^{-4}	3.213×10^{-4}	14.29	528.51
13	42653	2.466×10^{-4}	3.260×10^{-4}	16.24	563.39
14	45934	2.661×10^{-4}	3.338×10^{-4}	17.52	585.25
15	49215	2.904×10^{-4}	3.418×10^{-4}	19.11	611.34
16	52496	3.195×10^{-4}	3.500×10^{-4}	21.03	641.32
17	55777	3.561×10^{-4}	3.586×10^{-4}	23.44	677.08

Table VIII

Shuttle Altitude: 125 km

Storm Top (km)	Storm Top (ft)	Return Power On-Line (μw)	Return Power Off-Line (μw)	S/N Daylight	S/N Moonlight
10	32810	9.170×10^{-5}	1.862×10^{-4}	6.04	343.18
11	36091	1.102×10^{-4}	1.896×10^{-4}	7.25	376.28
12	39372	1.317×10^{-4}	1.949×10^{-4}	8.67	411.40
13	42653	1.488×10^{-4}	1.967×10^{-4}	9.80	437.46
14	45934	1.598×10^{-4}	2.004×10^{-4}	10.52	453.27
15	49215	1.734×10^{-4}	2.041×10^{-4}	11.41	472.24
16	52495	1.898×10^{-4}	2.079×10^{-4}	12.49	494.07
17	55777	2.103×10^{-4}	2.118×10^{-4}	13.85	520.20

Table IX

Shuttle Altitude: 150 km

Storm Top (km)	Storm Top (ft)	Return Power On-Line (μw)	Return Power Off-Line (μw)	S/N Daylight	S/N Moonlight
10	32810	6.187×10^{-5}	1.256×10^{-4}	4.07	281.68
11	36091	7.411×10^{-5}	1.275×10^{-4}	4.88	308.40
12	39372	8.828×10^{-5}	1.307×10^{-4}	5.81	336.69
13	42653	9.947×10^{-5}	1.315×10^{-4}	6.55	357.46
14	45934	1.064×10^{-4}	1.335×10^{-4}	7.01	369.78
15	49215	1.151×10^{-4}	1.355×10^{-4}	7.58	384.62
16	52496	1.256×10^{-4}	1.375×10^{-4}	8.27	401.74
17	55777	1.387×10^{-4}	1.397×10^{-4}	9.13	422.26

Table X

Shuttle Altitude: 175 km

Storm Top (km)	Storm Top (ft)	Return Power On-Line (μw)	Return Power Off-Line (μw)	S/N Daylight	S/N Moonlight
10	32810	4.454×10^{-5}	9.044×10^{-5}	2.93	238.78
11	36091	5.324×10^{-5}	9.160×10^{-5}	3.51	261.19
12	39372	6.327×10^{-5}	9.365×10^{-5}	4.17	284.86
13	42653	7.113×10^{-5}	9.402×10^{-5}	4.68	302.12
14	45934	7.594×10^{-5}	9.524×10^{-5}	5.00	312.18
15	49215	8.195×10^{-5}	9.645×10^{-5}	5.40	324.35
16	52496	8.918×10^{-5}	9.769×10^{-5}	5.87	338.41
17	55777	9.827×10^{-5}	9.896×10^{-5}	6.47	355.29

Table XI

Shuttle Altitude: 200 km

Storm Top (km)	Storm Top (ft)	Return Power On-Line (μw)	Return Power Off-Line (μw)	S/N Daylight	S/N Moonlight
10	32810	3.359×10^{-5}	6.821×10^{-5}	2.21	207.13
11	36091	4.009×10^{-5}	6.897×10^{-5}	2.64	226.43
12	39372	4.756×10^{-5}	7.040×10^{-5}	3.13	246.79
13	42653	5.339×10^{-5}	7.056×10^{-5}	3.52	261.54
14	45934	5.689×10^{-5}	7.136×10^{-5}	3.75	270.05
15	49215	6.130×10^{-5}	7.215×10^{-5}	4.04	280.35
16	52496	6.659×10^{-5}	7.295×10^{-5}	4.38	292.26
17	55777	7.325×10^{-5}	7.377×10^{-5}	4.82	306.60

Table XII

Shuttle Altitude: 225 km

Storm Top (km)	Storm Top (ft)	Return Power On-Line (uw)	Return Power Off-Line (uw)	S/N Daylight	S/N Moonlight
10	32810	2.624×10^{-5}	5.327×10^{-5}	1.73	182.82
11	36091	2.127×10^{-5}	5.379×10^{-5}	2.06	199.77
12	39372	3.705×10^{-5}	5.485×10^{-5}	2.44	217.63
13	42653	4.154×10^{-5}	5.490×10^{-5}	2.74	230.52
14	45434	4.421×10^{-5}	5.545×10^{-5}	2.91	237.87
15	49215	4.757×10^{-5}	5.599×10^{-5}	3.13	246.80
16	52496	5.161×10^{-5}	5.654×10^{-5}	3.40	257.14
17	55777	5.670×10^{-5}	5.710×10^{-5}	3.73	269.59

Table XIII

Shuttle Altitude: 250 km

Storm Top (km)	Storm Top (ft)	Return Power On-Line (uw)	Return Power Off-Line (uw)	S/N Daylight	S/N Moonlight
10	32810	2.105×10^{-5}	4.275×10^{-5}	1.34	163.56
11	36091	2.507×10^{-5}	4.313×10^{-5}	1.65	178.67
12	39372	2.968×10^{-5}	4.393×10^{-5}	1.95	194.58
13	42653	3.324×10^{-5}	4.393×10^{-5}	2.19	206.02
14	45934	3.534×10^{-5}	4.432×10^{-5}	2.33	212.50
15	49215	3.799×10^{-5}	4.471×10^{-5}	2.50	220.38
16	52496	4.117×10^{-5}	4.510×10^{-5}	2.71	229.50
17	55777	4.519×10^{-5}	4.550×10^{-5}	2.98	240.50

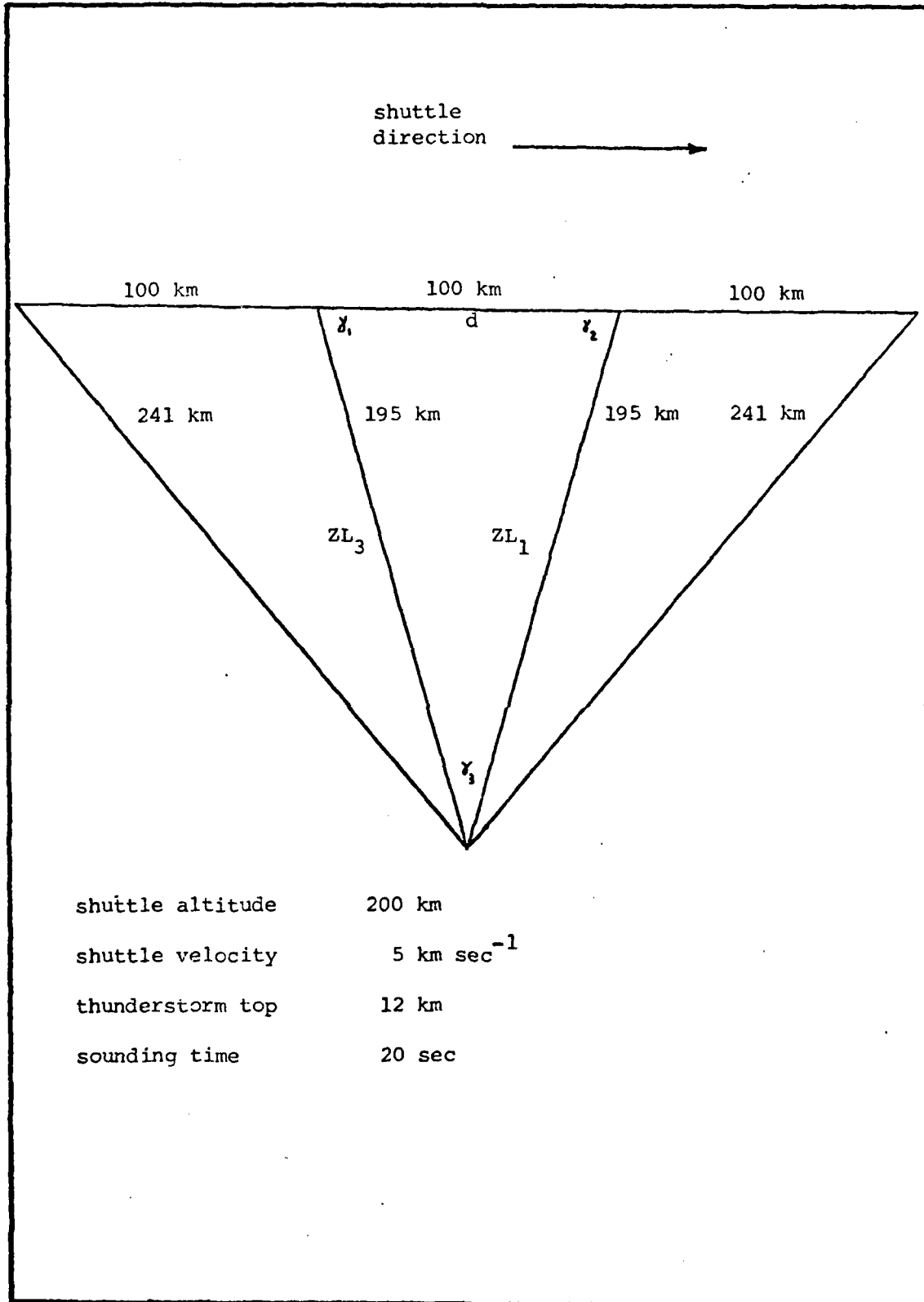


Figure 11. Shuttle overflight of a 12km thunderstorm.

limited or the aiming angle γ_2 becomes too small for shuttle guidance systems to properly aim the instrument. At night, S/N is very good and more than 4 data collection intervals are possible, but the pointing problem could be a factor. Figure 12 shows the same viewing scenario except now the sounding time t_s is 10 sec instead of 20 sec as in Figure 11. There are more intervals, but this does not imply that several thunderstorm tops can be surveyed.

The distance between the shuttle and a storm top Z_{L3} is found from the expression

$$Z_{L3} = (Z_{L1} + d - 2Z_{L1}d \cos \gamma_2)^{1/2} \quad (95)$$

where

Z_{L1} = shuttle altitude above storm top at start time t_o

Z_{L3} = shuttle altitude above storm top at $t_o + x$ sec

d = distance shuttle traveled at 5 km sec^{-1}

γ_2 = inclusive angle between Z_{L1} and d in degrees.

The time scale for temperature changes in storm tops reflecting changes in intensity is in the range of several degrees per minute (Mack et al, 1982). The shuttle-borne lidar would be within range of one thunderstorm top for 80 to 100 seconds (see Figure 11) before range reduces S/N or the aiming angle becomes too critical to ensure the same spot is being measured. Table XIV shows values of S/N for different values of sounding time t_s with the shuttle orbiting at 200 km. Storm tops from 10- 17 km were probed with $t_s = 10, 20,$ and 30 seconds for a worse case daylight situation.

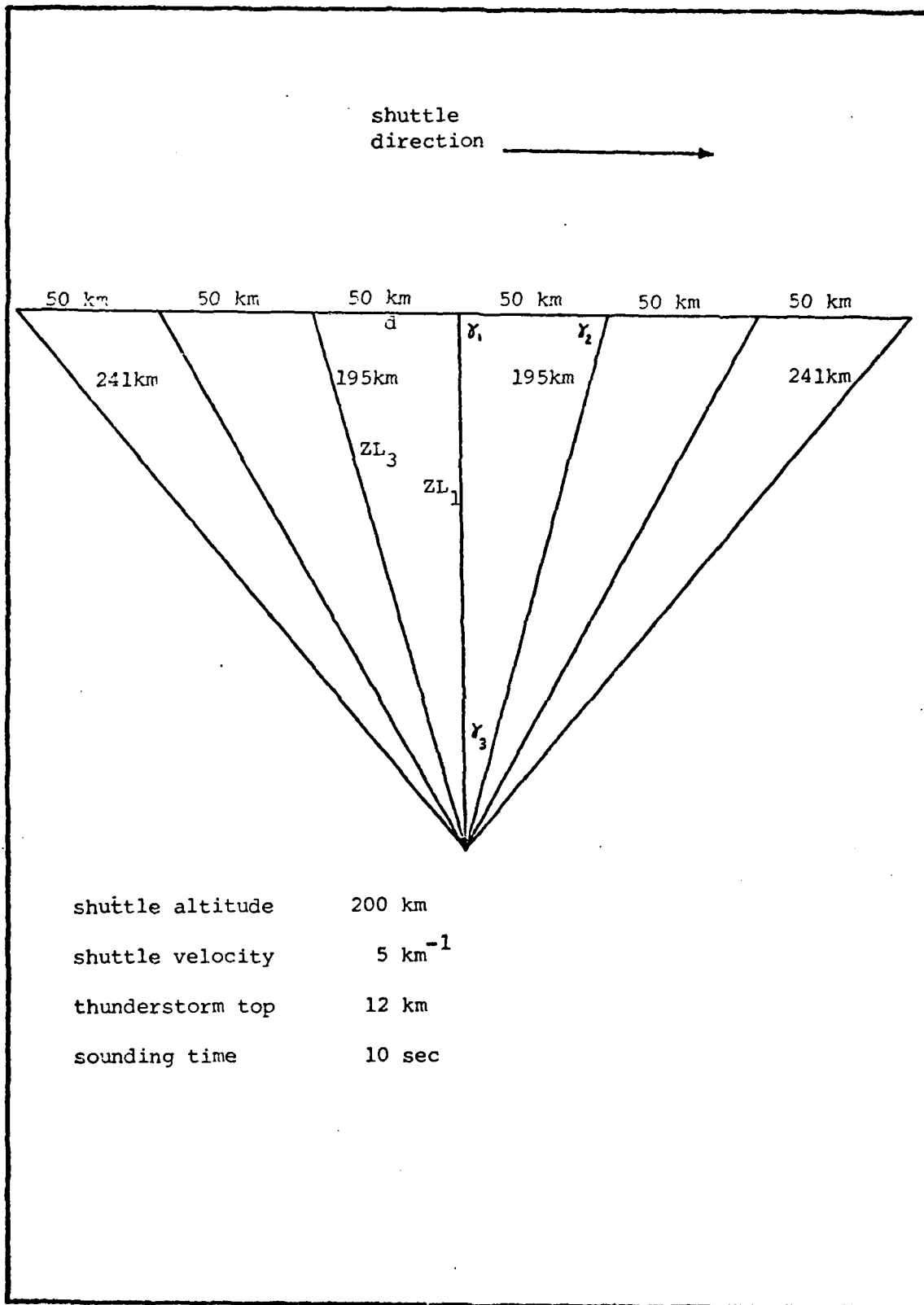


Figure 12. Shuttle overflight of a radar thunderstorm.

Table XIV

Sounding Time Tradeoff

<u>Top Height (km)</u>	<u>S/N $t_s = 10$ sec</u>	<u>S/N $t_s = 20$ sec</u>	<u>S/N $t_s = 30$ sec</u>
10	1.56	2.21	2.71
11	1.86	2.64	3.23
12	2.21	3.13	3.84
13	2.48	3.52	4.21
14	2.65	3.75	4.59
15	2.85	4.04	4.95
16	3.10	4.38	5.37
17	3.41	4.82	5.91

It is obvious that S/N increases as t_s increases as noted by Equation 85. Since a minute is required between temperature measurements, $t_s = 20$ sec will provide the largest S/N and ensure the cloud top stays within range. Thus, one storm top can be measured within a loitering time of 100 seconds if a rate of change in temperature is required. A maximum of 4 to 5 temperature measurements are possible if only single measurements are required within 80 to 100 seconds.

A possible operating sequence where $t_s = 20$ sec is for the lidar to lock onto a desired storm top and determine a temperature which would require 20 seconds. A minute later, a second measurement would be taken and the rate of change in temperature computed (Scenario II in Chapter IX will do this). The lidar could then be aimed at the next thunderstorm of interest.

IX. Thunderstorm Vertical Velocity

Vertical velocity is a fundamentally important variable which is required by all numerical weather prediction models; however, vertical velocities are not usually measured directly and are therefore obtained indirectly with empirical relations.

Adler and Fenn (1979 c) studied thunderstorm vertical velocities with 5 minute interval infrared geosynchronous satellite data. They computed vertical velocities by an adiabatic method expressed as

$$w = \frac{1}{\frac{\partial T}{\partial Z}} \frac{d T_{BB}}{dt} \quad (96)$$

where w = vertical velocity of cloud top

$\partial T/\partial Z$ = a reasonable vertical lapse rate (8°k/km)

T_{BB} = minimum black-body cloud-top temperature.

Adler and Fenn (1979 c) demonstrated that the intensity of a thunderstorm is correlated with the occurrence of severe weather on the ground. They discovered that the first report of a tornado took place during or just after a period of cloud top ascent. This was apparent in seven out of eight cases studied with an infrared geosynchronous satellite field of view (FOV) of 10 km on a side. Even with this poor spatial resolution, it was determined that a 30 minute lead time could be provided to the public of a potential tornado.

Figure 13 illustrates a time vs temperature trace for two tornado production thunderstorms. These storms are part of a large complex which existed on May 6, 1975 and covered an area stretching from South Dakota to Texas. Storm top temperatures were measured by Adler

AD-A163 834

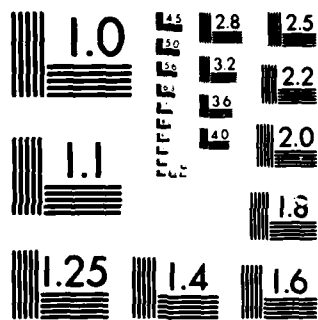
A FEASIBILITY STUDY THE DETERMINATION OF THUNDERSTORM
INTENSITY WITH A TE. (U) AIR FORCE INST OF TECH
WRIGHT-PATTERSON AFB OH SCHOOL OF ENGI.. C 2 LOWERY
DEC 82 AFIT/850/PH/82D-2 F/G 4/2

2/2

UNCLASSIFIED

NL

										END			
										FILED			
										DTL			



MICROCOPY RESOLUTION TEST CHART
NATIONAL BUREAU OF STANDARDS 1963-A

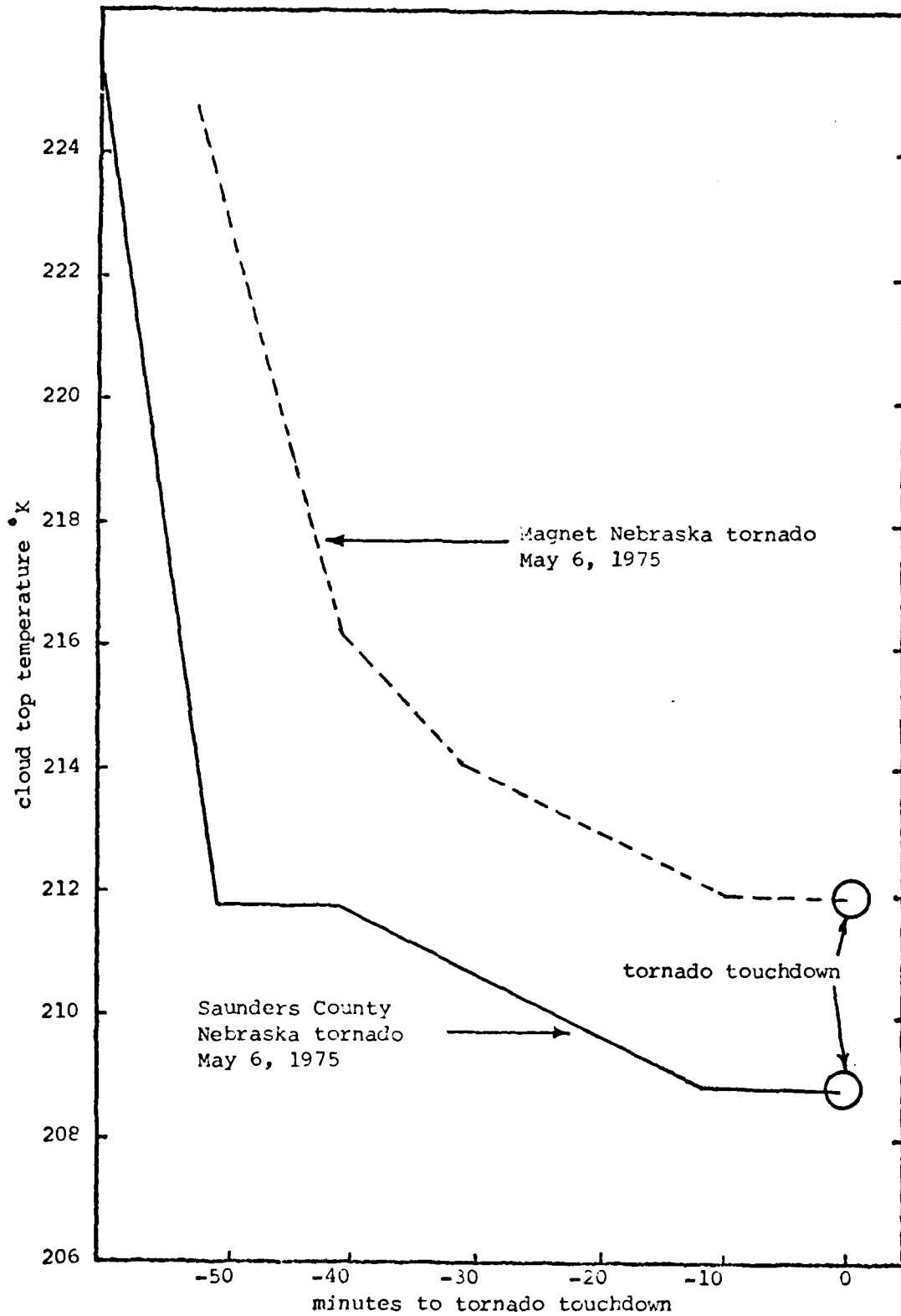


Figure 13. Profile of cloud top temperature vs time
90

and Fenn (1979 a) using an infrared geosynchronous satellite. The smoothed traces in Figure 13 illustrate the theory that severe weather occurs during, or soon after, a period of cloud top ascent indicating the storm is growing and cooling.

When studying thunderstorm vertical velocities, a distinction must be made between the vertical velocity of the cloud top and the vertical velocity of the updraft. Due to mixing of air at the cloud top, there is a difference between the two velocities. Kyle et al (1976) flew aircraft into updrafts and was able to fit a relationship to the results which can be written as

$$w = w_0 \exp \left[- a \left(\frac{r}{R} \right)^2 \right] \quad (97)$$

where w = updraft velocity at distance r

w_0 = peak updraft velocity

a = regression constant 2.3

r = radial distance from updraft core

R = radius of the updraft 1-3 km (Kropfli and Miller, 1976).

Adler and Fenn (1979 c) calculated an average vertical velocity \bar{w} over a circular area of radius r^1 . The result is

$$\bar{w} = \frac{w_0}{a} \left(\frac{R}{r^1} \right)^2 \left[1 - \exp \left[- a \left(\frac{r^1}{R} \right)^2 \right] \right] \quad (98)$$

This equation links the vertical growth of a thunderstorm to its updraft velocity.

Adler and Fenn (1979 a,b,c) used the SMS-2 and GOES-1 infrared satellites which have FOVs of 100 km^2 (10 km on a side). This implies that the circular radius of integration r^1 is 5.6 km. A typical

updraft radius R is 3 km according to Kropfli and Miller (1976).

Through Equation 98, it is seen that

$$\bar{w} = .12 w_0.$$

This implies that the updraft velocity of a thunderstorm is 8.3 times larger than the storm's mean vertical velocity as seen by a satellite. It is now quite evident that vertical velocity measurements are scale dependent.

Earlier, it was determined that a shuttle-borne lidar could illuminate 68.059 m² of cloud top. Using R = 3 km and r¹ = 4.655 m in Equation 98, it is seen that

$$\bar{w} \approx 1 w_0.$$

Vertical velocities can now be measured on the same scale as the actual updraft. For the first time, individual thunderstorm updrafts can be remotely sensed from orbit.

It is important to note that the lidar is actually measuring cloud top temperature and only through Equation 96 can the vertical velocity be determined.

Equation 96 can be rewritten for updraft velocities measured by the lidar as

$$w = 8.3 \frac{1}{\frac{\partial T}{\partial Z}} \frac{dT}{dt} \quad (99)$$

Thunderstorm top vertical velocities reported by Adler and Fenn (1979 c), for example, can now be altered to appear as if they were lidar derived (see Figures 14 and 15).

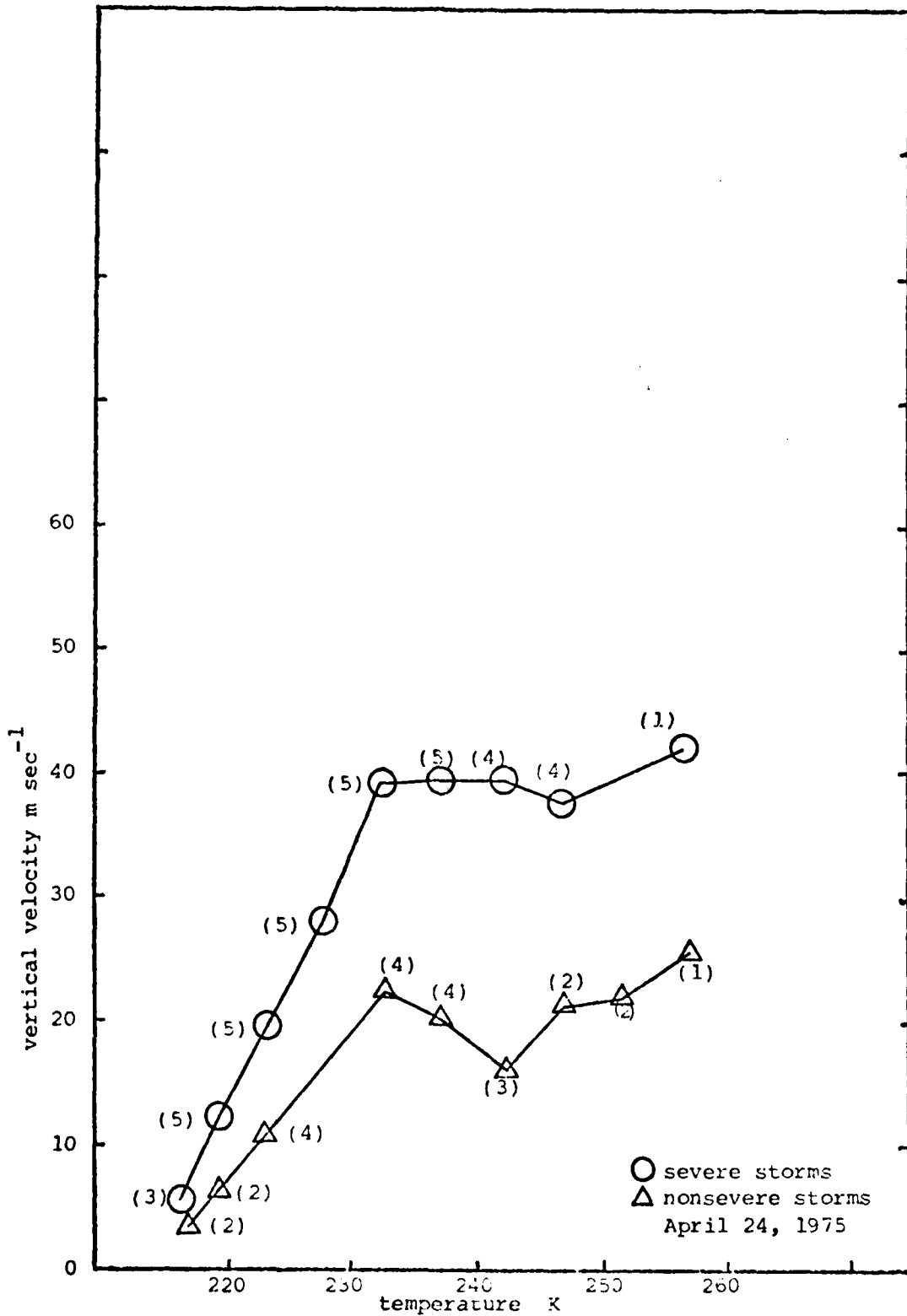


Figure 14. Vertical velocity vs cloud top temperature (after Adler and Dean, 1975 with changes)

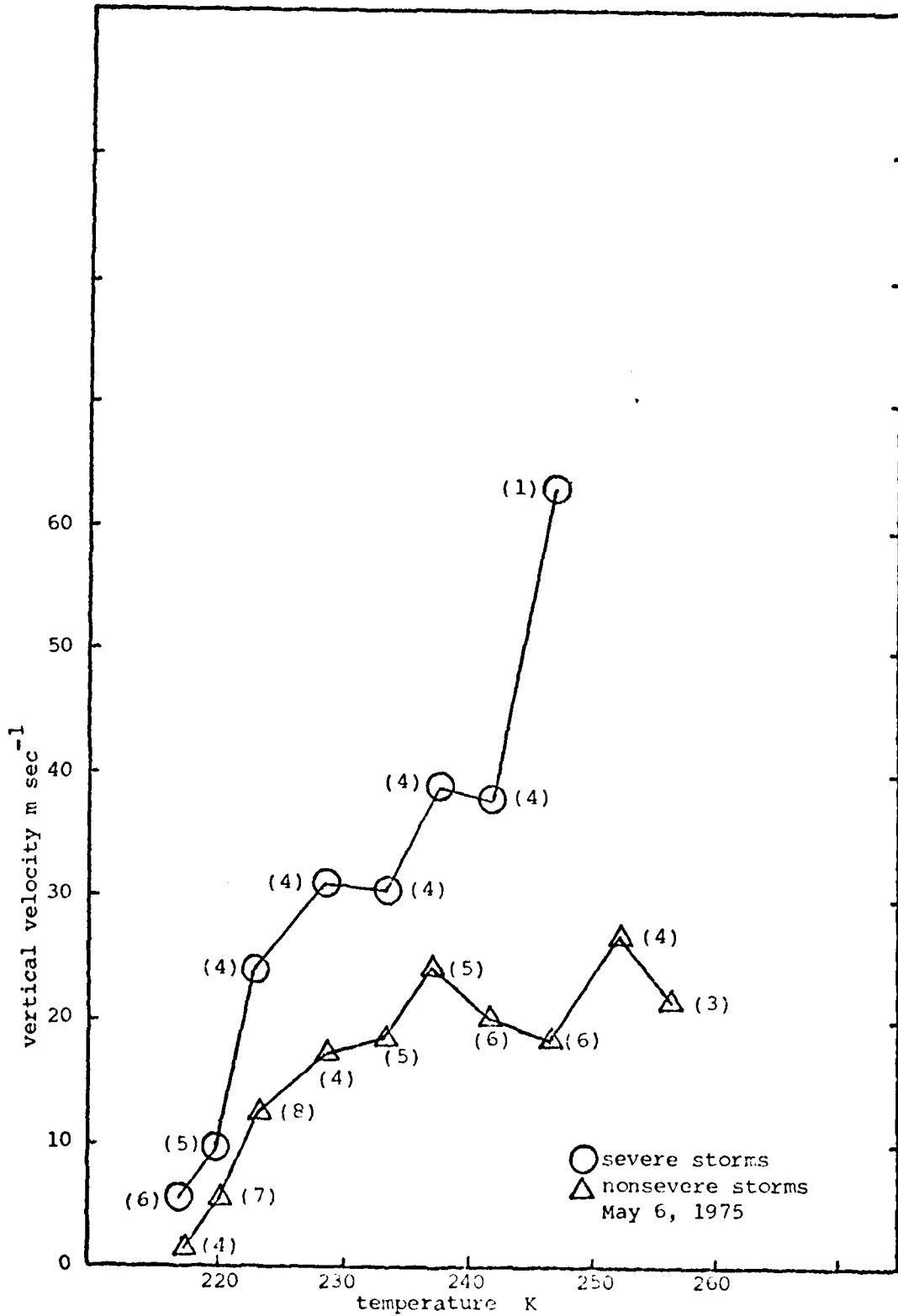


Figure 15. Vertical velocity vs cloud top temperature
 (after Allen et al., 1975, with changes)

Figure 14 is a composite profile of severe and non-severe thunderstorms observed in a storm complex stretching from Oklahoma to Missouri on 24 April 1975. The numbers in parentheses are the number of cases. Both severe and non-severe storms slow in their ascent as they approach the tropopause.

Figure 15 is similar except the storm complex runs from Texas to South Dakota and occurred on 6 May 1975. Table XV illustrates some statistical differences between severe and non-severe thunderstorms for the two storm complexes.

Table XV

Statistics on 24 April and 6 May 1975 Storm Complexes

24 April 1975 Storm Complex

Severe Storms:

Average Vertical Velocity	28.86 msec ⁻¹	@ 229°k
Standard Deviation	12.06 msec ⁻¹	

Non-severe Storms:

Average Vertical Velocity	15.54 msec ⁻¹	@ 231°k
Standard Deviation	6.81 msec ⁻¹	

6 May 1975 Storm Complex

Severe Storms:

Average Vertical Velocity	24.59 msec ⁻¹	@ 223°k
Standard Deviation	9.80 msec ⁻¹	

Non-severe Storms:

Average Vertical Velocity	15.62 msec ⁻¹	@ 227°k
Standard Deviation	7.53 msec ⁻¹	

The t-distribution test can be performed to see if there is a difference between vertical velocity of severe and non-severe storms for each storm complex.

The independent-t-test assumes the mean vertical velocity of severe and non-severe storms are normally distributed with variances unknown but equal. The following hypotheses can be established:

$$H_0: \mu_1 = \mu_2$$

$$H_1: \mu_1 \neq \mu_2$$

where H_0 = null hypothesis

H_1 = alternate hypothesis

μ_1 = population mean vertical velocity of severe storms

μ_2 = population mean vertical velocity of non-severe storms.

The formula for the independent-t-test is (Hines and Montgomery, 1980):

$$t = \frac{\bar{x} - \bar{y}}{\sqrt{\frac{1}{n_1} + \frac{1}{n_2}} \sqrt{\frac{\sum x_i^2 - n_1 \bar{x}^2 + \sum y_i^2 - n_2 \bar{y}^2}{n_1 + n_2 - 2}}} \quad (100)$$

with $n_1 + n_2 - 2$ degrees of freedom

where x_i, y_i = vertical velocity values for severe and non-severe cases respectively

n_1, n_2 = number of severe and non-severe data points

\bar{x}, \bar{y} = sample means for severe and non-severe cases.

The results of this t-test are displayed in Table XVI when using data from Figures 14 and 15.

Table XVI

More Statistics on the 24 April and 6 May 1975 Storm Complexes

24 April Storm Complex

$$t_0 = 2.63$$

$$df = 18$$

$$\alpha = .05$$

$$t_{.025, 18} = 2.101$$

$$t_0 > t_{.025, 18}$$

6 May Storm Complex

$$t_0 = 2.2$$

$$df = 14$$

using a 95% confidence interval ($\alpha = .05$)

$$t_{\frac{\alpha}{2}, n_1 + n_2 - 2} = t_{.025, 14} = 2.145$$

$$\text{so } t_0 > t_{.025, 14}$$

In both cases above, H_0 is rejected and there is a 95% chance that there is a difference between severe and non-severe thunderstorm updraft velocities.

Adler and Fenn (1979 c) examined 23 cases of storms near 10 km from both 24 April and 6 May 1975. Updrafts from severe and non-severe thunderstorms had average vertical velocities of 40.7 m sec^{-1} and 19.92 m sec^{-1} respectively. Using Equation 99, severe storms cooled at a rate of $2.4^\circ\text{k min}^{-1}$. An interesting exception to these numbers is the tornado that swept through Neosho, Missouri at 0040

Greenwich time on 25 April 1975. Updraft velocities at the cloud top reached 64.7 m sec^{-1} indicating a cooling of $4.0^\circ\text{k min}^{-1}$ (Adler and Fenn 1979 c).

Stereographic Observations

Hasler (1981) showed that stereographic observations of cloud heights and their temporal changes from two simultaneously scanning visible geosynchronous satellites is a fundamentally new tool for the atmospheric scientist. Stereographic measurements of cloud heights are based on simple geometric relationships and boast of horizontal resolution of 0.5 km. Conventional measurements with geosynchronous satellites have a spatial and temporal resolution of 1 km and 3 min. Stereographic capabilities are indeed impressive but are limited to daylight use. A shuttle-borne lidar only requires one instrument and can be used in day or night with horizontal resolution of several meters.

Mack et al (1982) analyzed stereographic data from several tropopause-penetrating thunderstorms over Oklahoma on 2 and 3 May 1979. He determined that moderate thunderstorms grew (cooled) at a rate of 2°k min^{-1} . These results agree closely with that of Adler and Fenn (1979 c) reported in the previous section.

Damaging Hailstorms

A large number of damaging hailstorm producing losses near \$100 million struck portions of New Mexico, Colorado, Wyoming, and Montana from May through August 1978. Reynolds (1980) examined these storms with visible and infrared data from a geostationary satellite. It was

determined that the coldest portion of the storm top was located near the area of hailfall. This cold portion of cloud top was 1-8 degrees colder than the surrounding anvil floor which was located at the tropopause. Reynolds was able to conclude that a strong correlation existed "between the onset of large hail (> 25 mm) and cloud-top temperatures becoming colder than the environmental tropopause temperature" (Reynolds, 1980: 345). Table XVII depicts typical data that Reynolds worked with.

Reynolds' discoveries pertaining to hailstorms implies another use for a shuttle-borne lidar. Instead of measuring rates of change in temperature, the lidar could take several measurements across the anvil floor within the 80 sec interval. Those towers with temperatures 1-8° colder than the surrounding top would be identified on the ground as locations of possible damaging hail. Figure 16 ideally shows a shuttle lidar making two measurements of a storm top well within the 80 second limit.

Scenario II

The first scenario considered in the previous chapter demonstrated that the shuttle lidar could recover a single temperature measurement from a hypothetical overshooting top. In that first scenario, the shuttle was orbiting at 200 km while the storm top was at 10 km. The retrieved temperature was 235°k. This second scenario will continue the first and measure the same cold area at a later time.

It is now known that the lidar can track the same target area for just over a minute. Assume a minute after the first measurement the same overshooting top is measured and through condition 12 the resultant

Table XVII
 Damaging Hailstorms of May-August 1978 (after Reynolds, 1980 with Changes)

Date	Location	Temperature Storm Top Ok	Trop Temp Ok	Max Hail Diameter mm	Area of Cloud Top Colder Than Trop (km ²)	Max Cloud Height (km)
7-18-78	Miles city, MT (GGW Sounding 7-19-78 OOGMT)	214	220	40-60	7630	14.4
6-15-78	Gillette, WY (RAP OOGMT 6-16-78)	210	214	40-80	3540	20.9
6-15-78	South Dakota (BIS OOGMT 6-16-78)	210	214	30-80	8575	18.5
6-27-78	Mosquard, NA (AMA OOGMT 6-28-78)	194	202	30-40	6900	19.1
5-23-78	Gillette, WY (RAP OOGMT 5-24-78)	209	211	40	2380	13.9
7-20-78	Casper, WY (RAP OOGMT 7-21-78)	210	216	40	3243	8.5
8-29-78	Loveland, CO (DEN OOGMT 8-30-78)	207	214	50-70	18,083	13.7
7-29-78	Miles City, MT (GGW OOGMT 7-30-78)	218	219	30	334	15.2
6-22-76	NHIRE	206	210	-	483	15.1

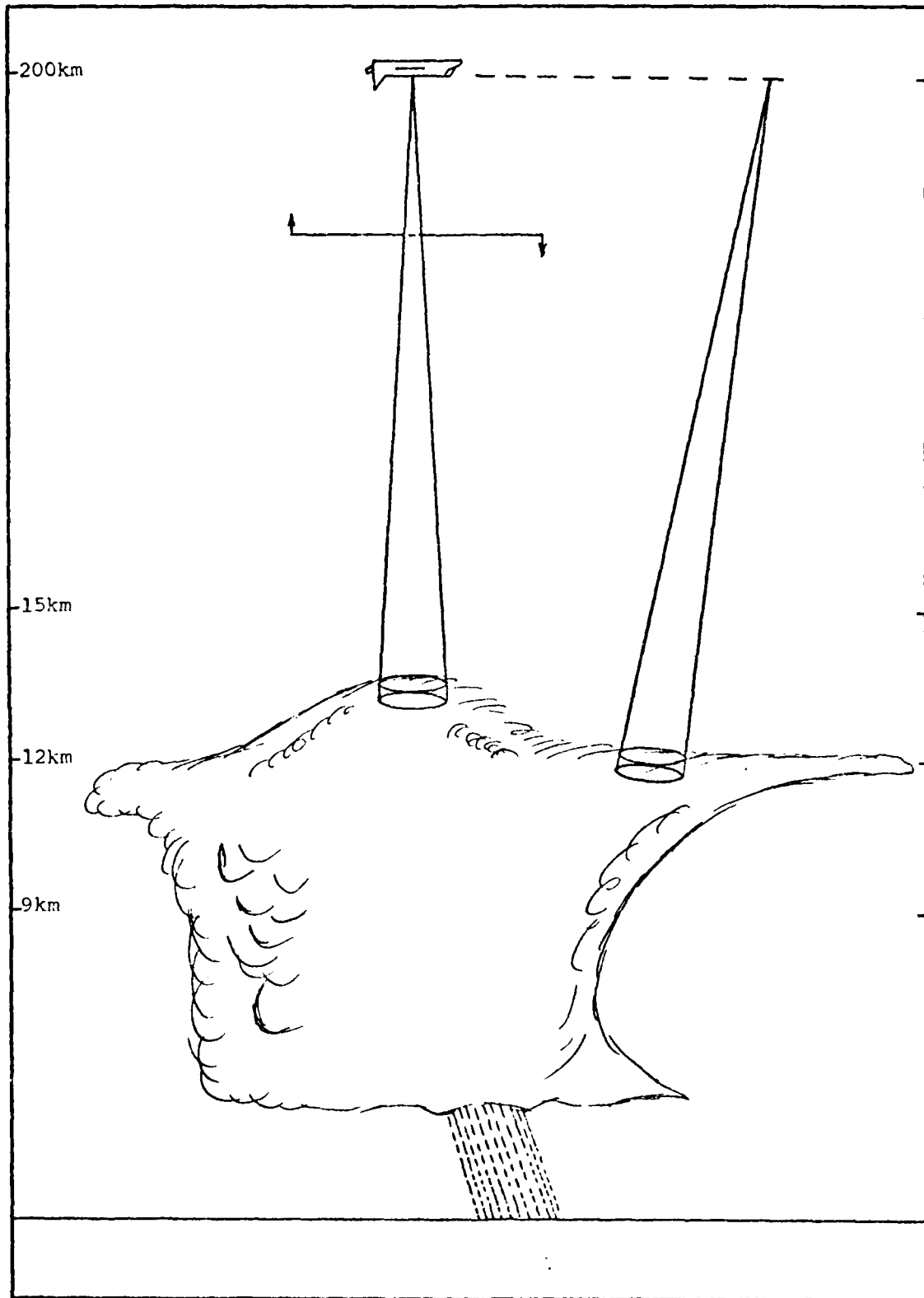


Figure 16. Historical of shuttle 1114 making general atmospheric measurements across the anvil flow.

absorption coefficient a_{g_0} is equal to $.0438 \text{ km}^{-1}$. At this time, the new storm top temperature and height are unknown except that the top is near 10 km. The value of A_0 from Equation 41 will still be $1742.73^\circ\text{k}^{3/2} \text{ m}^{-1}$. The new temperature T^* can be found still through Equation 43 using a seed guess temperature of 235° (value from the first measurement):

$$T^*_{i+1} = \frac{(1.439)(1421.436 \text{ cm}^{-1})}{\ln \left[(1742.73^\circ\text{k}^{3/2} \text{ m}^{-1})(.9999)(235^\circ\text{k}^{-3/2}) \right.}$$

$$\left. * \left(1 - \frac{e}{(10)(.7486)} \right) \frac{10^3}{.0438 \text{ km}^{-1}} \right]$$

$$= 230^\circ\text{k}.$$

So in one minute, an energetic updraft drove an already overshooting top upwards at which time the top cooled 5°k in one minute. A cooling rate of this magnitude would classify the thunderstorm as intense (Mack et al, 1982). The storm top vertical velocity according to Equation 96 is $.625 \text{ km min}^{-1}$.

The storm top is now located 10.625 km above the surface. The appropriate military and civilian organizations would be notified of the severe nature of the above storm and emergency action taken. The 80 second loitering time per storm top is now exceeded; therefore, the lidar would be aimed at the next suspicious thunderstorm.

X. Miscellaneous Considerations

Eye Safety

Table V (see Chapter VI) shows that the laser considered in this thesis develops a peak power of 1.8 MWatts. This is a great deal of power and would damage the human eye if the laser is viewed directly into the beam. The American Conference of Government Industrial Hygienists in 1973 established threshold values of energy density for intrabeam viewing. A pulsed laser operating near .7600 μm with pulse length less than 10^{-5} seconds has a threshold energy density of $6.5 \times 10^{-7} \text{ J cm}^{-2}$ according to the Conference (Smith and Platt, 1977). Therefore, there would be no eye damage if laser energy density remains below this threshold.

The space shuttle in this thesis orbits at 200 km. It must be determined if the eye could be damaged by observing the shuttle from the ground with the laser operating. The shuttle lidar has a full angle beam divergence of 1 mrad. The circular area illuminated A_L on the ground can be found by

$$A_L = \pi(Z_L \tan \theta/2)^2 \quad (101)$$

where Z_L = height of shuttle

θ = full angle beam divergence.

Table XVIII clearly shows that the shuttle-borne lidar poses no hazard to the naked eye of an observer on the ground. This will not be the case if the laser is viewed through a high powered telescope; however, this shuttle lidar is solely used to remote sense temperature

of thunderstorm tops and could never be viewed directly from the surface due to cloud attenuation.

Table XVIII

Laser Energy Density Reaching the Earth's Surface

Pulse Energy (J)	Energy Density at Surface (J cm ⁻²)
1	3.18x10 ⁻⁹
10	3.18x10 ⁻⁸
100	3.18x10 ⁻⁷

Calibration of the Lidar

The present instrument is a DIAL system featuring overlapping co linear transmission of two laser beams. DIAL theory according to Equation 19 requires that the extinction properties of the atmosphere be identified with exception to the resonant absorption effects which are to be determined. This implies that the instrument must be calibrated so that both lasers react in a similar manner.

Calibration could be accomplished by tuning the on-line laser to the off-line frequency. Simultaneous measurements from both lasers could be taken of transmitted and return signals. The differences would be used to normalize subsequent data runs. The on-line laser would then be tuned back to the absorbing wavelength and operations would begin. Calibration problems have been eliminated in this thesis by assuming atmospheric extinction at both wavelengths is the same except for the resonant absorption of oxygen.

Transmitter Configuration

Figure 17 is a block diagram of a lidar transmitter patterned after the DIAL device used by Kalshoven et al (1981). Solid lines indicate the passage of laser light while dashed lines indicate electrical power lines. The krypton gas laser is used to pump the two dye lasers.

Receiver Configuration

Figure 18 is a block diagram of a typical lidar receiver used for long range remote sensing taken from a variety of sources (Huffaker, 1978; Greco, 1980; Kalshoven et al, 1981; Spinhirne et al, 1982). This receiver features a 1.25 m diameter receiving telescope and a 1 nm spectral bandpass filter.

System Arrangement

Figure 19 portrays an idealized lidar system arranged in the shuttle cargo bay. Such an arrangement can easily interface with the space shuttle or Spacelab (Greco, 1980).

Viewing Geometry

Figure 20 shows possible viewing geometry and clearance angles for a downward viewing lidar (Huffaker, 1978). When considering the clearance angle of 75 degrees and nadir angle of 60 degrees, the lidar could search a maximum area of $3.8 \times 10^5 \text{ km}^2$ while operating from a 200 km orbit.

The Infrared Equivalent

This thesis has attempted to show that a laser operating from the space shuttle can measure the temperature of thunderstorm cloud tops.

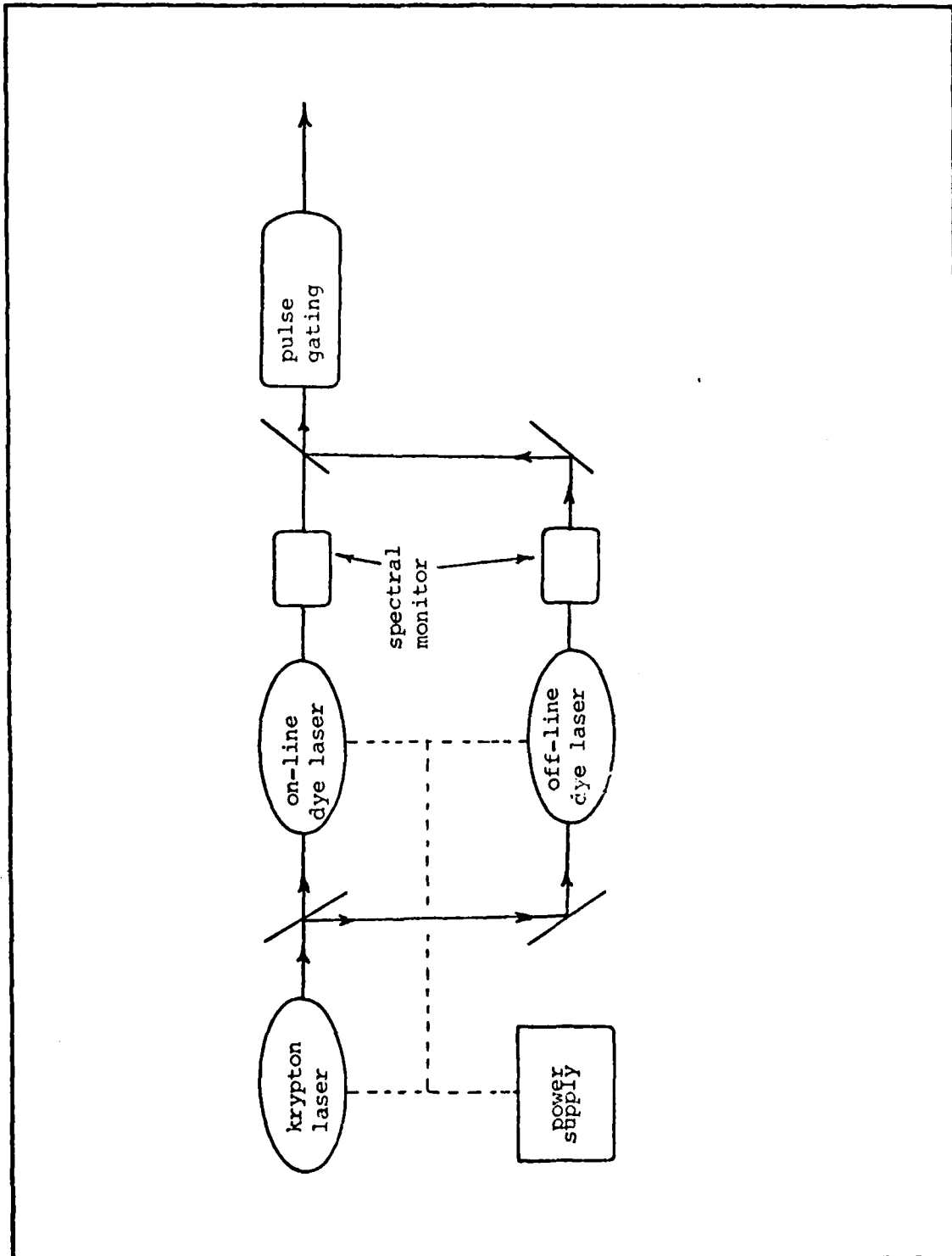


Figure 17. Idealized lidar transmitting system
 (after Kalshoven et al, 1981 with changes)

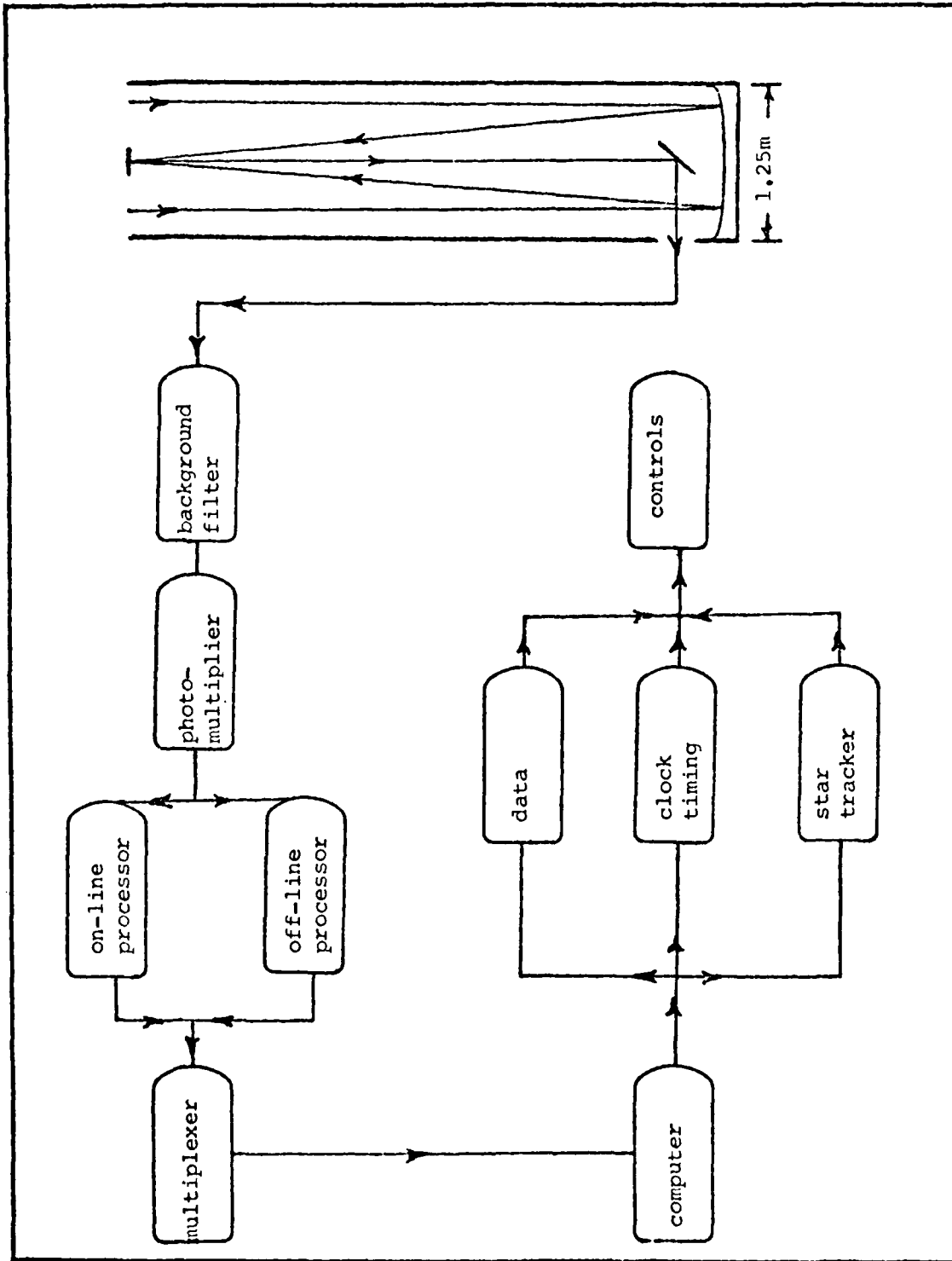


Figure 18. Idealized lidar receiving system (see text for references)

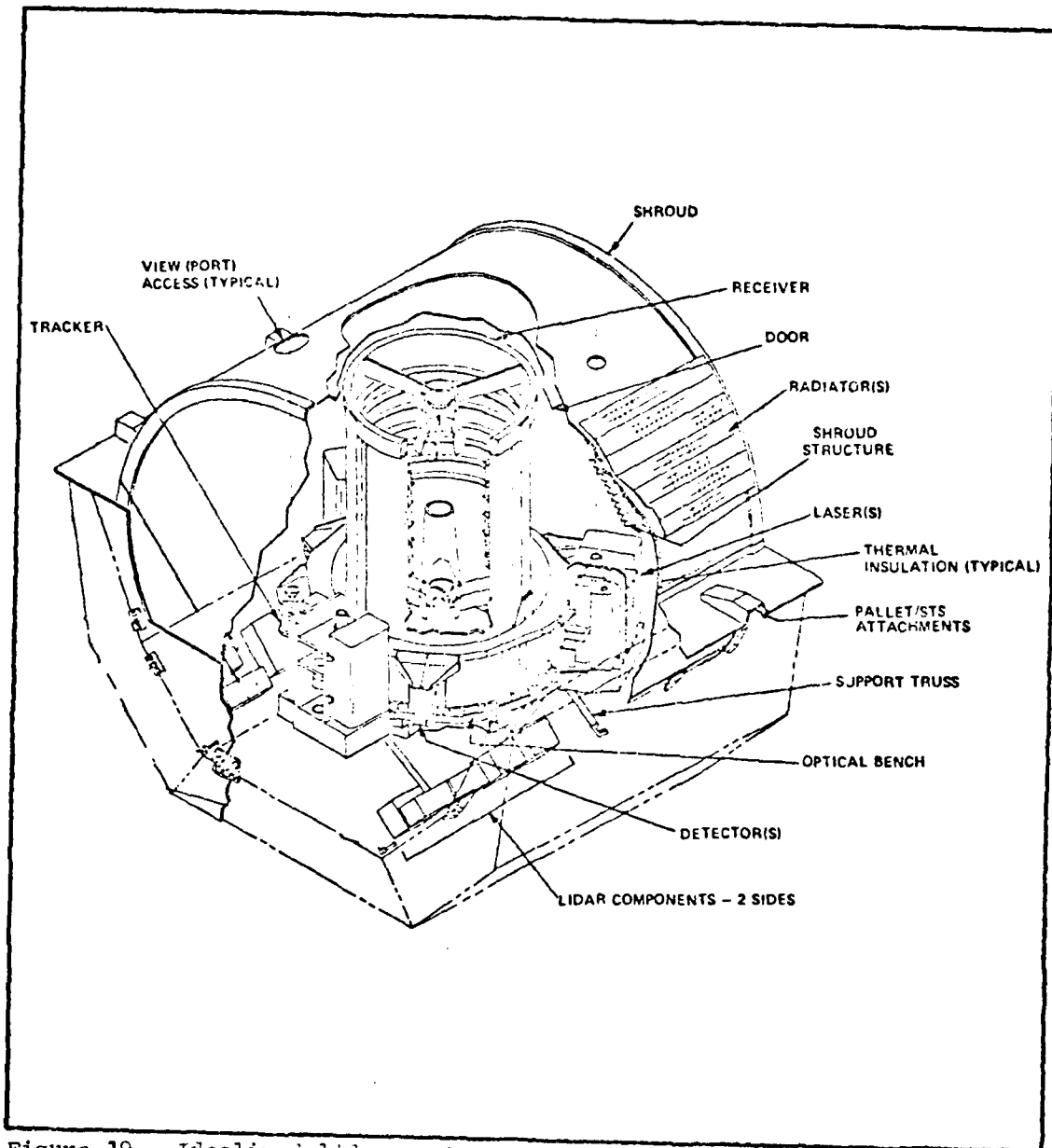


Figure 19. Idealized lidar system arrangement in shuttle cargo bay (after Greco, 1980 with changes)

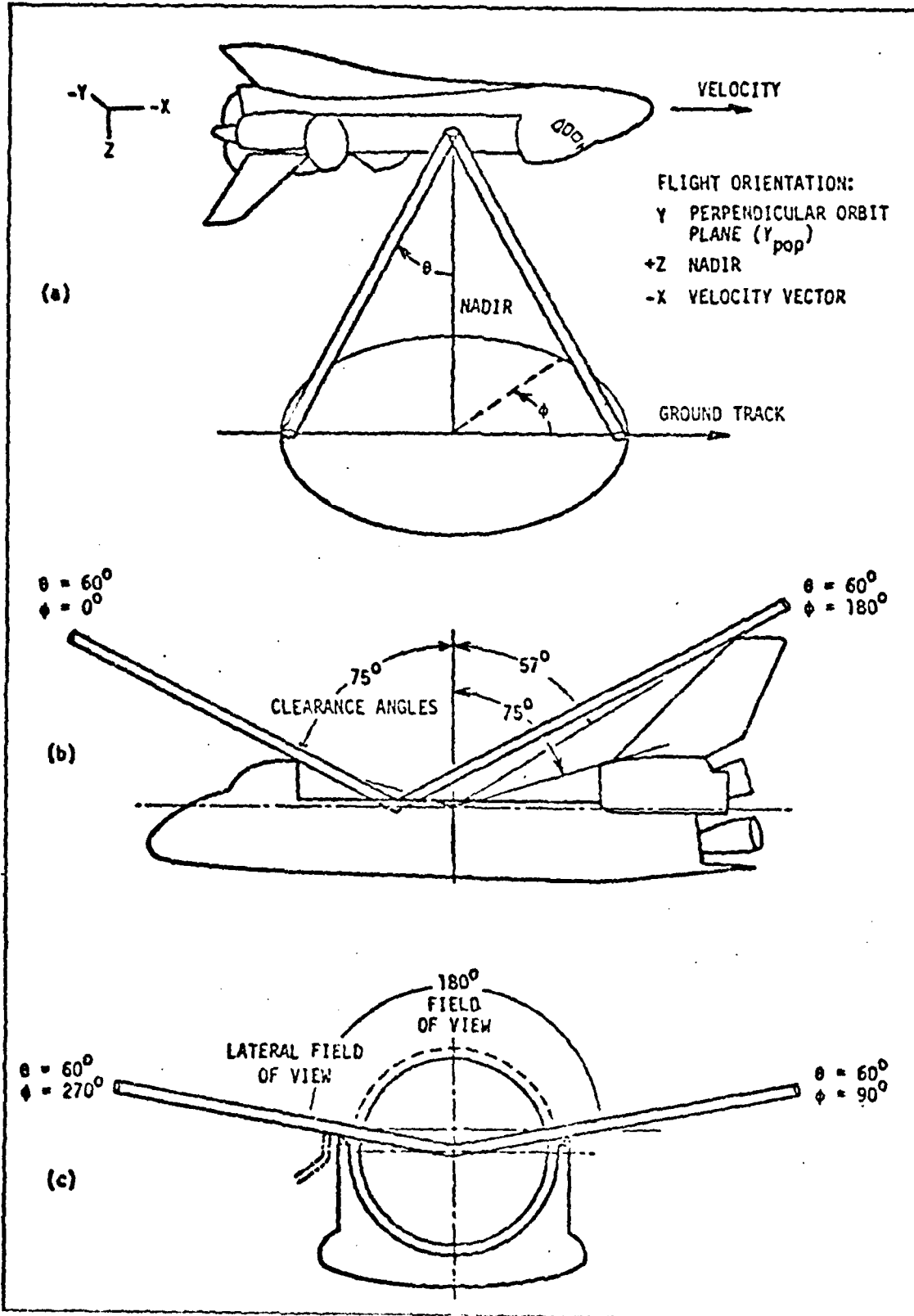


Figure 20. Linear viewing angles (after Hollander, 1977 with changes).

At this point, it would be interesting to know if an infrared radiometer operating from the shuttle could perform the same feat.

Adler et al (1982) flew at 18 km over thunderstorms in NASA's WB57F aircraft equipped with a 11 um scanning radiometer, a cloud top scanner (CTS). The CTS was accurate to approximately $\pm 2^{\circ}\text{K}$ at temperatures colder than 213°K . The instrument also features an 80 m resolution. Adler's general objective was to compare aircraft derived cloud top temperatures with those of geosynchronous satellites. In addition, he provides the first thunderstorm cloud top thermal mapping indicating the complex, continually changing nature of bubbling convective cells. It was determined that for typical thunderstorms the satellite derived temperatures were about 15°K warmer than the aircraft derived temperatures. This discrepancy results from the satellite's large field of view (FOV), 10×10 km, so that the temperature determined is some sort of average value for the 100 km^2 area. For small, growing thunderstorms, the satellite over estimated top temperatures by about $30\text{-}40^{\circ}\text{K}$ again due to FOV effects. According to Adler, a satellite FOV of 1 km would alleviate these problems.

The pioneering work of Adler et al (1982) seems to indicate that it would be feasible to operate a CTS with a FOV of 1 km and measure cloud top temperatures from the space shuttle. Nevertheless, high resolution infrared scanners generate a great deal of data which requires a large processing time before information can be passed onto the user. Processing time is 3 minutes for current geosynchronous infrared scanners (Hasler, 1981). The shuttle-borne lidar is not a scanning instrument and will deliver a temperature within 20 seconds depending on the sounding time used.

The lidar operating at 200 km achieves a horizontal resolution of 10 m for a storm top at 10 km. It is doubtful that an infrared scanner can ever be designed to match the lidar's super, high resolution. The shuttle lidar will therefore be capable of conducting a finely detailed thermal analysis of a storm top. Such an analysis could indeed reveal a very complex cloud top temperature structure which could provide new insight into thunderstorm dynamics.

The pointing of an orbiting lidar or infrared instrument at a particular overshooting top is a minor problem that could be solved in several ways. First, a shuttle qualified payload specialist could be trained to recognize and aim the instrument at a promising region on the cloud top. Second, a payload specialist could coordinate with meteorologist on the ground to help locate a suspicious storm top. Ground based personnel would use radar or satellite derived data to aid the payload specialist in locating a top that deserves special attention.

XI. Conclusion

This thesis has demonstrated for the first time that a lidar operating from the cargo bay of the space shuttle can successfully measure the intensity of thunderstorms. Thunderstorm intensity is monitored by measuring the time rate of change in temperature of a thunderstorm's overshooting top. Severe weather occurring on the ground takes place during, or just after a period of rapid cloud top cooling.

Temperature is measured using the differential absorption lidar (DIAL) technique. This technique features overlapping colinear transmission of two laser beams at different wavelengths. The first wavelength is set at .7696 μm which is a line center within the temperature sensitive, absorbing portion of the oxygen "A" band centered near .7700 μm . The second laser wavelength is set at .7614 μm which is a nearby spectral position where absorption from the oxygen "A" band is negligible. This DIAL technique is designed so that scattering and absorption properties of the atmosphere are identical except for oxygen resonant absorption at line center. It is shown that the lidar can measure the oxygen resonant absorption coefficient at the heights of typical thunderstorms. A temperature value is recovered by placing the retrieved absorption coefficient into a quickly converging iterative expression.

The two lasers required by the DIAL technique are dye lasers which are optically pumped by a krypton gas laser. The laser system output is a conservative 300 watts which is within space shuttle power constraints.

A variety of hypothetical thunderstorms are probed ranging in height from 10-17 km at different shuttle altitudes ranging from 100-250 km. Signal-to-noise calculations are performed considering the worse case at day with the sun directly overhead and at night with a full moon directly overhead. Success of the system is based on useful values of the signal-to-noise ratio.

The shuttle-borne lidar will remain within range of a given overshooting top for 80-100seconds while orbiting at 200 km. During this time, the rate of change in temperature can be determined by taking two measurements of the same overshooting top within a minute of each other. A storm is considered intense or severe if the rate of change in temperature is greater than $2^{\circ}\text{K min}^{-1}$. Alternately, during the 80-100 second loitering time, 4 single temperature measurements could be made of separate overshooting tops. Those tops determined to be 1-8 degrees colder than the tropopause correspond to locations on the ground where damaging hail (≥ 25 mm in diameter) can be expected.

A shuttle-borne temperature sensing lidar would be of great research value to the atmospheric sciences. Horizontal resolution is 10 m for a storm top at 10 km and shuttle operating at 200 km. This implies that, for the first time, high resolution thermal mapping of storm tops can be conducted from orbit. A shuttle-borne lidar could supplement existing severe storm monitoring networks by providing timely warnings of intensifying storms. In this way, such a sensor could prevent millions of dollars in property damage and possibly save lives.

Recommendations

As an effort to guide future research in the area of shuttle-borne lidars used to measure the intensity of thunderstorms, some recommendations can be made. The most obvious improvement that could be made is to investigate increasing the power available to the lidar. Nuclear power would not be needed. Additional fuel cells, each weighing 747 kg and delivering 840 kWh (Huffaker, 1978), could be placed in the shuttle's cargo bay.

Investigations could be conducted into increasing the pulse repetition rate (PRR) of dye lasers operating in the near infrared portion of the spectrum. As the PRR increases, small increases in the signal-to-noise ratio can be realized.

Chapter V mentions that a cirrus canopy resulting from previous convection will sometimes form above a thunderstorm thus masking the storm top from an orbiting sensor. This situation was not considered here but future work could attempt to model laser beam penetration of the cirrus canopy before the beam intercepts the storm top to determine if a useful signal can be recovered. Perhaps actual experimentation will be required.

Finally, current theory claims that a lidar can measure the atmospheric state variables (wind, humidity, pressure, and temperature according to Atlas and Korb, (1981)). It would be interesting to investigate developing an economical shuttle-lidar system which would be capable of measuring the atmospheric state variables. This innovation would lead to a complete orbiting weather station.

Bibliography

- Adler, Robert F. and Douglas D. Fenn. "Thunderstorm Monitoring from Geosynchronous Satellite," Preprints of Seventh Conference of Aerospace and Aeronautical Meteorology. 307-311. Boston, Mass: American Meteorological Society, 1976.
- . "Detection of Severe Thunderstorms Using Short Interval Geosynchronous Satellite Data," Preprints of Eleventh Conference on Severe Local Storms. 166-171. Boston, Mass: American Meteorological Society, 1979.
- . "Thunderstorm Intensity as Determined from Satellite Data." Journal of Applied Meteorology, 18: 502-517, April 1976.
- . "Thunderstorm Vertical Velocities Estimated from Satellite Data," Journal of Atmospheric Science, 36: 1747-1753, September 1979 c.
- , et al. "Thunderstorm Top Structure Observed by Aircraft Overflights with an Infrared Radiometer," Preprints of Twelfth Conference on Severe Local Storms. 160-163. Boston, Mass: American Meteorological Society, 1982.
- Anderson, Charles E. "Anvil Outflow Patterns as Indicators of Tornadic Thunderstorms," Preprints of Eleventh Conference on Severe Local Storms. 481-485. Boston, Mass: American Meteorological Society, 1979.
- Arn, Robert, M. Anvil Area and Brightness Characteristics as Seen from Geosynchronous Satellites. MS Thesis. Colorado State University, Colorado: Dept of Atmospheric Science, 1975.
- Atlas, David and C. Lawrence Korb. "Weather and Climate Needs for Lidar Observations from Space and Concepts for Their Realization," Bulletin of the American Meteorological Society, 62: 1270-1285, September 1981.
- Auvine, B. and C. Anderson. "The Use of Cumulonimbus Anvil Growth for Inferences About the Circulations in Thunderstorms and Severe Local Storms," Tellus, 26: 1001-1015, 1972.
- AWSM 105-124. Use of the Skew T, Log P Diagram in Analysis and Forecasting. Scott AFB, Illinois: Air Weather Service, July 1969.
- Barrell, H. and J. E. Sears. "The Refraction and Dispersion of Air for the Visible Spectrum," Philosophical Transactions of the Royal Society of London, 238: 1-64, 1939.
- Barton, I. J. and J. F. LeMarshall. "Differential-Absorption Lidar Measurements in the Oxygen "A" Band Using a Laser Lidar and Stimulated Raman Scattering," Optics Letters, 4: 78-80, March 1979.

- Beckman, Samuel K. "Relationship Between Cloud Bands in Satellite Imagery and Severe Weather," Preprints of the Twelfth Conference on Severe Local Storms. 483-486. Boston, Mass: American Meteorological Society, 1982.
- Boucher, R. J. "Relationship Between the Size of Satellite-Observed Cirrus Shields and the Severity of Thunderstorm Complexes," Journal of Applied Meteorology, 6: 564-572, March 1967.
- Brooks, E. M. "The Tornado Cyclone," Weatherwise, 2: 32-33, 1949.
- Brown, J. M. and K. R. Knupp. "The Iowa Cyclonic-Anticyclone Tornado Pair and its Parent Thunderstorm," Monthly Weather Review, 108: 1626-1646, October 1980.
- Brown, Rodger A., editor. The Union City, Oklahoma Tornado of May 24, 1973. NOAA Tech Memo. EPL NSSL 80. National Severe Storms Laboratory. Norman, Oklahoma, December 1976.
- Browning, K. A. "Airflow and Precipitation Trajectories Within Severe Local Storms which Travel to the Right of the Winds," Journal of Atmospheric Science, 21: 634-639, November 1964.
- "Hail: The Structure and Mechanisms of Hailstorms," edited by G. B. Foote and C. A. Knight. Meteorological Monogram, 38. 160-163. Boston, Mass: American Meteorological Society, 1977.
- Burch, Darrell E. and David A. Gryvnak. "Strengths, Widths and Shapes of the Oxygen Lines near $13,100 \text{ cm}^{-1}$ (7620Å)," Applied Optics, 8: 1493-1499, July 1969.
- Burgess, D. W. and D. R. Devore. "Doppler Radar Utility in Severe Weather Warnings," Preprints of Eleventh Conference on Severe Local Storms. 577-579. Boston, Mass: American Meteorological Society, 1979.
- Byers, Horace R. and Roscoe R. Braham, Jr. "The Thunderstorm," Report of the Thunderstorm Project. Washington, D.C.: Department of Commerce, 1949.
- Chanin, Marie-Lise and Alain Hauchecorne. "Lidar Observations of Density Waves and Temperature in the Stratosphere and Mesosphere," Tenth International Laser Radar Conference. 67. Silver Springs, Md: American Meteorological Society, 1980.
- Collis, R. T. H. "Lidar," Applied Optics, 9: 1782-1787, August 1970.
- Cohen, Ariel et al. "Atmospheric Temperature Profiles from Lidar Measurements of Rotational Raman and Elastic Scattering," Applied Optics, 15: 2896-2900, November 1976.

- DeLuise, J. J., et al. "Separation of Dust and Molecular Scattering Contributions to the Lidar Observation: a Method," Applied Optics, 14: 1917-1923, 1975.
- Derr, V. E. "Some Directions in Laser Meteorology," Eighth International Laser Radar Conference. Drexel University, Pa: American Meteorological Society, 1977.
- Edlen, B. "The Dispersion of Standard Air," Journal of Optical Society of America, 43: 339, 1953.
- Elasser, W. M. and M. F. Culbertson, "Atmospheric Radiation Tables," Meteorological Monogram, 23. Boston, Mass: American Meteorological Society, 1960.
- Elterman, L. UV, Visible, and IR Attenuation for Altitudes to 50 km, 1968. AFCRL 68-0153. Air Force Systems Command. Bedford, Mass, 1968.
- Ely, Robert I. A Laser Meteorological System Study. NWL Tech. Report No. TR 2839. U.S. Naval Weapons Lab., Dahlgren, Virginia, September 1972.
- Endemann, M. and R. L. Byer. "Simultaneous Remote Measurements of Atmospheric Temperature and Humidity Using a Continuously Turnable IR Lidar," Applied Optics, 20: 3211-3217, September 1981.
- . "Remote Single-Ended Measurements of Atmospheric Temperature and Humidity at 1.77 μm using a Continuously Tunable Source," Optics Letters, 5: 452-454, October 1980.
- Evans, W. E. Remote Probing of High Cloud Cover via Satellite-Boring Lidar. NASA CR 96893. Stanford Research Institute, 1968.
- Fernald, F. G., et al. "Determination of Aerosol Height Distribution by Lidar," Journal of Applied Meteorology, II: 482-489, April 1972.
- Fiacco, G. and L. O. Smullin. "Detection of Scattering Layers in the Upper Atmosphere (60-140 km) by Optical Radar," Nature, 199: 1275-1276, September 1963.
- Fujita, T. T. "Proposed Mechanism of Tornado Formation from Rotating Thunderstorms," Preprints of Eighth Conference on Severe Local Storms. 191-196. Boston, Mass: American Meteorological Society, 1973.
- . "Tornadoes Around The World," Weatherwise, 26: 56-57, 1973 b.
- . "Manual of Downburst Identification for Project Nimrod," SMRP #156, 1978.

- . "Infrared, Stereo-height, Cloud-Motion, and Radar-Echo Analysis of SESAME-DAY Thunderstorms," Preprints of Twelfth Conference on Severe Local Storms. 213-216. Boston, Mass: American Meteorological Society, 1982.
- "Global Atmospheric Reserach Project," GARP Publications Series 11, World Meteorological Organization, March 1973.
- Gill, R., et al. "Measurement of Atmospheric Temperature Profiles Using Raman Lidar," Journal of Applied Meteorology, 18: 225-227, February 1979.
- Goyer, G. G. and R. Watson. "The Laser and its Application to Meteorology," Bulletin of the American Meteorological Society, 44: 564-570, September 1963.
- Grams, Gerald W. "Laser Atmospheric Studies: An Overv iew of Recent Work and Potential Contributions to the Atmospheric Sciences," Bulletin of the American Meteorological Society, 59: 1160-1164, September 1978.
- Greco, R. V. Atmospheric Lidar Multi-User Instrument System Definition Study. NASA CR 3303, August 1980.
- Gucker, F. T. and Basu, S. Right-Angle Molecular Light Scattering from Gases. Scientific Report No. 1, Contract AF 19122-400. University of Indiana, 1953.
- Harrison, H., et al. "Mie-Theory Computations of Lidar and Nephelometric Scattering Parameters for Power Law Aerosols," Applied Optics, 11: 2880-2885, December 1972.
- Hasler, A. F. "Stereographic Observations from Geosynchronous Satellites: An Important New Tool for the Atmospheric Sciences," Bulletin of the American Meteorological Society, 62: 194-212, February 1981.
- Hess, Seymour L. Introduction to Theoretical Meteorology. New York: Holt, Rinehart and Winston, 1959.
- Heymsfield, Gerald M., et al. "Evolution of the Upper-level Structure of Thunderstorms on May 2, 1979," Preprints of Twelfth Conference on Severe Local Storms, 197-200. Boston, Mass: American Meteorological Society, 1982.
- Hines, William W. and Douglas C. Montgomery. Probability and Statistics in Engineering and Management Science (second edition). New York: John Wiley and Sons, Inc., 1980.
- Hinkley, E. D., editor. Laser Monitoring of the Atmosphere. New York: Springer-Verlag Berlin Heidelberg, 1976.

- Hobbs, Peter V. (editor) and Deepak Adarsh. Clouds Their Formation, Optical Properties and Effects. New York: Academic Press, 1981.
- Huffaker, R. M., editor. Feasibility Study of Satellite-Borne Lidar Global Wind Monitoring System. NOAA Tech Memo. ERL WPL 37. Boulder, Colorado, 1978.
- Johnson, Conrad L. "Public Response to Severe Weather Alerts ... Apathy or Alarm?," Preprints of Tenth Conference on Severe Local Storms. 448-452. Boston, Mass: American Meteorological Society, 1977.
- Johnson, L. A. Coherent Lidar As a Tool for Remote Temperature Sensing in the Troposphere. NOAA Tech Memo. ERL WPL-41. Boulder, Colorado, 1979.
- Junge, C. E. "Our Knowledge of the Physics-Chemistry of Aerosols in the Undisturbed Marine Environment". Journal of Geophysical Research, 77, 5183-5200, 1972.
- Kalshoven, James E., Jr., et al. "Laser Remote Sensing of Atmospheric Temperature by Observing Resonant Absorption of Oxygen," Applied Optics, 20: 1967-1971, June 1981.
- Kerker, M. The Scattering of Light and Other Electromagnetic Radiation. New York: Academic Press, 1969.
- Ketter, Robert L. and Sherwood P. Prawell, Jr. Modern Methods of Engineering Computation. New York: McGraw-Hill Book Co., 1969.
- Korb, C. L. and C. Y. Weng. "A Two-Wavelength Lidar Technique for the Measurement of Atmospheric Temperature Profiles," Nineth International Laser Radar Conference, 185. Munich, Germany: American Meteorological Society, 1979.
- Kyle, T. G., et al. "Fitting Measurements of Thunderstorm Updraft Profiles to Model Profiles," Monthly Weather Review, 104: 611- 617, May 1976.
- Lebow, P., et al. "Remote Laser Measurement of Temperature and Humidity Using Differential Absorption in Atmospheric Water Vapor," Eleventh International Laser Radar Conference, 30-32. Madison, Wis: American Meteorological Society, 1982.
- Lemon, L. R., et al. "Tornado Production and Storm Sustenance," Preprints of Ninth Conference on Severe Local Storms. 100-104.
- "Doppler Radar Application to Severe Thunderstorm Study and potential Real-Time Warnings," Bulletin of the American Meteorological Society, 58: 1187-1193, November 1977.

- Lemon, L. R. "On Improving National Weather Service Severe Thunderstorm and Tornado Warnings," Preprints of Eleventh Conference on Severe Local Storms. 569-572. Boston, Mass: American Meteorological Society, 1979.
- Lemon, L. R. and Charles A. Doswell III. "Severe Thunderstorm Evaluation and Mesocyclone Structure as Related to Tornadogenesis," Monthly Weather Review, 107: 1184-1197, September 1979b.
- Ligda, M. G. H. Proceedings of First Conference on Laser Technology. (Secret). Office of Naval Research, Boston, Mass Office, 1: 63, 1964.
- Marshall, Timothy P. and Richard E. Peterson. "Explosive Development of an Eastern Kansas Thunderstorm," Preprints of Eleventh Conference on Severe Local Storms. 64-71. Boston, Mass: American Meteorological Society, 1979.
- Marwitz, J. D. "The Structure Motion of Severe Hailstorms. Part I: Supercell Storms," Journal of Applied Meteorology, 11: 166-179, February 1972.
- "The Structure and Motion of Severe Hailstorms, Part III: severely Sheared Storms," Journal of Applied Meteorology, 11: 189-201, February 1972b.
- Murray, E. R., et al. "Measurement of Average Atmospheric Temperature Using a CO₂ Laser Radar," Applied Optics, 19: 1794-1797, June 1980.
- McCann, Donald W. "On Overshooting-Collapsing Thunderstorm Tops," Preprints of Eleventh Conference on Severe Local Storms. 427-432. Boston, Mass: American Meteorological Society, 1979.
- McClatchey, R. A., et al. Optical Properties of the Atmosphere. AFCRL 71-0279. Air Force Systems Command. Bedford, Mass, 1971.
- NASA 2228. Eleventh International Laser Radar Conference. University of Wisconsin, Wis., 1982.
- NASA SP 433. Shuttle Atmospheric Lidar Research Program, Washington, D.C., 1979.
- , et al. Satellite Observations of the Onset and Growth of Severe Local Storms. NASA CR 157046. Washington, D.C., 1977.
- Negri, A. J. and Robert Mack. "Satellite Infrared, Stereo, and Radar Observations of Tornadic Thunderstorms on April 10, 1979," Preprints of Twelfth Conference on Severe Local Storms. 164-167. Boston, Mass: American Meteorological Society, 1982.

- Newton, C. W. "Dynamics of Severe Convective Storms," Meteorological Monogram, 27. 33-58. Boston, Mass: American Meteorological Society, 1977.
- Nielsen, Philip E. Power Engineering for Directed Energy Weapons. Report No. 1815-80. Air Command and Staff College: Maxwell AFB, Alabama, 1980.
- O'Shea, Donald C., et al. Introduction to Lasers and Their Applications. Reading, Mass: Addison-Wesley, 1978.
- Ostby, Frederick P. and David M. Higginbotham. "Tornado Predictability As a Function of Geography and Intensity," Preprints of Twelfth Conference on Severe Local Storms. 176-179. Boston, Mass: American Meteorological Society, 1982.
- Penner, S. S. Quantitative Molecular Spectroscopy and Gas Emissivities. Boston: Addison-Wesley, 1959.
- Platt, C.M.R. "Lidar and Radiometric Observations of Cirrus Clouds," Journal of Atmospheric Science, 30: 1191-1204, 1973.
- . "Lidar Backscatter From Horizontal Ice Crystal Plates," Journal of Applied Meteorology, 4: 482-488, April 1978.
- . et al. "Some Microphysical Properties of an Ice Cloud From Lidar Observations of Horizontally Oriented Crystals," Journal of Applied Meteorology, 17: 1220-1224, August 1978.
- . "Remote Sounding of High Clouds: I. Calculations of Visible and infrared Optical Properties From Lidar and Radiometer Measurements," Journal of Applied Meteorology, 18: 1130-1143, September 1979.
- Pruppacher, Hans R. and James D. Klett. Microphysics of Clouds and Precipitation. Boston: D. Reidel Publishing Company, 1980.
- Pryor, S. P. Measurement of Thunderstorm Cloud-Top Parameters Using High Frequency Satellite Imagery. MS Thesis. Colorado State University, Colorado: Dept of Atmospheric Science, 1978.
- Purdom, James. "Satellite Imagery and Severe Weather Warnings," Preprints of Seventh Conference on Severe Local Storms. 120-137. Boston, Mass: American Meteorological Society, 1971.
- . "Some Uses of High-Resolution GOES Imagery in the Mesoscale Forecasting of Convection and its Behavior," Monthly Weather Review, 104: 1474-1483, December 1976.
- Reynolds, David W. "Observations of Damaging Hailstorms From Geosynchronous Satellite Digital Data," Monthly Weather Review, 103: 337-343, March 1980.

- Rubeska, I. and B. Moldan. Atomic Absorption Spectroscopy. Cleveland: CRC Press, 1969.
- Russel, P. B. and B. M. Morley. "Orbiting Lidar Simulations, 2: Density, Temperature, Aerosols, and Cloud Measurements by a Wavelength-Combining Technique," Applied Optics, 21: 1554-1563, May 1982.
- Rust, David W., et al. "Research on Electrical Properties of Severe Thunderstorms in the Great Plains," Bulletin of the American Meteorological Society, 62: 1286-1293, September 1981.
- Sikdar, D., et al. "Convective Transport of Mass and Energy in Severe Storms over the United States--An Estimate from Geostationary Altitude," Tellus, 22: 521-532, 1970.
- Smith, William L. and C. M. R. Platt. A Laser Method of Observing Surface Pressure and Pressure--Altitude and Temperature Profiles of the Troposphere from Satellites. NOAA Tech Memo. Ness 89. Washington, D.C., 1977.
- Spinhirne, J. D., et al. "Cloud-Top Remote Sensing by Airborne Lidar," Applied Optics, 21: 1564-1571, May 1982.
- Suchman, David. "Combining and Comparing Satellite and Radar Brightness Statistics During SESAME 1979," Preprints of Twelfth Conference on Severe Local Storms. 232-235. Boston, Mass: American Meteorological Society, 1982.
- Tecson, Jaime J., et al. "Thunderstorm Associated Cloud Motions as Computed from 5-Minute SMS Pictures," Preprints of Tenth Conference on Severe Local Storms. 22-29, Boston, Mass: American Meteorological Society, 1977.
- Thekaekara, Matthew P. "Extraterrestrial Solar Spectrum, 3000-6100 Å at 1Å Intervals," Applied Optics, 13: 518-522, March 1974.
- Wark, D. Q. and D. M. Mercer. "Absorption in the Atmosphere by the Oxygen "A" Band," Applied Optics, 4: 839-844, July 1965.
- , and S. Fritz. "A Tornado-Producing Cloud Pattern Seen from TIROS 1," Bulletin of the American Meteorological Society, 42: 447-460, September 1971.
- Whitney, L. F., Jr. "Severe Storm Clouds as Seen from TIROS," Journal of Applied Meteorology, 2: 501-507, April 1963.
- Wilson, J., et al. "Operational Application of Meteorological Doppler Radar," Bulletin of the American Meteorological Society, 61: 1154-1168, October 1980.
- Yuen, C. W. Observations of Severe Convective Storms from SMS-1 Satellite Studies of Soundings and Imaging Measurements. NASA CR 521798. University of Wisconsin, Wis., 1977.

Vita

Craig Zalmar Lowery was born on 24 February 1955 in Los Angeles, California, the son of James A. Lowery and his wife, Marie Eileen. In August 1978, he received his bachelor's degree in meteorology from Texas A&M University in College Station, Texas. Upon graduation, he was selected to attend the USAF Officer Training School where he was commissioned a Second Lieutenant. In December 1978, he was assigned to the North American Aerospace Defense Command (NORAD) in Cheyenne Mountain, Colorado Springs, Colorado. There he served as a team chief for the Atmospheric/Solar Forecasting Detachment. He received the Air Force Joint Service Commendation Award for his work at NORAD prior to his selection to the first class in space operations at the Air Force Institute of Technology in 1981.

Permanent address: 308 Sheryl Drive
Victoria, Texas 77901

This thesis was typed by Mrs Anna L. Lloyd.

UNCLASSIFIED

SECURITY CLASSIFICATION OF THIS PAGE (When Data Entered)

REPORT DOCUMENTATION PAGE		READ INSTRUCTIONS BEFORE COMPLETING FORM
1. REPORT NUMBER AFIT/GSO/PH/82D-2	2. GOVT ACCESSION NO. AD-A163 834	3. RECIPIENT'S CATALOG NUMBER
4. TITLE (and Subtitle) A FEASIBILITY STUDY: THE DETERMINATION OF THUNDERSTORM INTENSITY WITH A TEMPERATURE SENSING SHUTTLE-DORNE LIDAR	5. TYPE OF REPORT & PERIOD COVERED MS THESIS	
	6. PERFORMING ORG. REPORT NUMBER	
7. AUTHOR(s) Craig Z. Lowery, Capt., USAF	8. CONTRACT OR GRANT NUMBER(s)	
9. PERFORMING ORGANIZATION NAME AND ADDRESS AIF FORCE INSTITUTE OF TECHNOLOGY DEPARTMENT OF PHYSICS WRIGHT-PATERSON AFB OH 45433	10. PROGRAM ELEMENT, PROJECT, TASK AREA & WORK UNIT NUMBERS	
11. CONTROLLING OFFICE NAME AND ADDRESS	12. REPORT DATE Dec 1982	
	13. NUMBER OF PAGES 123	
14. MONITORING AGENCY NAME & ADDRESS (if different from Controlling Office)	15. SECURITY CLASS. (of this report) UNCLASSIFIED	
	15a. DECLASSIFICATION/DOWNGRADING SCHEDULE	
16. DISTRIBUTION STATEMENT (of this Report) Approved for public release; distribution unlimited		
17. DISTRIBUTION STATEMENT (of the abstract entered in Block 20, if different from Report)		
18. SUPPLEMENTARY NOTES Approved for public release LAW AFB 150-1 LEN E. WOLAVER 16 JAN 86 Dean for Research and Professional Development Air Force Institute of Technology (AFIT) Wright-Patterson AFB OH 45433		
19. KEY WORDS (Continue on reverse side if necessary and identify by block number) Laser Meteorological Instruments Lidar Thunderstorms Remote Sensing Temperature Space Shuttle		
20. ABSTRACT (Continue on reverse side if necessary and identify by block number) This thesis examines the feasibility of operating a lidar (laser radar) from the space shuttle and having this instrument measure the intensity of thunderstorms. Thunderstorm intensity is monitored by measuring the time rate of change in temperature of the top 0.5 km of a thunderstorm. Severe weather occurring on the ground takes place during, or just after a period of rapid cloud top cooling. Temperature is measured with two channels using a differential absorption lidar (DIAL) beam which determines the differential absorption of oxygen in the oxygen "A" band near .7700um. Cont'd		

DD FORM 1 JAN 73 1473

EDITION OF 1 NOV 65 IS OBSOLETE

UNCLASSIFIED

SECURITY CLASSIFICATION OF THIS PAGE (When Data Entered)

Abstract (cont'd)

One wavelength is set at .7696 μm which is a temperature sensitive oxygen absorbing line while the second wavelength is set at .7614 μm where oxygen absorption is negligible. The lidar can measure the oxygen resonant absorption coefficient at the heights of typical thunderstorm tops. A temperature value is recovered by placing the retrieved O_2 absorption coefficient into a quickly converging iterative expression. Hypothetical thunderstorms with heights from 10-17 km are probed at shuttle altitudes ranging from 100-250 km. Success of the system is based on useful values of the signal-to-noise ratio.

END

FILMED

3-86

DTIC